Doctoral Dissertation

Comprehension of $Mg(OEt)_2$-based Ziegler-Natta Catalyst Structure in Heterophasic Polypropylene Characteristics

GOOND HONGMANEE

Supervisor: Professor Dr. Minoru Terano

School of Materials Science
Japan Advanced Institute of Science and Technology

September 2016

Contents

Chapter I

General introduction

1.1 Ziegler-Natta catalysts

1.1.1 Introduction to Ziegler-Natta catalysts

Generally there are three main types of catalyst; Phillips catalyst (or supported chromium catalyst), metallocene (or single-site catalyst) and Ziegler-Natta catalyst, which are industrially used at present besides radical polymerization. However, when focused on propylene polymerization, Ziegler-Natta catalyst takes the largest part for producing polypropylene because of its high productivity and low operating cost compared to the others.[1] Ziegler-Natta catalyst was named according to Karl Ziegler (Germany) and Gulio Natta (Italy), who discovered ethylene polymerization catalyst in the 1950s. This catalyst has been continuously developed over fifty years after its discovery. The development of Ziegler-Natta catalyst can be classified in to five generations as summarized in **Table 1.1**.

Table 1.1 evolution of Ziegler-Natta catalysts for propylene polymerization.[2]

Generation	**Catalyst**	**Yield (kPP gcat^{-1})**	**Isotactic index**[(a)]
First	δ-$TiCl_3$/DEAC	2 – 4	90 – 94
Second	δ-$TiCl_3$/isoamylether/$AlCl_3$/DEAC	10 – 15	94 – 97
Third	$MgCl_2$/ester/$TiCl_4$/TEA/ester	15 – 30	95 – 97
Fourth	$MgCl_2$/ester/$TiCl_4$/TEA/$PhSi(OEt)_3$	> 100	> 98

[(a)] Determined by percent weight of heptane soluble content of polymer

The generation of Ziegler-Natta catalyst is divided by the discovery of $MgCl_2$ as a support and the usage of electron donors. In the first generation, Ziegler-Natta catalysts were composed of crystalline $TiCl_3$ in four different geometries: hexagonal (α), fibrous (β), cubic (γ), and a mixed hexagonal-cubic form (δ). The

δ-$TiCl_3$ complex is the most active for propylene polymerization and is obtained as porous particles with diameters varying from 20 to 40 μm (secondary particles), resulting from the agglomeration of even smaller $TiCl_3$ particles with diameters in the range 0.03 – 0.04 μm (primary particles).[2]

In the second generation, electron donor (Lewis bases) was used to improve stereoselectivity and productivity of the catalyst. However, it was not sufficient to neglect post-reactor processes. The catalysts from first two generations were formed from crystalline $TiCl_3$. The drawbacks of them were low productivity because monomer could not access to the active sites locating inside the particle. Therefore, they also required post-reactor processes such as catalyst residue removal and the elimination of atactic polypropylene.

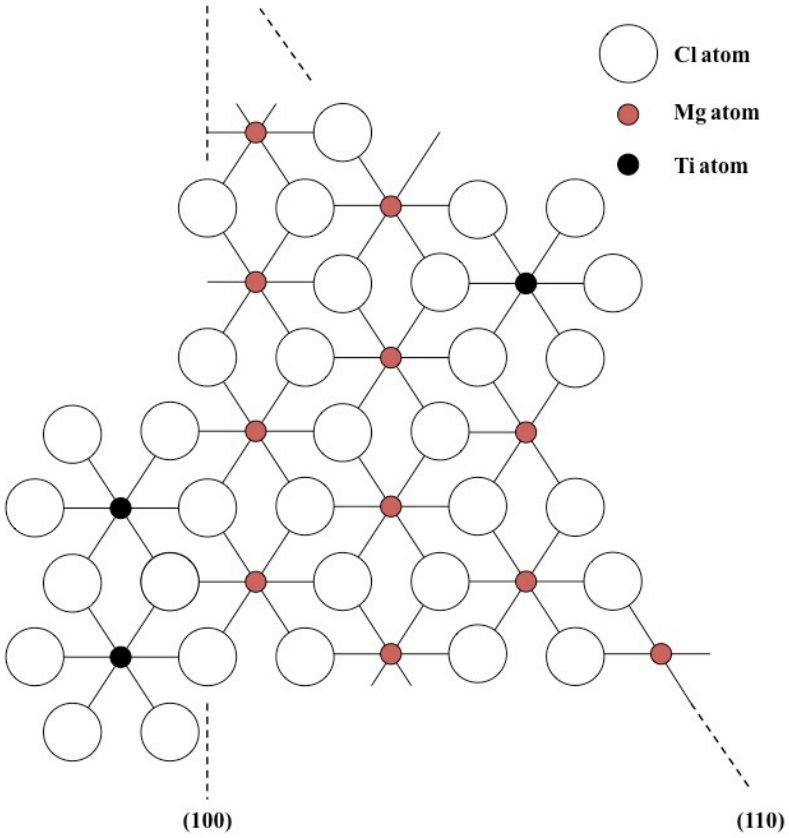

Figure 1.1 structure of $TiCl_4/MgCl_2$ Ziegler-Natta catalyst.

An idea to improve the accessibility of monomer to active sites led to the invention of supported-catalyst. Magnesiumchloride ($MgCl_2$) was the most appropriate support. This support gave high productivity in both of ethylene and propylene polymerization and improve stereoselectivity. The structure of $TiCl_4/MgCl_2$ catalyst is shown in **Figure 1.1**.[3] The discovery of $MgCl_2$ lead to the reduction of operating cost, because the post-reactor processes can be neglected.

The improvement on catalyst morphology control and stereoselectivity seemed to be the main target of the fourth generation Ziegler-Natta catalyst. The catalyst morphology was enlarged in order to form enough large spherical polymer particle to be able to neglect pelletization process. Also, the pair of electron donor was changed in order to improve stereoselectivity. Electron donors can be classified into two types; internal and external donor. For internal donor, it is added during catalyst preparation, while the external donor is directly charged to a reactor before polymerization. The main objective of the electron donor is to control the distribution of $TiCl_4$ on $MgCl_2$ surfaces. The development of electron donor system is summarized in **Table 1.2**.[2]

Table 1.2 Electron donor development of propylene polymerization catalyst

Internal donor	External donor	Isotactic index (wt%)
Aromatic monoesters (EB)	−	60
Aromatic monoesters (EB)	Aromatic monoesters (methyl *p*-toluate)	95
Aromatic diesters (DIBP)	Silanes	97 – 99
Diethers (1,3-diether)	−	97 – 99

1.1.2 Ziegler-Natta catalyst preparations

Typically, $TiCl_4/MgCl_2$ catalyst preparation is composed of four steps: digestion,

activation, washing, and drying. The digestion step includes the reaction of an organomagnesium (MgOR) compound, $TiCl_4$, and an internal electron donor in chlorinated organic solvent. The active $TiCl_4$ is dispersed in the porous precursor surface and form $MgCl_2$ crystal and $TiCl_3 \cdot OR$, simultaneously. $TiCl_3 \cdot OR$ is removed by $TiCl_4$ and solvent. Then, the formed catalyst is washed using a volatile organic compound. Finally, after the volatile organic compound is evaporated, the catalyst is obtained as a free-flowing powder.

Generally, there are mainly three preparation methods for preparing Ziegler-Natta catalyst ball-milling[4-6], alcohol-adduct[7-10], and magnesiumethoxide[11-12]. For the first method, magnesiumchloride and internal electron donor are mixed by ball-milling and further treated by $TiCl_4$. The other two methods, alcohol-adduct and magnesiumethoxide ($Mg(OEt)_2$), are prepared though morphology controlled precursor to form well-shaped $MgCl_2$ by chemical reaction to be a support for $TiCl_4$. Considering the identical characteristic of each method, grinding catalyst gave the highest initial activity followed by rapid the deactivation. On the contrary, alcohol-adduct and $Mg(OEt)_2$-based catalysts, both of them exhibited build-up-type kinetics. However, there are many studies reported that $Mg(OEt)_2$-based catalyst showed the highest overall catalytic activity among these methods.

1.1.3 Researches in magnesiumethoxide-based Ziegler-Natta catalyst

$Mg(OEt)_2$-based Ziegler-Natta catalyst got attention from many researchers because of its high performances. There were many researches relating to kinetics, morphology control, and catalyst performances. For example, Tait et al.[13] conducted propylene polymerization by using three platforms of catalyst in with and without external electron donor. They reported that ball-milling catalyst gave decay-type rate

profile, while adduct and ethoxide-based catalyst gave build-up type. These results were consistent with Dashti's work.[12] Furthermore, they emphasized the relationship between kinetics and polymer morphology. Although concentration of active sites of $Mg(OEt)_2$-based catalyst was less compared to the other methods, it could gave more stable activity and also better polymer particle morphology. The active sites was well-dispersed all over the $Mg(OEt)_2$-based catalyst particle.

The initial-stage development of polymer morphology was intensely investigated by many researchers. Besides reaction kinetics, nature and architecture of support materials, as well as kind of polymerization also influences polymer morphology development.[14] There are two patterns of fragmentation depending on pore size and volume. Layer-by-layer (LbL) is usually occurred when catalyst suffers from mass transfer limitation.[15, 16] In contrast, the enhancement of catalyst pore volume makes catalyst particle brittle, which employed homogeneous fragmentation mechanism as usually seen in propylene polymerization. However, the pattern can be changed regarding to polymerization procedure. Vestberg et al.[17] reported that pre-contact of catalyst with cocatalyst and external donor could lead to homogeneous fragmentation in low pore volume catalyst, because the active sites were already activated uniformly before polymerization was started. Focusing on $Mg(OEt)_2$-based catalyst, the inner structure of the catalyst is composed of three layers; outermost surface, porous layer, and compact core (**Figure 1.2**). Taniike et al.[14] purposed that the nascent-formed polymer located on the particle surface and in the macropores. As the reaction was carried out, the polymer filled the pore in the porous layer and created stress on the pore walls. The generated stress expanded the porous layer, which induced fragmentation of the outermost shell and polymer/catalyst lamellae on the surfaces of

compact core. Their concept of morphology development is summarized in **Figure 1.3**.

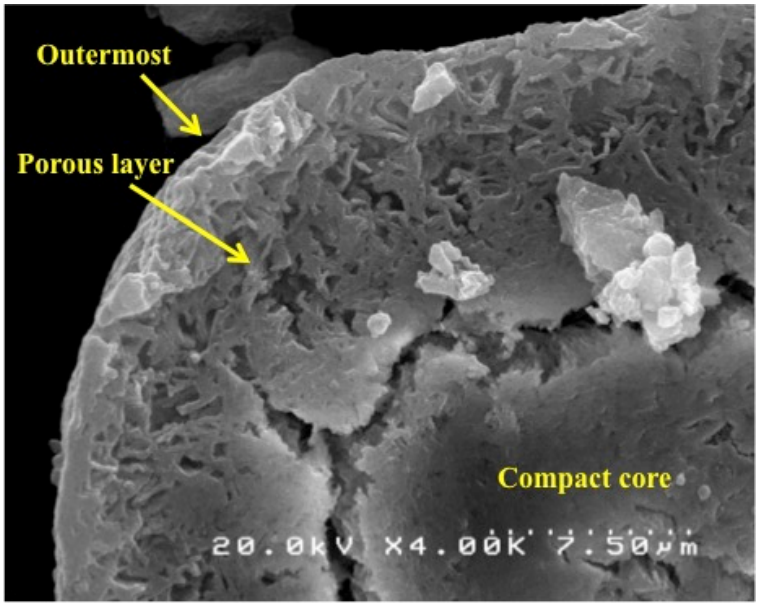

Figure 1.2 structure of $Mg(OEt)_2$-based catalyst.

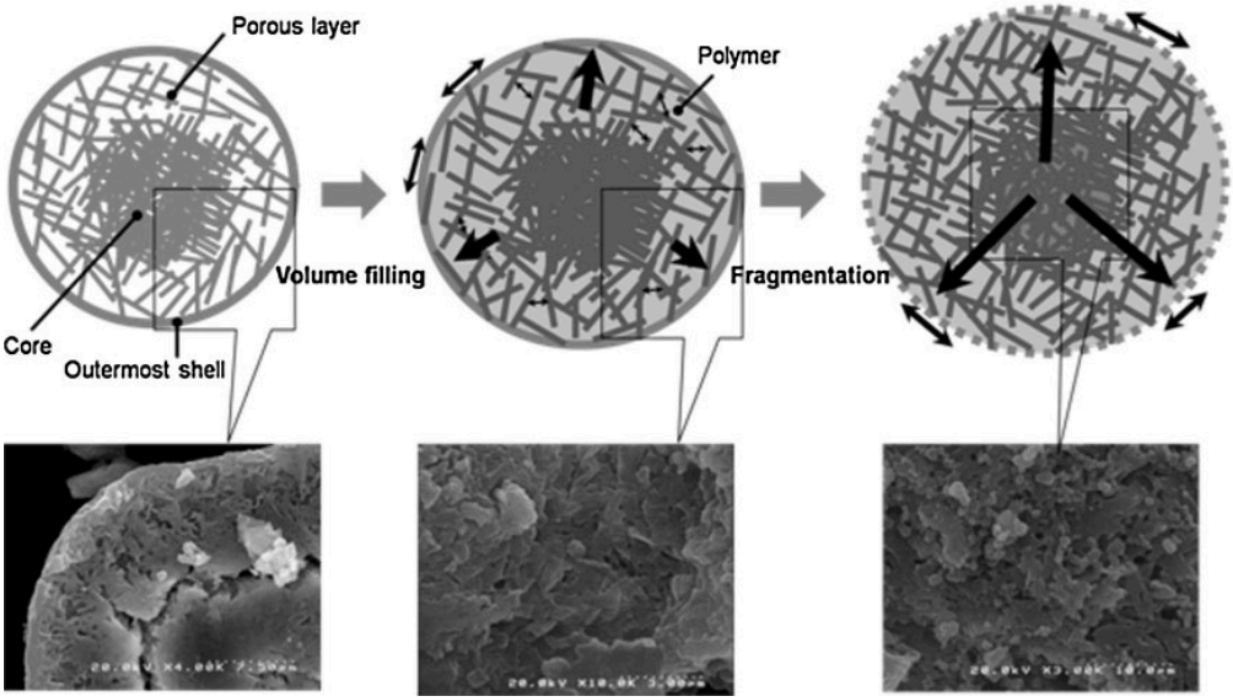

Figure 1.3 initial-stage polymer morphology development proposed by Taniike et al.

In addition to the polymer morphology, the performances of $Mg(OEt)_2$-based Ziegler-Natta catalyst are also attractive for both of industrial and academic field. It is known that the performances of catalyst are depended on the reaction conditions and catalyst itself. The catalyst performances can be improved by modification of either chemical composition of catalyst or reaction environment. However, less attention has been paid on the study of relationship between catalyst structure and performances especially on Ziegler-Natta catalyst.

Structure-Performance relationship (SPR) is a study aiming to correlate materials structure and their performances. By integrating statistical analysis, SPR is useful for exploration and prediction of material performances which become more and more important for materials science. Especially in catalysis, SPR can provide a guideline of catalyst design in a quantitative way. Unfortunately, SPR study is still limited for Ziegler-Natta catalyst because its structure composed of complex arrangement, which leads to multivariable problem. In addition, its heterogeneity makes difficulty in characterization both of catalyst structure and polymer properties. However, the study by Taniike and coworkers showed a relationship between catalyst structure (pore volume and particle size) and its performances (catalytic activity and comonomer incorporation ability) in ethylene/1-hexene copolymerization.[18] The study showed large catalyst size had negative effect on catalytic activity, while meso- and macropore volume had positive effect on 1-hexene incorporation ability.

1.2 Magnesiumethoxide

1.2.1 Magnesiumethoxide formation mechanisms

Magnesiumethoxide (MGE) was a high performance material as a precursor of Ziegler-Natta catalyst as shown in the previous section. It is known that MGE

particle is composed of many platelet crystals. However, the formation mechanism is still unclear.

The growth mechanism of $Mg(OEt)_2$ was studied by Tanase and coworkers.[19] They employed Mg ribbon as a source of magnesium to synthesize $Mg(OEt)_2$ in order to minimize the influence of collision between particles. Then, they tracked the particle development from the samples collected from different times of reaction. The schematic concept of their proposed is shown in **Figure 1.4**.

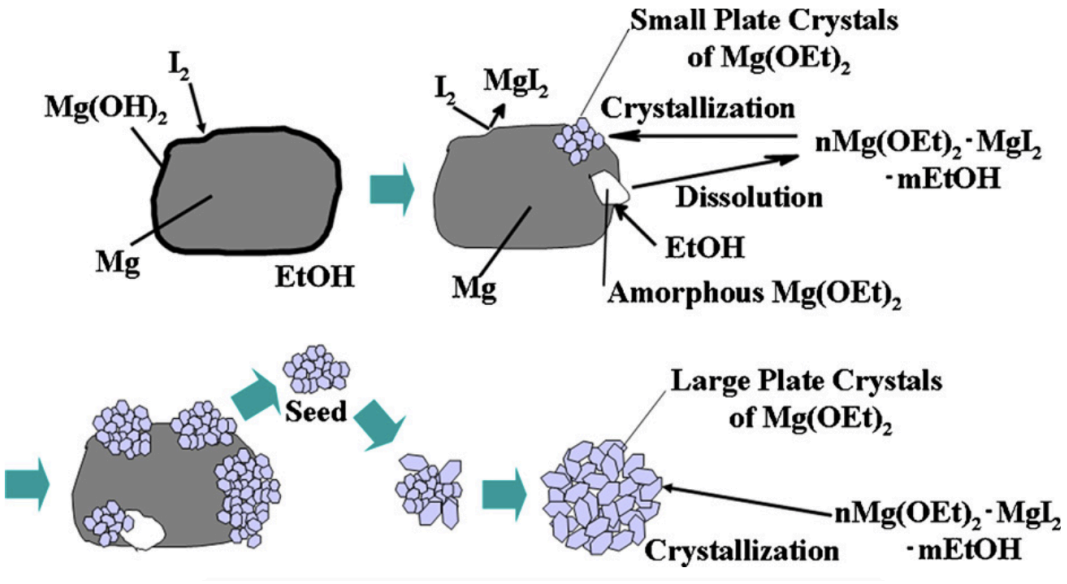

Figure 1.4 mechanism for $Mg(OEt)_2$ particle growth proposed by Tanase et al.

Brief explanation of their mechanism was summarized as follow. $Mg(OEt)_2$ seeds were initially formed on Mg surfaces and subsequently detached due to the collision and other shear force. The isolated particles continued to grow further from the precipitation of quasi-stable nMg(OEt)$_2$.MgI$_2$.mEtOH soluble complex. The related chemical reactions are shown in equation 1.1-1.3.

$$Mg + 2EtOH \longrightarrow Mg(OEt)_2 + H_2 \quad (1.1)$$

$$Mg + I_2 \longrightarrow MgI_2 \quad (1.2)$$

$$n\text{Mg(OEt)}_2 + \text{MgI}_2 + m\text{EtOH} \longrightarrow n\text{Mg(OEt)}_2.\text{MgI}_2.m\text{EtOH} \quad (1.3)$$

Joseph et al.[20] also studied $Mg(OEt)_2$ particle growth and its kinetics. However, in their research, they employed magnesium powder instead of ribbon to be comparative the industrial-scale production. Their observed mechanism was not different from the previous proposal by Tanase et al. The growth mechanism consisted of three main steps; $Mg(OEt)_2$ particle formation, particle growth, and separation. They also found the relationship between reaction rate and particle morphology by changing system parameters such as size of magnesium source, reaction pressure, and stirring speed. The results showed that the increase of reaction rate and shear force could reduce $Mg(OEt)_2$ particle size.

1.2.2 Modifications of magnesiumethoxide morphology

As seen in the proposed mechanism, it is known that the formation of $Mg(OEt)_2$ was sensitive to the conditions. Utilizing the knowledge from the proposed mechanism, it led to various possibilities to modify the morphology of resulting $Mg(OEt)_2$ and/or catalyst particle.

The achievement of enlargement of $Mg(OEt)_2$ was found in Tanase and coworkers's work.[21] They added other metalchloride (MCl_x) compound, besides I_2, to replace magnesium atom in the crystal structure (**Figure 1.5**). From the results, the additional of $MnCl_2$ could enlarge particle size of carrier. However, $MnCl_2$ did not co-crystallize as expected, but it adsorbed on the surface of plate $Mg(OEt)_2$ crystal as proven by XRD.

Besides the addition of metal compound, Funako et al.[22, 23] also found that the addition of other alcohol (in addition to ethanol) could change the morphology of building unit. The addition of *i*-propanol to some extent could change pore structure of the carrier from broad dimension and slit shape to microporous and cylindrical shape. They also varied alcohol type in the experiment. The pore distribution of carrier was also changed depending on molecular structure of alcohol. This was ascribed to the disturbance of dissolution/precipitation equilibrium during $Mg(OR)_2$ formation.

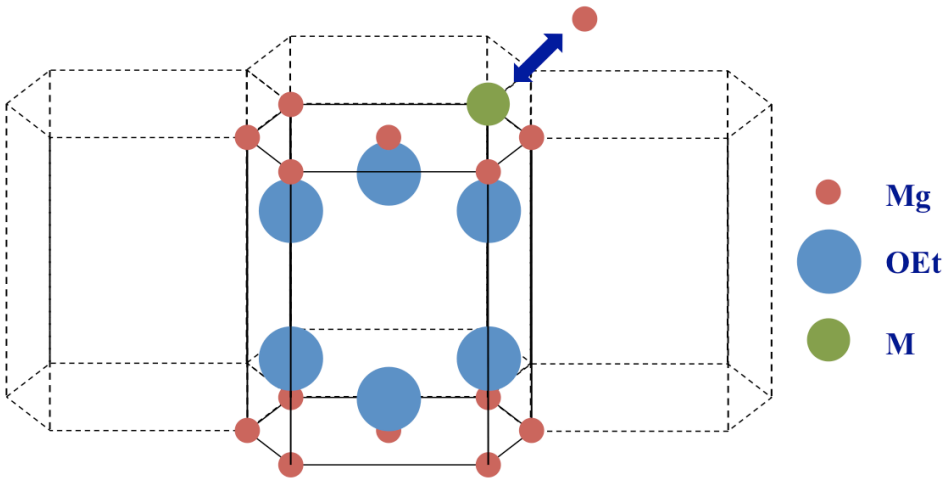

Figure 1.5 crystal structure of carrier material co-crystallizing with another metal atom in $Mg(OEt)_2$ synthesis.

1.3 Introduction to polyolefins

Polyethylene (PE) and polypropylene (PP) are two main classes of polyolefins. They have been widely used to produce many general commodities such as films, plastic bag and bottle. In addition, they also have been used in advanced materials such as high impact resistant materials and conductive materials. It is known that the properties of polymer are controlled by its microstructure, which can be designed

through the control of production process. There are three components, which are important for determining polymer microstructure; (i) monomer (or comonomer), (ii) catalyst, and (iii) reactor. In this section, each component is emphasized for more comprehension of polyolefin, especially on polypropylene.

1.3.1 Polypropylene and its comonomer

Homopolypropylene (PP) is produced from many chemically connected propylene molecules. Generally, it has density of ~0.9 g/ml, which is lower than polyethylene (PE). PP can be produced through many routes such as free radical and cationic polymerization. However, in practical, PP is catalytically polymerized by transition metal and metal alkyl cocatalyst as shown in equation 1.4.

$$n\ CH_2 = CHCH_3 \longrightarrow \sim (CH_2\underset{\displaystyle CH_3}{\underset{|}{C}}H)_n \sim \qquad (1.4)$$

Propylene is an asymmetric molecule, which differs from ethylene. There is possibility for molecules to cooperate with the previous molecules in different direction leading to various configuration of methyl group in main polypropylene chain. This characteristic is called “tacticity”. Also, the different tacticity of polypropylene gives the different polymer properties such as mechanical properties, crystallinity, melting behavior and solubility. The orientation of methyl group can produce three different configurations as shown in **Figure 1.6**.

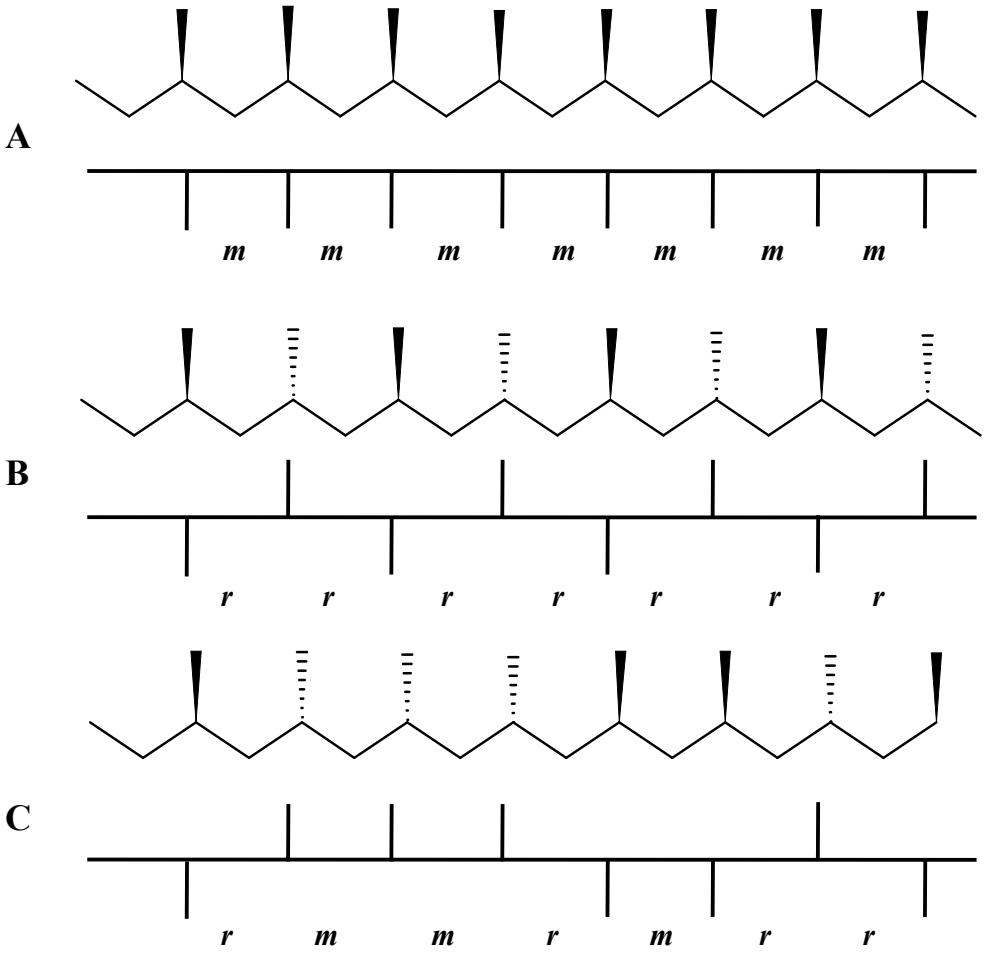

Figure 1.6 stereoisomers of polypropylene: (a) isotactic, (b) syndiotactic, and (c) atactic polypropylene.

Isotactic polypropylene (iPP) contains orderly oriented methyl group in the main chain. Because of its structure, it can crystalize up to the crystallinity of 70% and has relatively high melting temperature (160 to 180 °C). iPP is widely used in fibers, films, and houseware products. For syndiotactic polypropylene (sPP), it contains alternated methyl group. Although its properties are lower than iPP such as melting temperature, toughness etc., it is used in specific application such as healthcares and electrical power cables. Atactic polypropylene (aPP) has randomly arranged methyl group in main chain. The crystallinity of aPP is the lowest among PP polymers, so aPP is generally undesired, because of its poor mechanical properties.

Comparing to other polymers, PP has relatively low operating cost with many excellent properties such as high chemical resistance and toughness. In addition, propylene can be copolymerized with other α-olefins such as ethylene, 1-butene or 1-hexene to improve polymer properties. However, among these comonomers, ethylene is the most common used comonomer.

There are two possible copolymer structures obtained from propylene-ethylene copolymerization, random and sequential copolymer. Random copolymer is obtained when copolymer content is up to 7%. For, sequential copolymer or impact copolymer, ethylene molecules are linked among propylene chain. Thus, the polymer structure is contained with segmented polyethylene and polypropylene. The characteristics of polypropylene are summarized in **Table 1.3**.[24]

Table 1.3 characteristics of polypropylene.

Type of polypropylene[(a)]	Comonomer content (wt%)	Impact resistance	Film Clarity	Tensile strength
Homopolymer	0	Poor	Poor	Good
Random copolymer	1-7	Medium	Good	Medium
Impact copolymer	5-25	Good	-	Poor

[(a)] Densities of all types are in the range of 0.89 – 0.91 g/mL

1.3.2 In situ high impact polypropylene

Polypropylene is used in many applications, because it has many special properties compared to other polymer, especially its high tensile strength. It has been used to produce general commodities such as films, and textiles. To widen range of application, blending with other co-/polymer to form a polymer alloy can also be one of the effective ways.

High impact polypropylene (hiPP) is a polymer alloy between polypropylene (PP) and ethylene-propylene rubber (EPR). The addition of EPR can improve impact property especially at low temperature.

An in situ hiPP overwhelms many advantages compared to the external blending. In economic aspect, the in situ process can reduce energy consumption in the production process. Technically, in situ blending can provide extraordinary polymer properties, since it can produce more than two compositions to fulfill the extra requirements of materials. Also, it allows producing well-dispersed components that discard compatibility of two components.[25] For Ziegler-Natta catalyst, active sites locate on the surfaces of porous support. Polymerization continuously occurs at the active sites and replicates the catalyst particle. According to mass transfer resistance, the polymer can be faster generated at an outer layer comparing to an inner layer. This expands the surface of polymer and produces a polymer, which has porous internal structure. The porous polymer is obtained and behaves as a polymerization reactor, which other olefins can be polymerized. This technology is named "reactor granule technology (RGT)".[26]

Generally, hiPP is produced in two-stage reactor in series. First, isotactic polypropylene particles are produced in the first reactor, which can be either slurry- or gas-phase. Then, these particles are transferred to a gas-phase reactor, where the copolymer is produced within the isotactic polypropylene pores. There are many factors affecting the properties of hiPP.

Fan et al.[27] studied the influences of random and segmented copolymer on impact property and flexural modulus of in situ hiPP. They observed that both random and segmented copolymer had positive effects on the impact property. While the increase of random copolymer content decreased flexural modulus. They also

investigated the impact strength at low temperature (−30 °C) and room temperature (23 °C) of hiPP absented random copolymer. At room temperature, impact strength was slightly lower after removing the random copolymer, while the impact strength strongly affected at low temperature. However, the observed improvement of impact strength by random copolymer at low temperature conflicted with the result of L. D'Orazio et al.[28] They blended isotactic polypropylene with random copolymer and found that the impact strength of the blend was slightly improved at low temperature.

Besides the content, quality of rubber also plays a key role in determining the properties. As the reaction keeps proceeding, the active sites (amount, oxidation state, etc.) are also altered along the process. These changes of active sites also affect copolymerization resulting in variation of copolymer composition. As reported by many researchers, propylene-rich EPR reduced the interfacial tension against the PP matrix resulting in fine dispersion of EPR.[28, 29] It also affected on the polymer properties after processing. It gave excellent transparency, and low shrinkage. These effects were also ascribed to a partial dissolution of the propylene-rich EPR in the amorphous region between the PP lamellae. On the contrary, ethylene-rich EPR, which the ethylene content above 50 wt%, comprised of polyethylene fraction incorporated as inclusions in the amorphous EPR domains to form core-shell (single inclusion) and salami-like (multiple inclusions) structures.[1, 30, 31] HiPP impact copolymers with an ethylene-rich dispersed phase have very good low-temperature toughness and the scratch as well as stress-whitening resistance. In terms of the mechanical properties, the optimum composition rendering an EPR phase sufficiently immiscible with the matrix to maintain phase separation and adequately miscible to assure proper matrix/dispersed-phase adhesion is reported to be 35–45 wt % of ethylene.[27, 32]

1.3.3 Rubber growth mechanisms in high impact polypropylene

As described in the previous section, the properties and morphology of dispersed phase in hiPP particle are significantly important on determining the properties of hiPP. Thus, it is meaningful and necessary to study how the dispersed phase is formed. However, it is still controversial among the researchers about the formation mechanisms.

In Debling and Ray's model [33], the isotactic polypropylene particle consisted of many clusters of microparticles, where the catalyst fragment existed. As copolymerization processed, the rubber phase formed in small micropores, and then expanded into larger macropore. The obtained hiPP particle remained large pores, macro cracks, and voids which was similar to homopolymer (**Figure 1.7**). Interestingly, the diffusion limitation was not found even the copolymer was up to 70 wt% of whole polymer. They reasoned that macropores, large cracks, and channels were sufficient to overwhelm the diffusion limitation.

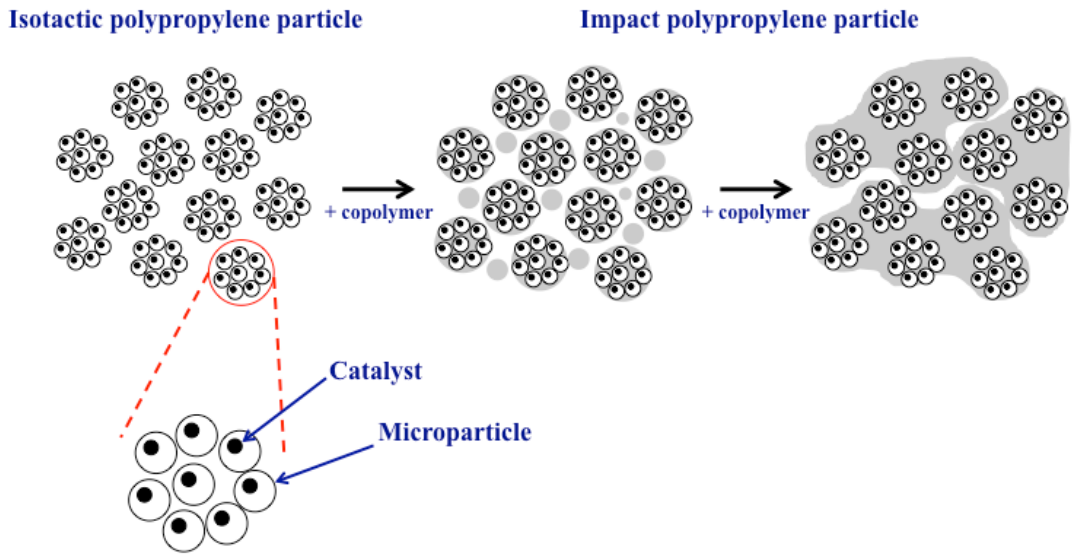

Figure 1.7 proposed model of hiPP particle growth by Debling and Ray.

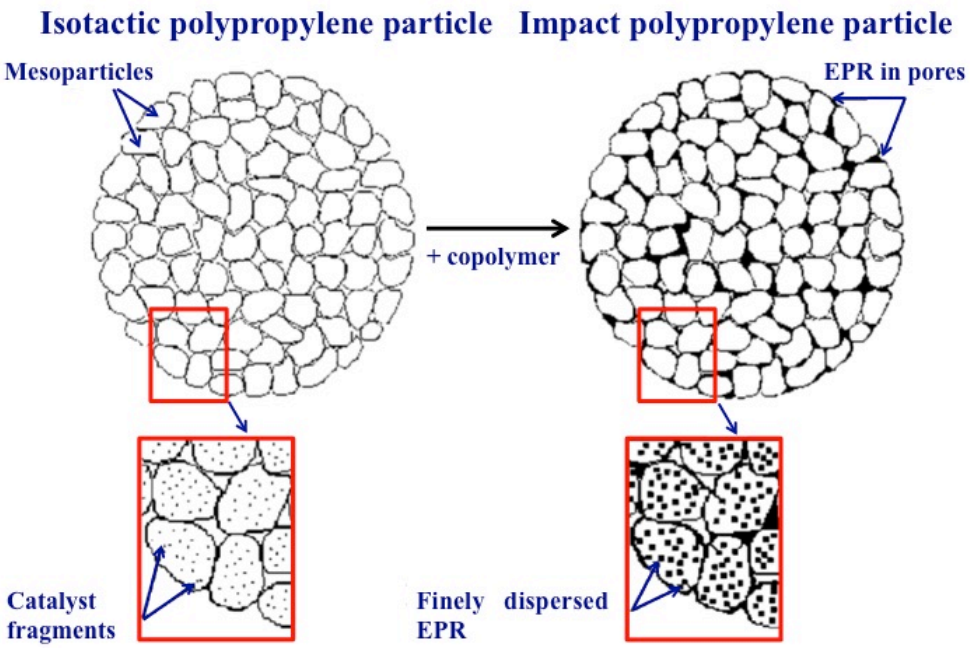

Figure 1.8 proposed model of hiPP particle growth by Urdampilleta et. al.

Urdampilleta et al.[34] observed the porosity of hiPP (rubber content of 24 wt%) by microtome technique and mercury porosimetry. They could not observe apparent pores from the cut particle. It contradicted the result from porosity measurement, which showed only 46% of pore was filled by rubber. Comprising of calculation and AFM technique, they concluded that EPR was formed around the catalyst fragments which resulted in the dispersed EPR domains in polypropylene matrices. Then, some of EPR broke polypropylene matrices and flowed to the pores. The concept of the purposed model is shown in **Figure 1.8**.

McKenna et al.[35] proposed pore filling model in the case of small and large pore size of catalyst. In both cases, layer of polypropylene was formed on the internal surfaces of catalyst after the first stage polymerization (propylene polymerization). EPR was formed underneath the polypropylene layer. Then, it broke propylene layer and flowed out to the pore of catalyst. For small pore size, the rubber occluded the pore as shown in **Figure 1.9a**. While large pore size needed larger amount of EPR to

completely fill the pore.

Cecchin et al.[36] proposed that at the end of the homopolymerization stage the polypropylene particle is composed by quite a few polymer mesoparticles. The catalyst fragments were located at the surface of the polymer mesoparticles because they segregated during the homopolymerization. Therefore, the EPR formed in the second stage was located at the surface of these mesoparticles filling the pores between them. This led to continuous network of EPR.

Zhou et al.[37] described the hiPP particle morphology as the dispersion of nanosized rubbery droplets along iPP primary particles. The rubbery droplets can then agglomerate to the continuous EPR phase.

Although these models were different in the details of rubber formation, these works emphasized the importance of catalyst design. Polymer formed at the active sites located on the surfaces of catalyst, and duplicated the catalyst morphology. Thus, the catalyst preparation could also affect the polymer morphology, especially pore characteristics.

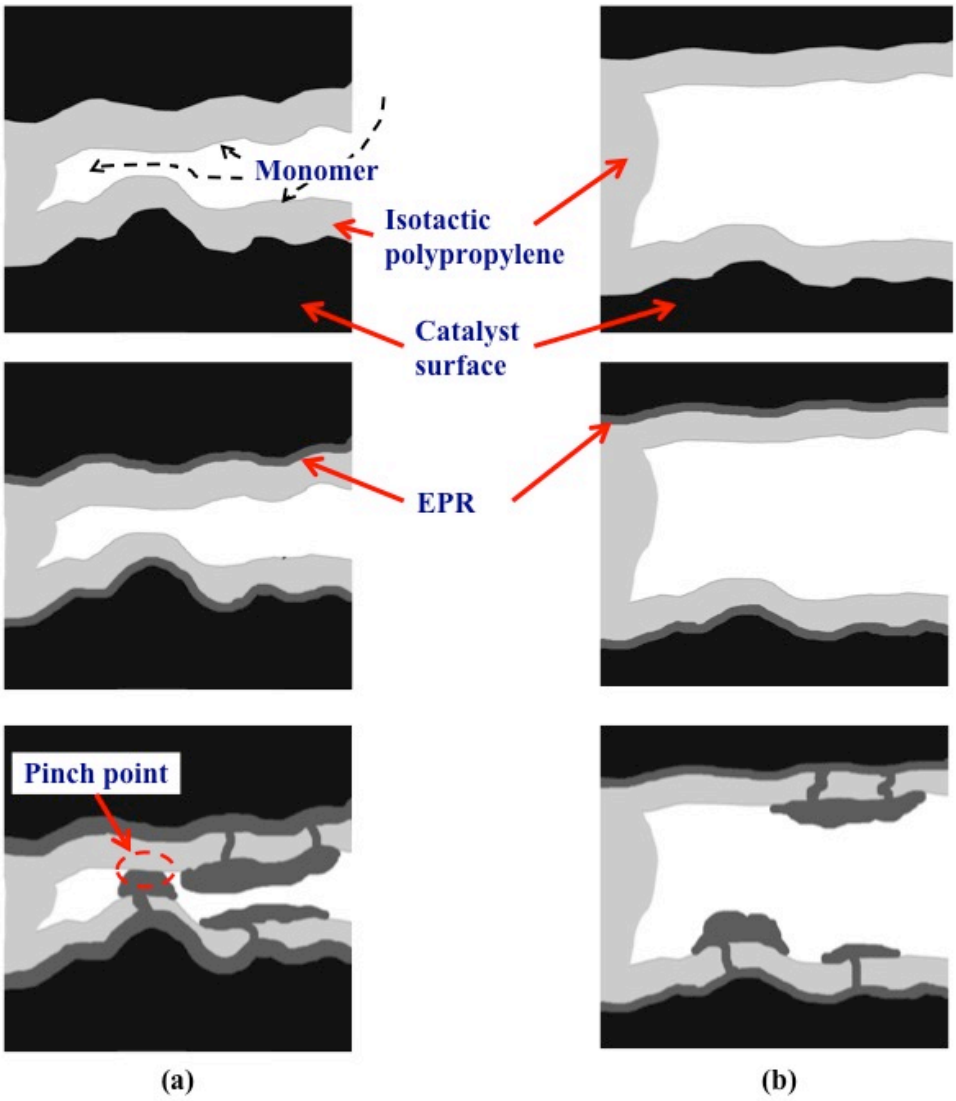

Figure 1.9 EPR filling model proposed by McKenna et al. (a) small pore size filling, and (b) large pore size filling.

1.4 Objectives of this study

Polypropylene is an interesting polyolefin, which the production rate has been increasing annually. Because polypropylene has excellent properties and low operating cost, it has been used in many applications. The development of technology and the research in polyolefin also expand range of usage and make polypropylene more and more advanced material.

The background of the achievement in excellent properties has to be looked back

to the step of catalyst design. It is known that polymer properties are determined by its microstructure. However, it is a big challenge for researchers to control polymer microstructure in Ziegler-Natta catalyst. One of the difficulties to understanding this catalyst is the characterization. Ziegler-Natta catalyst is composed of multicomponent and irregularly hierarchic structures from micro- to macro-scale. It is difficult to reveal all of the structures and their characteristic. Moreover, because of it hierarchy, it is difficult to change only a target structure without changing other parameters. Thus, a specific role of each structure on catalyst performance is still unclear. Finally, the relationship between structure and performances is not one-to-one relationship. According to the problems, most of polyolefin researches have been done in an empirical way.

In this dissertation, the author intensively investigated performances of Ziegler-Natta catalyst in polypropylene/(ethylene-*co*-propylene) copolymerization since the stage of catalyst structure design, evaluation of the reactor performance, and the catalyst performances. The study was divided into three chapters.

Chapter 2: Probing into morphology evolution of magnesium ethoxide particles as precursor of Ziegler-Natta catalysts. In this chapter, the formation of magnesiumethoxide was investigated in the course of synthesis. The origination of particle size and circularity was concluded.

Chapter 3: Establishment of experimental procedure for high impact propylene copolymerization in a gas-phase reactor. Polypropylene/(ethylene-*co*-propylene) copolymer or high impact polypropylene (hiPP) is generally produced in a two-stage reactor in series. To obtain both of excellent polymer properties and morphology, it is important to determine the proper reaction conditions and the operating procedure.

Chapter 4: Reactor granule technology for evaluating rubber distribution of high

impact polypropylene in $Mg(OEt)_2$-based Ziegler-Natta catalyst. The structure of polypropylene was continuously changing during the reaction according to the fragmentation phenomena. Thus, copolymerization occurred on the surface of the produced polymer was also influenced from the different polymer structure. In this chapter, the changes of polymer properties were ascribed as the performances of polymer template.

References

[1] N. Pasquini (Ed.), *Polypropylene Handbook,* Hanser, Munich, Germany 2005.

[2] J. B. P. Soares, T. F. L. McKenna, *Polyolefin Reaction Engineering,* WILEY-VCH, Boschstr, Germany 2012.

[3] V. Busico, P. Corradini, L. De Martino, A. Porto, V. Savino, E. Albizzati, *Macromol. Chem. Phys*., 186 (1985) 1279-1288.

[4] S. Poonpong, S. Dwivedi, T. Taniike, M. Terano, *Macromol. Chem. Phys.*, 215 (2014) 1721-1727.

[5] H. Mori, K. Ohnishi, M. Terano, *Macromol. Chem. Phys.*, 199 (1998) 393-399.

[6] H. Mori, K. Ohnishi, M. Terano, *Macromol. Rapid Commun.*, 17 (1996) 25-29.

[7] Z. Y. Ye, L. Wang, L. F. Feng, X. P. Gu, H. H. Chen, P. Y. Zhang, J. Pan, S. Jiang. L. X. Feng, *J. Polym. Sci. A Polym. Chem.*, 40 (2002) 3112-3119.

[8] S. Miya, M. Tachibana, Y. Karasawa US Patent 5100844, 1992.

[9] M. Kioka, H. Kitani, N. Kashiwa US Patent 4330649, 1982.

[10] A. A. Batinas-Geurts, N. H. Friederichs, T. Schoffelen, E. Zuidema US Patent 20140296454, 2014.

[11] G. H. Zohuri, F. Azimfar, R. Jamjah, S. Ahmadjo, *J. Appl. Polym. Sci.*, 89 (2003) 1177-1181.

[12] A. Dashti, A. Ramazani SA, Y. Hiraoka, S. Y. Kim, T. Taniike, M. Terano, *Polym. Int.*, 58 (2009) 40-45.

[13] P. J. T. Tait, G. H. Zohuri, A. M. Kells, I. D. McKenzie, *Ziegler Catalysts*, Springer Berlin Heidelberg, Heidelberg, Germany 1995.

[14] T. Taniike, V. Q. Thang, N. T. Binh, Y. Hiraoka, T. Uozumi, M. Terano, *Macromol. Chem. Phys.*, 212 (2011) 723-729.

[15] G. Fink, B. Steinmetz, J. Zechlin, C. Przybyla, B. Tesche, *Chem. Rev.*, 100 (2000) 1377-1390.

[16] X. Zheng, M. Smith, J. C. Chadwick, J. Loos, *Macromolecules*, 38 (2005) 4673-4678.

[17] T. Vestberg, P. Denifl, C.-E. Wilen, *J. Appl. Polym. Sci.*, 110 (2008) 2021-2029.

[18] T. Taniike, T. Funako, M. Terano, *J. Catal.*, 311 (2014) 33-40.

[19] S. Tanase, K. Katayama, S. Inasawa, F. Okada, Y. Yamaguchi, T. Konakazawa, T. Junke, N. Ishihara, *Appl. Catal. A Gen.*, 350 (2008) 197-206.

[20] J. Joseph, S. C. Singh, V. K. Gupta, *Particul. Sci. Technol.*, 27 (2009) 528-541.

[21] S. Tanase, K. Katayama, S. Inasawa, F. Okada, Y. Yamaguchi, T. Sadashima, N. Yabunouchi, T. Konakazawa, T. Junke, N. Ishihara, *Macromol. React. Eng.*, 350 (2008) 197-206.

[22] T. Funako, P. Chammingkwan, T. Taniike, M. Terano, *Macromol. React. Eng.*, 9 (2005) 325-332.

[23] T. Funako, P. Chammingkwan, T. Taniike, M. Terano, *Polyolefins J.*, 2 (2015) 65-71.

[24] D. B. Malpass, E. Band, *Introduction to Industrial Polypropylene: Properties, Catalysts Processes*, Wiley-Scrivener, Massachusetts, United States of America.

[25] P. Galli, *Macromol. Symp.*, 78 (1994) 269-284.

[26] P. Galli, *J. Macromol. Sci.*, Pure Appl. Chem., 36 (1999) 1561–1586.

[27] Z.-Q. Fan, Y.-Q. Zhang, J.-T. Xu, H.-T. Wang, L.-X. Feng, *Polymer*, 42 (2001) 5559-5566.

[28] L. D'Orazio, C. Mancarella, E. Martuscelli, G. Sticotti, *J. Mater. Sci.*, 26 (1991) 4033-4047.

[29] T. Nomura, T. Nishio, T. Fujii, J. Sakai, M. Yamamoto, A. Uemura, *Polym. Eng. Sci.*, 35 (1995) 1261-1271.

[30] R. Zacur, G. Goizueta, N. Capiati, *Polym. Eng. Sci.*, 40 (2000) 1921-1930.

[31] P. Doshev, G. Lohse, S. Henning, M. Krumova, A. Heuvelsland, G. Michler, H.-J. Radusch, *J. Appl. Polym. Sci.*,101 (2006) 2825-2837.

[32] C. Grein, M. Gahleitner, B. Knogler, S. Nestelberger, *Rheol. Acta.*, 46 (2007) 1083-1089.

[33] J. A. Debling. W. H. Ray, *J. Appl. Polym. Sci.*, 81 (2001) 3085-3106.

[34] I. Urdampilleta, A. González, J. J. Iruin, J. C. de la Cal, J. M. Asua, *Macromolecules*, 28 (2005) 2795-2801.

[35] T. F. McKenna, D. Bouzid, S. Matsunami, T. Sugano, *Polym. React. Eng.*, 11 (2003) 177-197.

[36] G. Cecchin, E. Marchetti, G. Baruzzi , *Macromol. Chem. Phys*, 202 (2001) 1987-1994.

[37] Y. Zhou, H. Niu, Y. Zhao, J.-Y. Dong, D. Wang, *Polymer*, 50 (2009) 4690-4695.

Chapter II

Probing into morphology evolution of magnesium ethoxide particles as precursor of Ziegler-Natta catalysts

2.1 Introduction

In Ziegler-Natta catalyzed olefin polymerization, polymer morphology is one of major concerns in plant production efficiency. For instance, polymer with narrow particle size distribution and high bulk density can enhance the production throughput, while inappropriate morphology can cause transportation and plugging problems.[1] It is widely accepted that the morphology of polymer replicates that of catalyst particles.[2]

Polymer is generated at active sites located inside catalyst pores and accumulates hydraulic pressure, leading to particle fragmentation and exposure of new active sites. This process repeatedly proceeds in catalyst particles to yield polymer particles that imitate the catalyst morphology. To achieve well-controlled polymer morphology, intensive consideration must be paid on the catalyst design.

Nowadays, a variety of techniques have been established to control the morphology of Zielger-Natta catalysts, whose details depend on employed precursors. For instance, if adduct solution of $MgCl_2$ and ethanol is used, the solidification into desired morphology is done either by quenching after forming emulsion in inert solvent[3] or spray drying[4] prior to contacting with $TiCl_4$. In the cases of adduct solution of $MgCl_2$ and longer alcohol (such as 2-ethyl-1-hexanol)[5] and solution of magnesium-titanium alkoxide complex[6], the solidification is often done by reaction-induced precipitation using $TiCl_4$ or other halogenating reagents, in which the morphology is tunable mainly through the reaction rate and shear force. When a pre-formed solid precursor is used, the solidification that is an essential step to obtain good particle morphology can be omitted, giving rise to a production advantage in terms of the ease of morphology control. $Mg(OEt)_2$ powder with spherical morphology is frequently selected owning to relatively high and stable activity of

resultant catalysts. The morphology of catalysts is known to duplicate the morphology of $Mg(OEt)_2$ as long as the pre-formed precursor is not fragile.[7] Thus, achieving well-controlled morphology of $Mg(OEt)_2$ with sufficient particle strength is an essential step for the production of $Mg(OEt)_2$-based Ziegler-Natta catalysts.

Generally, $Mg(OEt)_2$ is synthesized from the reaction of metallic Mg and ethanol in the presence of a halide initiator. The control of particle morphology is done by optimizing synthesis conditions in an empirical way with prerequisites of narrow particle size distribution, no fine particles, sufficient particle strength and high circularity degree. It was reported that kinetics of the reaction is crucial in controlling the particle morphology, in which too fast kinetics tends to cause particle breakage and fine generation.[8] To control kinetics using Mg with an appropriate size [8], stepwise heating[9] or gradual addition of precursors[10-12] is a typical way to refine the particle size and particle size distribution. The presence of organic halide or alkaline earth metal halide produced irregular particles, while I_2 and magnesium halides yielded spherical particles.[13, 14] According to Tanase et al., I_2 increases the solubility of $Mg(OEt)_2$ by forming quasi-stable complex before precipitating into plate-like building units.[13] These building units further grow and aggregate in a hierarchical manner to form spherical macro-particles. Minor presence of certain alcohols (in addition to ethanol) can alter the shape of building units from usual plate-like to rod-like or irregular shape, affecting the sphericity of resultant macro-particles.[15, 16] The particle size distribution and sphericity of $Mg(OEt)_2$ are also influenced by the morphology of Mg, in which plate-like Mg morphology leads to more spherical $Mg(OEt)_2$ particles.[7] Likewise, many ways have been empirically developed to control the morphology of $Mg(OEt)_2$ particles, while systematic understanding is still lacking on the origin of the particle morphology in the synthesis of $Mg(OEt)_2$: The

majority of researchers examined the influences of certain parameters by observing the morphology of final particles without paying attention on how particles are formed and shaped in the synthesis.

In this study, the morphological development of $Mg(OEt)_2$ particles and building units was observed in the course of the reaction and the influence of Mg sources was studied in detail on the morphological development. It was found that $Mg(OEt)_2$ particles were formed through i) seed generation on surfaces of Mg, ii) isolation of growing seeds as separate macro-particles, and iii) further growth with the increase of the sphericity. The Mg sources affected the reaction rate, by which the growth and isolation processes were significantly altered. Especially, slower reaction enabled the continuous growth of both macro-particles and crystals of $Mg(OEt)_2$. Structural characteristics and ethylene/1-hexene copolymerization performance of resultant Ziegler-Natta catalysts were also studied.

2.2 Experiment

2.2.1 Materials

Ethanol (purity > 99.5%) was purchased from Wako Pure Chemical Industries Ltd. and dried over 3Å molecular sieves with N_2 bubbling for 2 h prior to use. Two types of Mg sources, denoted as MgA and MgB, were donated from Yuki Gousei Kogyo Co., Ltd. and obtained from Merck Co., Ltd., respectively. The particle size and particle size distribution from light scattering measurement were 87.8 μm and 1.48 for MgA and 278.0 μm and 0.98 for MgB. Iodine (I_2, purity > 99%) was used as an initiator in the $Mg(OEt)_2$ synthesis. Titanium tetrachloride ($TiCl_4$, purity > 99%) and di-n-butylphthalate (DnBP, purity > 98%) were used without further purification. n-Heptane (purity > 99.5%), toluene (purity > 99.5%) and 1-hexene (purity > 97%)

were dried over 4Å molecular sieves with N_2 bubbling for 2 h prior to use. Triethylaluminium (TEA) used as an activator for polymerization was supplied from Tosoh Finechem Co. Ethylene of polymerization grade was donated from Sumitomo Chemical Co., Ltd.

2.2.2 $Mg(OEt)_2$ synthesis

$Mg(OEt)_2$ was prepared based on a patent[10] in a 500 mL jacket-type glass reactor equipped with a mechanical stirrer. After sufficient N_2 replacement, the reactor was heated to 75 °C. The amount of 0.67 g of flake I_2 and 32.0 mL of ethanol were added into the reactor. The mixture was stirred at 180 rpm for 10 min to assure the complete dissolution of I_2. Then, 2.5 g of Mg and 32.0 mL of ethanol were introduced for nine times at an interval time of 10 min. After the last addition, the mixture was kept stirring for the desired aging time. The resultant solid was washed with 190 mL of ethanol twice before drying in a rotary evaporator.

The morphological development of $Mg(OEt)_2$ particles was tracked by collecting samples according to the sampling scheme in **Scheme 1**. 10.0 mL of suspension was taken from the reactor, and then immediately quenched in 20.0 mL of heptane at 5 °C before drying in vacuo. The samples were denoted as A (or B)- MGE010-320, in which the numeric value indicates the residence time of samples in the reactor while A or B indicates the Mg source.

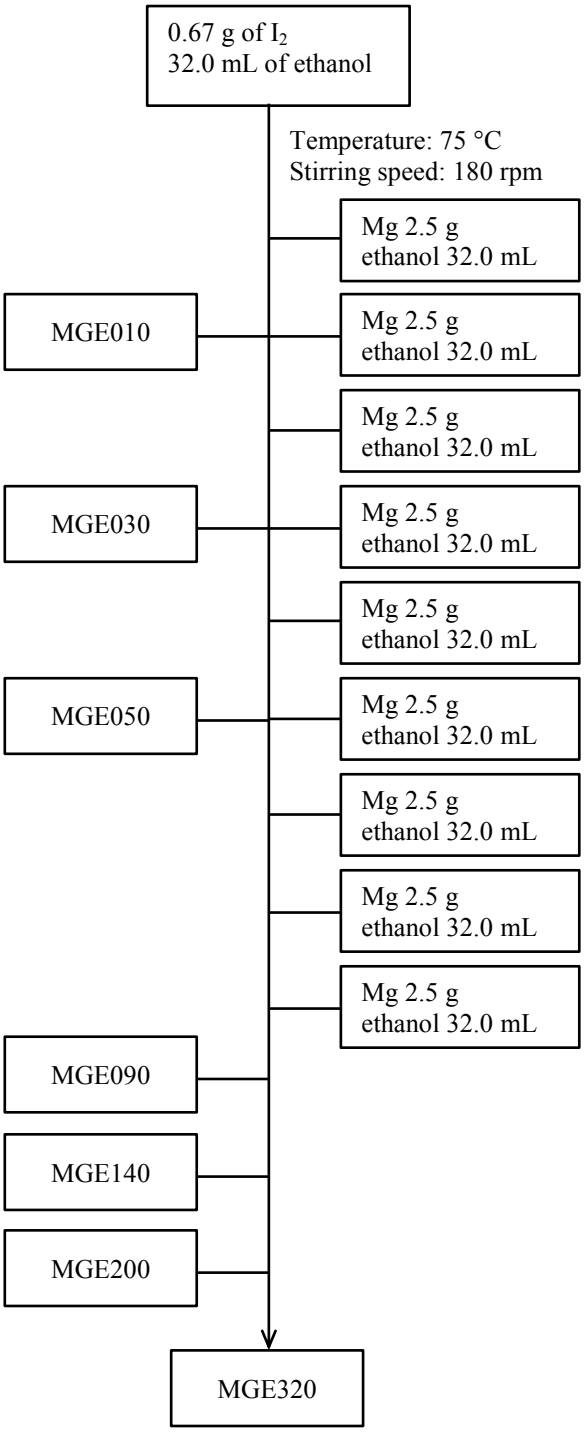

Scheme 1 $Mg(OEt)_2$ synthesis and sampling procedure, where the numeric values after "MGE" refer to residence time (min) in the reactor.

2.2.3 Catalyst synthesis

$Mg(OEt)_2$-based Ziegler-Natta catalysts were prepared based on a patent[17] in a

500 mL three-neck round bottom flask equipped with a mechanical stirrer rotating at 180 rpm under N_2 atmosphere. The amount of 15.0 g of $Mg(OEt)_2$ and 150 mL of toluene were added into the flask under N_2 atmosphere. $TiCl_4$ (30.0 mL) was tardily dropped, where the temperature was kept at 3-5 °C. Followed by the gradual increase of temperature to 90 °C, 4.5 mL of DnBP was added. Thereafter, the reaction mixture was heated to 110 °C and stirred for 2 h. The product was washed with 150 mL of toluene twice at 90 °C and further treated with 30.0 mL of $TiCl_4$ in 150 mL of toluene at 110 °C for 2 h. Finally, the product was repetitively washed with heptane at 70 °C and at room temperature to obtain the final catalysts. Two catalyst samples, denoted as A-CAT200 and B-CAT200, were prepared from the corresponding $Mg(OEt)_2$ samples.

2.2.4 Copolymerization

Copolymerization of ethylene with 1-hexene was performed in a 1 L autoclave equipped with a mechanical stirrer rotating at 750 rpm. First 500 mL of heptane and 30.0 mL of 1-hexene were introduced into the reactor under N_2 atmosphere. 1.0 mmol of TEA was added into the reactor, and then the solution was saturated with 0.8 MPa of ethylene at 70 °C. Then 15 mg of a catalyst was fed into the reactor to initiate the reaction. The copolymerization was conducted for 30 min at 70 °C and 0.8 MPa with the continuous feed of ethylene. Finally, the monomer was vented off and the polymer was collected and dried at 60 °C for 6 h.

3.2.6 Characterization

The particle morphology of $Mg(OEt)_2$ and catalyst samples was observed by scanning electron microscopy (SEM, Hitachi S-4100) at an accelerate voltage of 20

kV. The samples were prepared under N_2 atmosphere, and then subjected to Pt-Pd sputtering for 60 s before the measurement. The particle morphology in SEM micrographs was quantified using an image processing software.[7] The relative span factor (RSF) and the circularity were respectively calculated based on equations (2.1) and (2.2),

$$\text{Relative span factor} = \frac{D_{90}\text{-}D_{10}}{D_{50}} \tag{2.1}$$

$$\text{Circularity} = \frac{4 \times \pi \times \text{area}}{(\text{boundary length})^2} \tag{2.2}$$

where, D_{10}, D_{50}, and D_{90} correspond to the cumulative number-based particle sizes at 10%, 50%, and 90%, respectively. The area and boundary length for a two-dimensionally projected particle were determined over 500 particles. The crystal structure of $Mg(OEt)_2$ was analyzed by X-ray powder diffraction (XRD, Smart Lab., RIGAKU) using CuKα radiation at 40 kV and 30 mA. The measurement was performed based on a stepwise scanning in the range of 6-14 degree with the step of 0.1 degree per 30 s. A sample was loaded onto a glass holder under N_2 atmosphere, and then covered by a Mylar film to prevent the contact with moisture. The crystal size was estimated based on the Scherrer's equation[18] for each specified diffraction peak.

The pore architecture of catalysts was determined by N_2 adsorption/desorption measurement (BELSORP-max) at 77 K. A pyrex tube was heated at 200 °C over-night in vacuo for eliminating moisture. The amount of 50.0 mg of a catalyst was added in the pyrex tube under N_2 atmosphere. Then, the sample was outgassed at 80 °C for 3 h. The micropore volume ($D < 2$ nm) was calculated based on the previously proposed equation.[7] The mesopore volume ($2 \text{ nm} < D < 50$ nm) was analyzed by the INNES method.[19] The chemical compositions of catalysts were measured based on

previously reported procedures.[7] The Ti and donor contents were determined by UV/vis spectroscopy (JASCO V-670) and IR spectroscopy (FTIR-4100, JASCO), respectively. The n-butyl branch content in copolymer was determined by ^{13}C NMR (Bruker 400 MHz) operating at 100 MHz at 120 °C. 1,2,4-Trichlorobenzene and 1,1,2,2-tetrachloroethane-d_2 were used as solvent and an internal lock, respectively.

2.3 Results and discussion

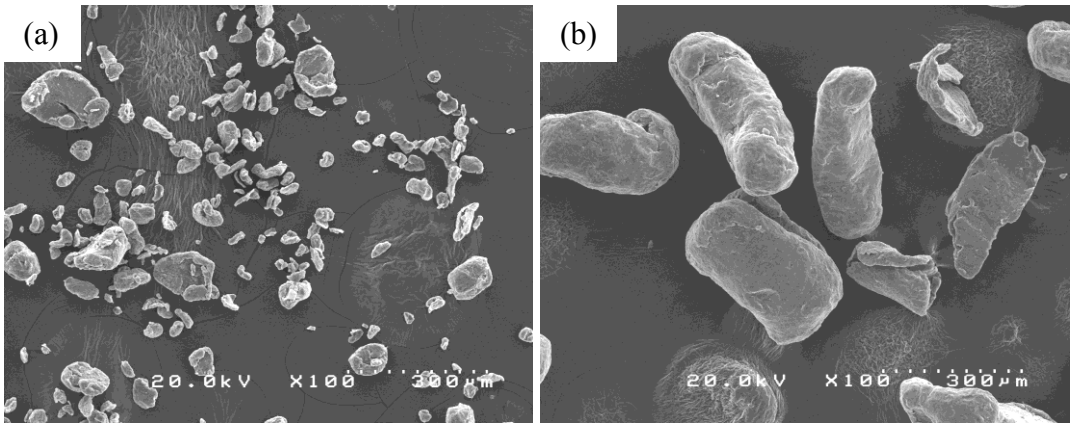

Figure 2.1 SEM micrographs of Mg powder: (a) MgA (x100) and (b) MgB (x100).

Morphological evolution of $Mg(OEt)_2$ synthesized using different Mg sources was tracked. Both of the Mg sources, denoted as MgA and MgB, have similar platelet morphology with smooth surfaces (**Figure 2.1**). However, the particle size of MgA was in the range of 30-100 μm, much smaller than that of MgB, whose size was in the range of 100-300 μm, in accordance to light scattering measurement. **Figure 2.2** and **2.3** show SEM micrographs for A- and B-MGE, respectively. In the case of A-MGE, huge chunks having surfaces fully covered by aggregated small seeds were observed at the first 10 min of the reaction (**Figure 2.2a**). Considering the size of MgA, it was reasonable that the chunks were MgA particles with the reaction product formed on the surfaces. After the repetitive addition of the reagents, the small seeds continued to

grow and transform into spherical-like particles on the surfaces (**Figure 2.2c**), followed by breakage of the chunks into clusters of spherical-like particles as well as single spherical-like particles (**Figure 2.2e**). As the reagent addition progressed (from 50 to 90 min), the spherical-like particles continuously grew and the clusters broke up into single particles (**Figure 2.2g**). The aging of reaction products (from 90 to 320 min) did not have a significant effect on the particle characteristics, except the improvement of the particle sphericity (**Figure 2.2g,i,k,m**).

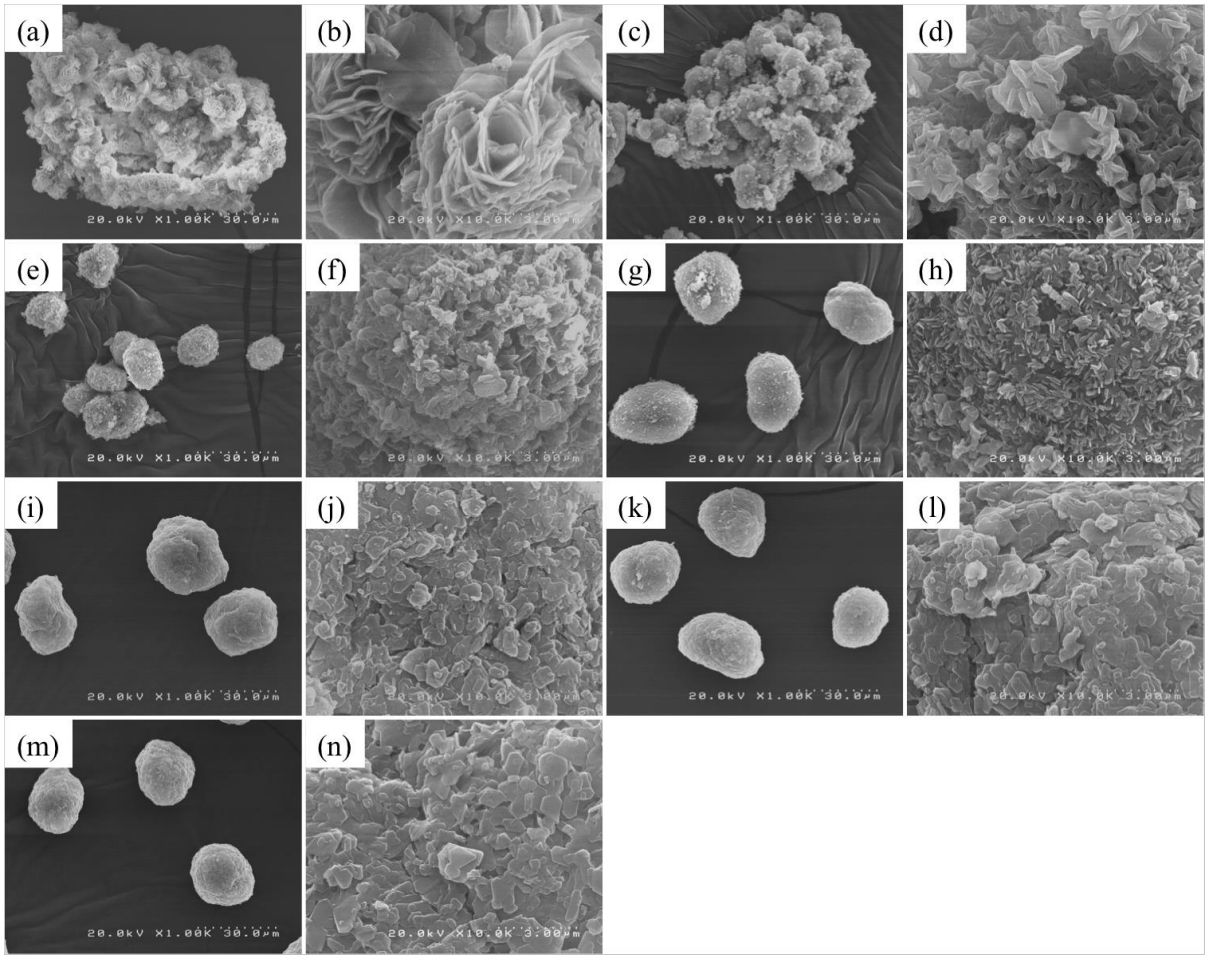

Figure 2.2 SEM micrographs of $Mg(OEt)_2$ samples: (a,b) A-MGE010 (x1000, x10000), (c,d) A-MGE030 (x1000, x10000), (e,f) A-MGE050 (x1000, x10000), (g,h) A-MGE090 (x1000, x10000), (i,j) A-MGE140 (x1000, x10000), (k,l) A- MGE200 (x1000, x10000), and (m,n) A-MGE320 (x1000, x10000).

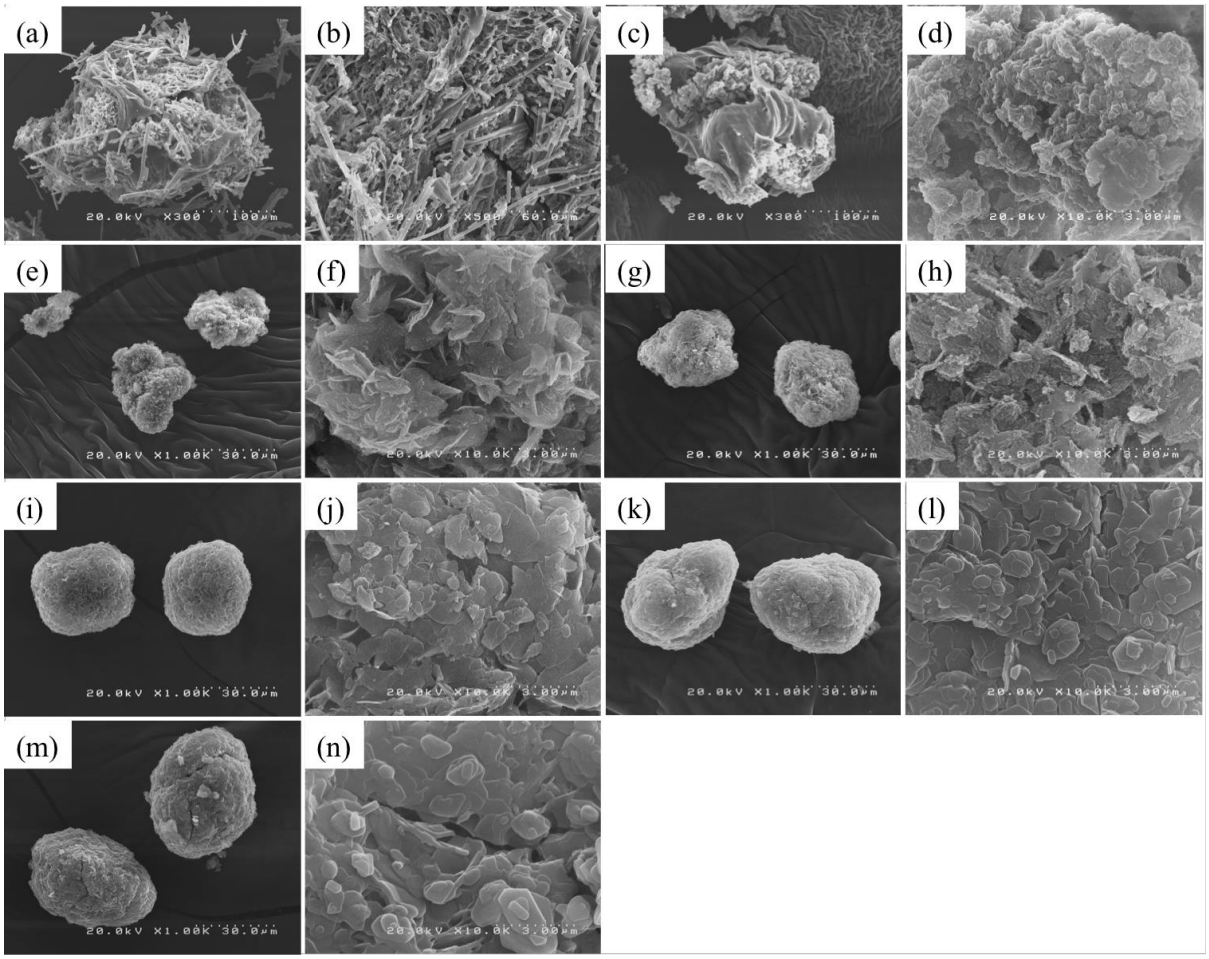

Figure 2.3 SEM micrographs of $Mg(OEt)_2$ samples: (a,b) B-MGE010 (x300, x500), (c,d) B-MGE030 (x300, x10000), (e,f) B-MGE050 (x1000, x10000), (g,h) B-MGE090 (x1000, x10000), (i,j) B-MGE140 (x1000, x10000), (k,l) B-MGE200 (x1000, x10000), and (m,n) B-MGE320 (x1000, x10000).

In the case of B-MGE, the needle-like rods, whose presence was not detected in A-MGE, were observed at the first 10 min (**Figure 2.3a**). These rods (with the longer dimension around 30-60 μm) were mainly attached on the MgB particles. Along the repetitive addition of the reagents, these needle-like rods transformed into aggregated seeds with irregular shapes (**Figure 2.3c**). It was notable that smooth surfaces, characteristic for MgB, were still observable. At 50 min, clusters of $Mg(OEt)_2$ seeds with irregular shapes appeared (**Figure 2.3e**) as separate particles. Judging from the

persistence of original MgB particles (not shown here), these clusters resulted from the detachment of aggregated seeds from the MgB surfaces. The growth of the detached clusters continued even in the aging (from 90 to 200 min) to reach the maximum particle size (**Figure 2.3g,i,k**). Further extension of the aging from 200 to 320 min improved the sphericity of particles without significant change in the particle size. However, fractures on the particle surfaces started to appear, which is not promising in catalyst preparation (**Figure 2.3m**).

Table 2.1 Particle characteristics of $Mg(OEt)_2$

	D_{10} [(a)] (μm)	D_{50} [(a)] (μm)	D_{90} [(a)] (μm)	RSF[(b)]	Circularity[(c)]
A-MGE050	12.4	18.3	38.9	1.448	0.746
A-MGE090	21.7	26.8	41.8	0.750	0.822
A-MGE140	22.4	27.2	42.9	0.754	0.833
A-MGE200	21.8	26.3	41.1	0.734	0.849
A-MGE320	20.5	25.3	40.2	0.779	0.893
B-MGE050	12.9	19.8	29.5	0.838	0.683
B-MGE090	15.9	27.3	38.0	0.809	0.774
B-MGE140	16.8	30.6	46.2	0.961	0.761
B-MGE200	27.5	39.3	48.5	0.534	0.823
B-MGE320	23.2	38.3	47.5	0.634	0.855

[(a)] D_{10}, D_{50}, and D_{90} are the particle diameters at 10%, 50% and 90% in the cumulative number-based particle size distribution obtained by the analysis of SEM micrographs over 500 particles.

[(b)] Determined based on Equation (2.1).

[(c)] Determined based on Equation (2.2).

The characteristics of $Mg(OEt)_2$ particles were acquired from SEM micrographs (**Table 2.1**). It should be noted that the image analysis was not conducted on A- and B-MGE010-030 samples, because the co-presence of irregular particles on the Mg surfaces largely misled the analysis results. In **Table 2.1**, the D_{50} value of isolated (or detached) particles was found to be similar for both of A- and B-MGE050. Even though huge chunks were still observed in B-MGE050, their fraction was too small to affect the particle size calculation based on number average. The particle size increased with the increase of residence time and converged at 90 and 200 min for A- and B-MGE, where the maximum D_{50} values were 27 and 39 μm, respectively.

The convergence of the particle sizes for A- and B- MGE indicated the complete consumption of metallic Mg, where A-MGE required shorter time to reach the consumption and to stop the growth. The smaller particle size and faster convergence for A-MGE could be ascribed to the faster reaction rate: MgA accompanied faster seed formation, thus generating a larger number of particles. In addition, MgA was more rapidly consumed, and consequently the particle growth converged at an earlier timing than that for MgB. The RSF value for both of the samples decreased with the increase of the residence time and became stable when the particles stopped obvious growth. The circularity degree increased over the addition and aging period for both of the samples, indicating that morphological shaping occurred in a continuous manner.[7]

Whilst the morphological development of $Mg(OEt)_2$ particles was more or less similar for the two Mg sources, the morphology of building units was quite unique, especially during the reagent addition period. The large micron-sized platelets were firstly observed for A-MGE (**Figure 2.2b**) before converting into much smaller building units having irregular shapes and sizes (**Figure 2.2d,f,h**). In the case of B-

MGE, the needle-like rods were firstly formed (**Figure 2.3b**) and subsequently experienced several morphological transformations (**Figure 3d,f,h**). Finally, the plate-like building units, which are typically observed for $Mg(OEt)_2$, were formed during the aging period (at 140 min) for both of A- and B-MGE and persevered upon extending the aging time (**Figure 2i,l,n** and **3j,l,n**). These observations revealed that the evolution of building units into the stable form went through several metastable forms, whose pathway was dependent on the Mg sources.

From the SEM micrographs, the particle evolution was found to be consistent with a scheme previously proposed by Tanase et al.[13] $Mg(OEt)_2$ seeds were initially formed on Mg surfaces and subsequently detached due to the collision and other shear force. The isolated particles continued to grow further from the precipitation of quasi-stable nMg(OEt)$_2$.MgI$_2$.mEtOH soluble complex. This mechanism holds regardless Mg sources (ribbon or powder form). However, it is interesting to address that the isolation of seeds was greatly affected by the Mg sources. A-MGE was mainly isolated as single particles, while B-MGE was predominantly isolated as clusters (**Figure 2.2e** and **2.3e**). This difference was believed to be relevant to the reaction rate. MgA offered a higher reaction rate, thus seeds could be rapidly developed as single particles before the isolation. On the contrary, the seed formation and growth of B-MGE particles were much slower and seeds were detached as clusters. The subsequent aging helped to gradually improve the circularity. However, the final circularity was still influenced by the morphology of initially isolated particles, in which higher circularity was obtained when the seeds were isolated as single particles. Our findings are summarized in **Scheme 2.2**.

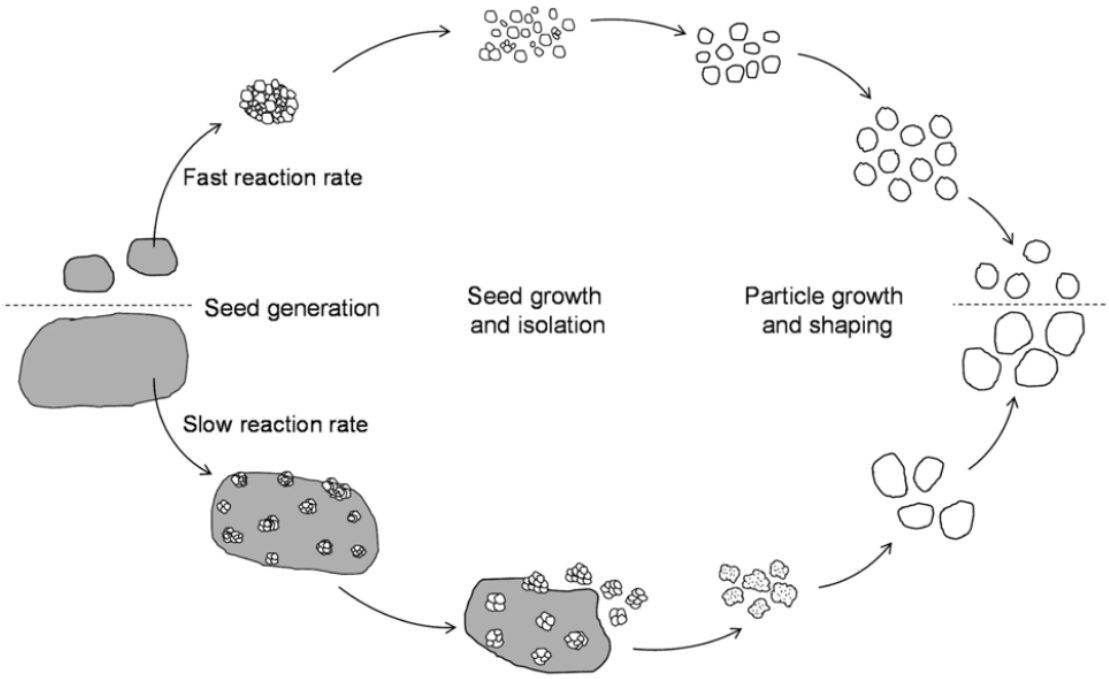

Scheme 2.2 $Mg(OEt)_2$ particle formation and evolution.

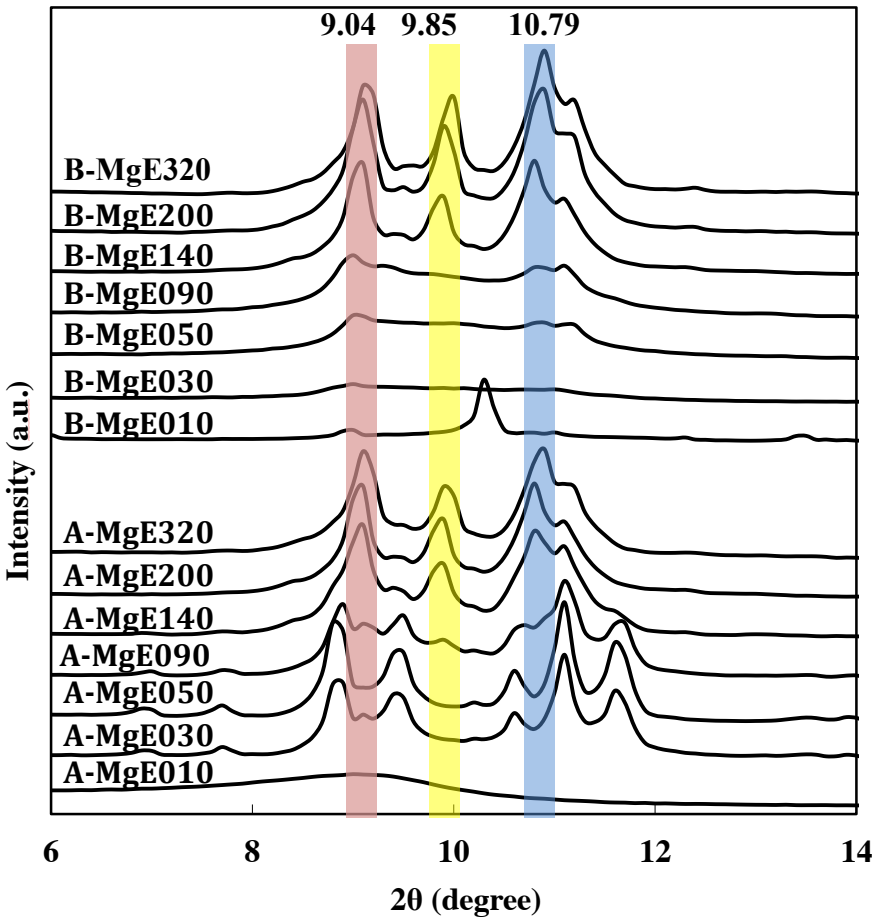

Figure 2.4 XRD patterns of $Mg(OEt)_2$: (a) A-MGE and (b) B- MGE.

The crystal structure of $Mg(OEt)_2$ during the reaction was observed by XRD and the results are shown in **Figure 2.4**. A-MGE010 exhibited a single broad peak, demonstrating that the initially formed seeds were poorly crystalline. Thereafter, several diffraction peaks appeared in the 2θ range of 8-12 degree, indicating the formation of crystal phases. As designated in **Figure 2.4**, the intensity of peaks in the regions I, III, V, VI, VIII and IX decreased with the increase of the residence time and the peaks finally disappeared at 140 min. At the same time, the intensity of peaks in the regions II, IV and VII gradually increased and became dominant during the aging period. In the case of B-MGE, the XRD patterns in the initial stage were different from those of A-MGE. B-MGE010 exhibited a sharp main peak positioned in the region V. At 30 min, this peak completely disappeared, while the broad peak between the regions I and II started to develop. The co-existence of several peaks between regions III-VIII was also recognized for B-MGE030-090 samples. The XRD patterns of B-MGE eventually became similar to those of A-MGE at 140 min, where the three main characteristic peaks in the regions II, IV and VII became dominant. The appearance and disappearance of several peaks along the residence time specified the co-presence of different crystal phases, especially during the repetitive addition of the reagents in the initial stage. The transformation of XRD peaks synchronized well with the transformation of building units in SEM micrographs. It was deduced that the unique morphology of building units in the initial stage might correspond to the metastable forms (MGE010-090). Accordingly, the plate-like building units with the crystal structure typical for $Mg(OEt)_2$ plausibly corresponded to the stable form (MGE140-320). The difference in the reaction rate between MgA and MgB was believed to alter the composition of $n\text{Mg(OEt)}_2.\text{MgI}_2.m\text{EtOH}$ soluble complex, resulting in the formation of different metastable forms.[20] The formation of the

stable phase induced the undersaturation of solution with respect to the metastable phases, which resulted in the gradual disappearance of metastable phases.[21] The crystal size of the stable phase was calculated from the three main peaks (in the regions II, IV and VII) using the Scherrer's equation (**Figure 2.5**).

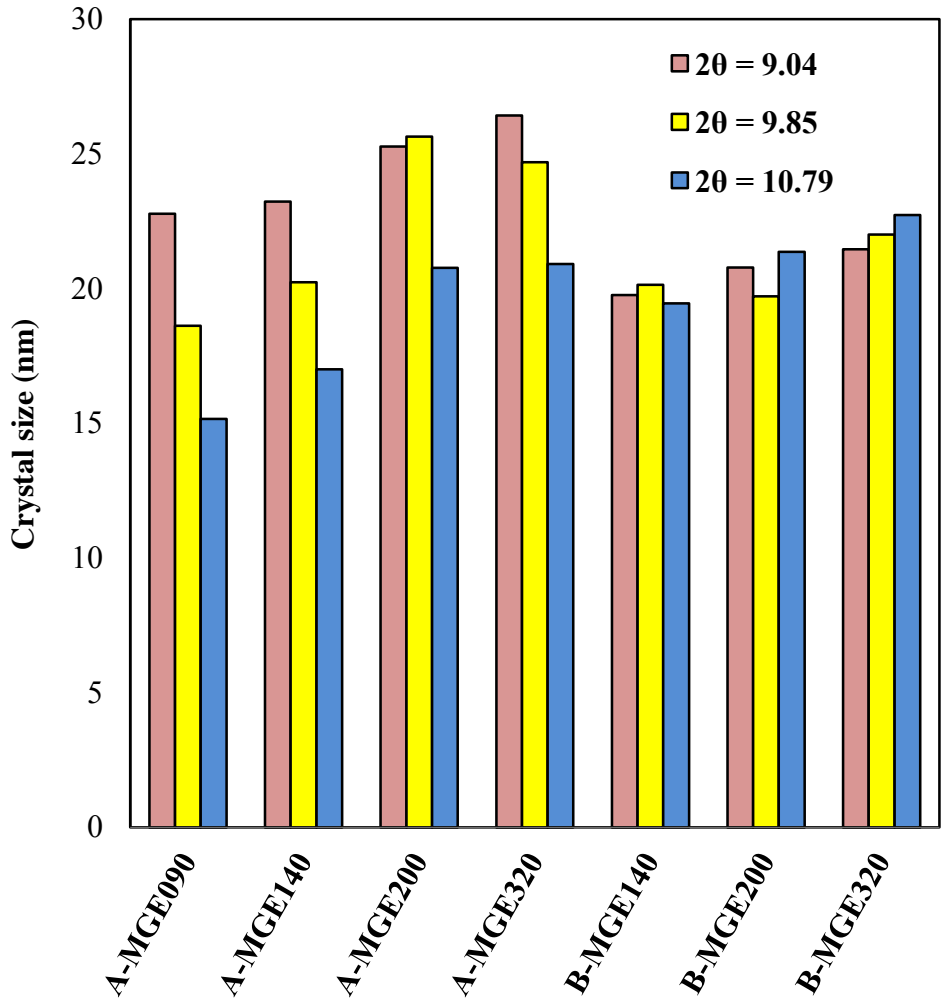

Figure 2.5 Calculated crystal sizes based on specified diffraction peaks for A- and B-MGE.

Even though the crystal phase was similar, the dimension of crystal was different. The crystal size of A-MGE exhibited significant difference for the three peaks, while B-MGE exhibited similar sizes. The aging increased the crystal size for both of the

samples. However, the crystal size for A-MGE converged at the residence time of 200 min, while no convergence of the crystal size was found for B-MGE within 320 min of the reaction. It should be noted that the particle size was converged earlier than the crystal size (at 90 min for A-MGE and at 200 min for B-MGE), suggesting that the repining process continued even after the particles stopped obvious growth. According to our previous works, the pore architecture of $Mg(OEt)_2$-based catalysts was essentially decided by the structural characteristics of $Mg(OEt)_2$.[15, 16] Therefore, the influence of the Mg sources was investigated on the pore characteristics of catalysts. $Mg(OEt)_2$ samples with the residence time of 200 min were chosen to ensure not only the complete conversion of Mg, but also the best balance in terms of the $Mg(OEt)_2$ morphology. A- and B-MGE200 samples were converted into catalysts and denoted as A- and B-CAT200, respectively. SEM micrographs in **Figure 2.6** exhibit that the morphology of both catalysts replicates that of original $Mg(OEt)_2$ except the molten edges and smoother surfaces, which are generally observed for $Mg(OEt)_2$-based Ziegler-Natta catalysts.[7] Note that no fine particles were observed after catalyzation for both of the samples, indicating the adequate physical stability of both samples.

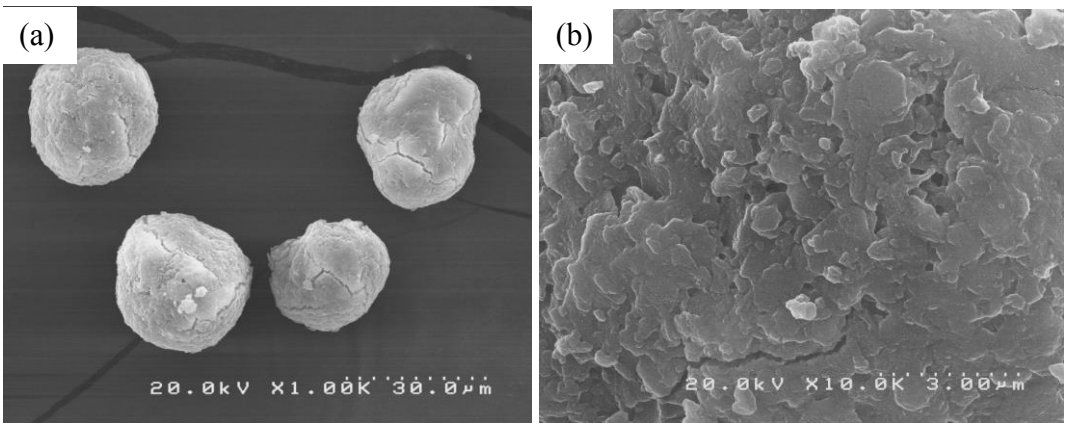

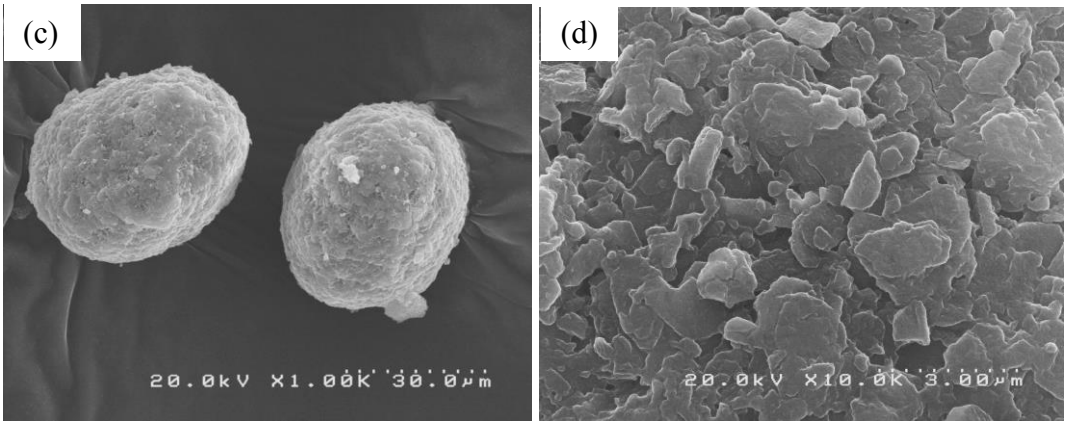

Figure 2.6 SEM micrographs of catalyst particles: (a,b) A-CAT200 (x1000, x10000) and (c,d) B-CAT200 (x1000, x10000).

The N_2 adsorption/desorption isotherms of the catalysts are shown in **Figure 2.7**. Both of the catalysts exhibited similar adsorption isotherms, classified as type II in IUPAC for macroporous solid.[22] The hysteresis loop of type H3 in IUPAC classification indicated slit-shape mesopores, whose size and shape were non-uniform.[22] The pore size distributions are shown in **Figure 2.8**. In both of the catalyst samples, the pore distribution exhibited bimodal characteristics typically observed for $Mg(OEt)_2$-based Ziegler-Natta catalysts.[15] The micropore volume was found to be similar for both of the Mg sources. This is in accordance with our previous work, where the micropores were believed to derive from the volumetric shrinkage during catalyzation and insensitive to the variation of $Mg(OEt)_2$ synthesis conditions.[15] Meanwhile, the mesopore volume was found to be smaller for B-CAT200. The suppression of mesopore volume of B-CAT200 is yet unknown. However, in considering characteristics of B-MGE compared to A-MGE, this difference might be relevant to the smaller and more uniform crystal size for B-MGE.

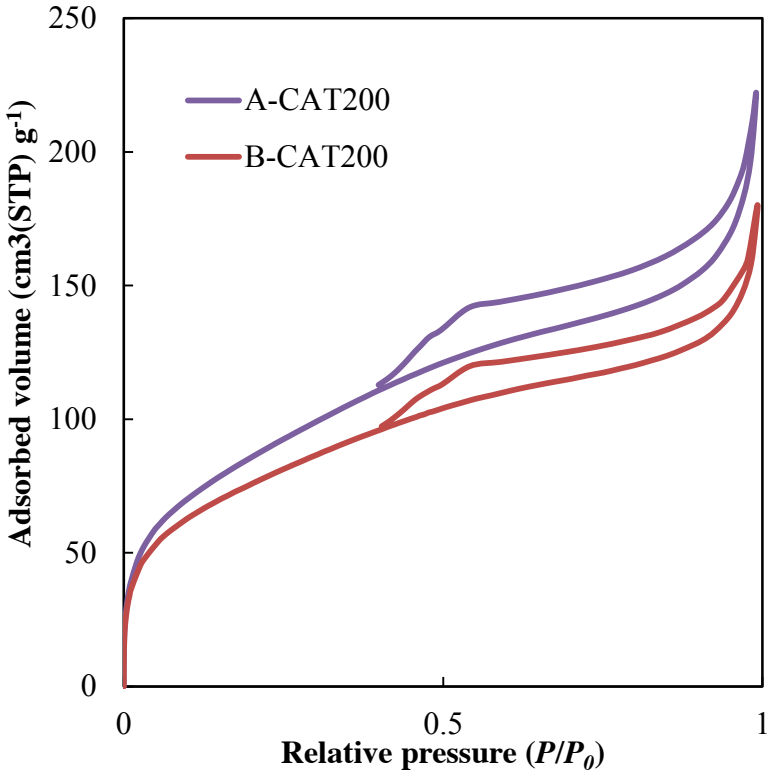

Figure 2.7 N_2 adsorption/desorption isotherms for catalyst samples.

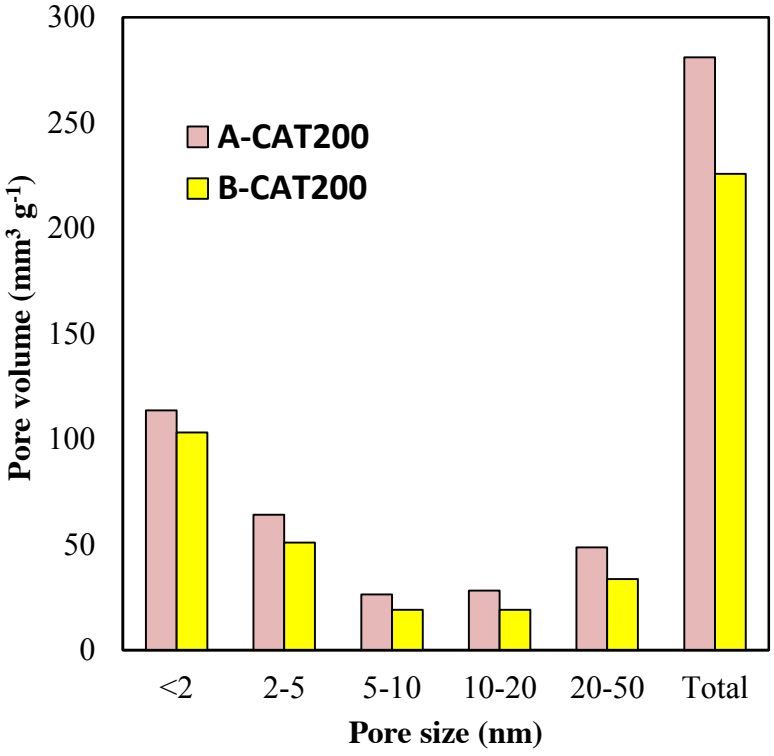

Figure 2.8 Pore size distribution of catalyst samples.

The compositions of catalysts are reported in **Table 2.2**. B-CAT200 contained the lower Ti and donor contents compared to A-CAT200, while the molar ratio between donor and Ti was similarly kept at 1.6. This result indicated the competitive adsorption between Ti and donor[23], which was not affected by $Mg(OEt)_2$ structural differences. Thus, the lower Ti and donor contents in B-CAT200 was believed to originate from the smaller pore volume, i.e. smaller surface area of original B-MGE200.

Ethylene/1-hexene copolymerization was performed to investigate the performance of catalysts, especially for the insertion ability of relatively large monomer. The catalytic activities and *n*-butyl branch contents are reported in **Table 2.2**. The activity per Ti-mol was found to be similar for both of the catalysts. Contrary, the 1-hexene incorporation efficiency for B-CAT200 was slightly lower than that for A-CAT200, which attributed to the suppression of mesopore volume [7].

Table 2.2. Chemical compositions and polymerization results

	Ti content[(a)] (wt%)	**Donor content[(b)] (wt%)**	**Activity[(c)] (kg-polymer Ti-mol $^{-1}$h^{-1}atm^{-1})**	**n-Butyl branch content[(d)] (mol%)**
A-CAT200	2.8	17	3.3×10^3	0.75
B-CAT200	1.8	11	3.2×10^3	0.56

[(a)] Determined by UV/vis spectroscopy.

[(b)] Determined by FTIR.

[(c)] Ethylene/1-hexene copolymerization was conducted at 70 °C in 500 mL of heptane with 1.0 mmol of TEA, 0.2 mol of 1-hexene, and 0.8 MPa of continuously supplied ethylene for 30 min.

[(d)] Determined by ^{13}C NMR.

2.4 Conclusion

The influence of Mg sources on the evolution of $Mg(OEt)_2$ particles was investigated by observing the morphology of $Mg(OEt)_2$ particles during the synthesis. We found that Mg sources influenced not only the growth of initially formed seeds, but also the detachment behavior of growing seeds. The smaller size of Mg offered a higher reaction rate, resulting in the rapid development of seeds into spherical-like $Mg(OEt)_2$ particles on Mg surfaces, which were afterward isolated as single particles. The morphology of the isolated particles determined the sphericity of $Mg(OEt)_2$ particles, even though subsequent aging gradually improved it. Mg sources also influenced the morphology of $Mg(OEt)_2$ building units as well as the crystal growth, differentiating the pore size distribution of catalysts (mainly for mesopores). The mesopore volume of the catalysts became larger when $Mg(OEt)_2$ was prepared using the smaller size of Mg, and caused enhanced comonomer incorporation in ethylene/1-hexene copolymerization. Thus, the present study has successfully clarified the origin of the morphology of $Mg(OEt)_2$ particles in a comprehensive manner, which must contribute to finer design of the morphology and performance of Ziegler-Natta catalysts.

References

[1] J. T. M. Pater, G. Weickert, W. P. M. Van Swaaij, *J. Appl. Polym. Sci.*, 87 (2003) 1421-1435.

[2] P. Galli, P. C. Barbè, L. Noristi, Angew. Makromol. Chem., 120 (1984) 73-90.

[3] Z. Y. Ye, L. Wang, L. F. Feng, X. P. Gu, H. H. Chen, P. Y. Zhang, J. Pan, S. Jiang, L. X. Feng, *J. Polym. Sci. Part A: Polym. Chem.*, 40 (2002) 3112-3119.

[4] S. Miya, M. Tachibana, Y. Karasawa, (1992) US Patent 5100844.

[5] M. Kioka, H. Kitani, N. Kashiwa, (1982) US Patent 4330649.

[6] A. A. Batinas-Geurts, N. H. Friederichs, T. Schoffelen, E. Zuidema (2014) US Patent 20140296454.

[7] T. Taniike, T. Funako, M. Terano, *J. Catal.*, 311 (2014) 33-40.

[8] J. Joseph, S. C. Singh, V. K. Gupta, *Part. Sci. Technol.*, 27 (2009) 528-541.

[9] V. Gupta, S. Singh, U. Makwana, J. Joseph, K. Singala, S. Rajesh, V. Patel, M. Yadav, G. Singh (2014) US Patent 8633124B2.

[10] H. Nomura, N. Kurihara, K. Higuchi, (1991) JP Patent 199174341.

[11] A. Yamanaka, H. Kumai, M. Suyama, (2007) JP Patent 2007297371.

[12] A. Yamanaka, H. Kumai, M. Suyama, (2014) US Patent 8632882

[13] S. Tanase, K. Katayama, S. Inasawa, F. Okada, Y. Yamaguchi, T. Konakazawa, T. Junke, N. Ishihara, *Appl. Catal. A: Gen*, 350 (2008) 197-206.

[14] S. Tanase, K. Katayama, S. Inasawa, F. Okada, Y. Yamaguchi, T. Sadashima, N. Yabunouchi, T. Konakazawa, T. Junke, N. Ishihara, *Macromol. React. Eng.*, 2 (2008) 233-239.

[15] T. Funako, P. Chammingkwan, T. Taniike, M. Terano, *Macromol. React. Eng.*, 9 (2015) 325-332.

[16] T. Funako, P. Chammingkwan, T. Taniike, M. Terano, *Polyolefins J.*, 2 (2015) 65-71.

[17] M. Terano, A. Murai, M. Inoue, K. Miyoshi, (1987) JP Patent S62158704.

[18] P. Scherrer, *Math-Phys Kl.*, 2 (1918) 98-100.

[19] W. B. Innes, *Anal. Chem.*, 29 (1957) 1069-1073.

[20] N. Y. Turova, E. P. Turevskaya, *J. Organomet. Chem.*, 42 (1972) 9-17.

[21] R. C. Snyder, M. F. Doherty, *AIChE J.*, 53 (2007) 1337-1348.

[22] G. Leofanti, M. Padovan, G. Tozzola, B. Venturelli, *Catal. Today*, 41 (1998)

207-219.

[23] A. G. Potapov, G. D. Bukatov, V. A. Zakharov, *J*. *Mol*. *Catal*. *A: Chem*., 301 (2009) 18-23.

Chapter III

Establishment of experimental procedure for high impact propylene copolymerization in gas-phase reactor

3.1 Introduction

In polyolefin production process, reactor is one of the most important components, which its operating conditions strongly relate to polymer properties. Generally, propylene polymerization reactor is classified into two types according to the media of reaction, slurry-phase and gas-phase reactor.[1] Slurry-phase polymerization is a heterogeneous phase reaction. Propylene is dissolved into the inert solvent such as heptane, hexane, toluene etc. Then, propylene diffuses to catalyst particles, where the reaction occurs at the active sites locating on the surfaces of catalyst. The prominent point of this process is its excellent heat transfer and precision of pressure and heat control.[2] However, the main drawback of slurry-phase polymerization was high operating cost because it consumes large amount of solvent. On the other hand, gas-phase polymerization process can well overcome this drawback because the reaction is carried out in a gaseous phase, which noticeably decreases the consumption of solvent. The disappearance of solvent leads to the expansion of production ability. The copolymer such as ethylene-propylene random copolymer is easily dissolve in hydrocarbon solvent, so it cannot be produced in slurry-phase process. According to this fact, an engineering grade polypropylene such as high impact polypropylene is usually produced in gas-phase reactor.

The instance of industrial process for hiPP production is shown in the Spheripol process (Bassel) as seen in **Figure 3.1**.[3] The prepolymerized polypropylene is fed into loop reactors to produce isotactic polypropylene (iPP). Then, iPP particles are transfer to the second reactor, which is gas-phase fluidized bed reactor. In this second stage, ethylene-propylene copolymer is formed inside iPP particles. In laboratory scale, the first-stage reaction can be either gas- or slurry-phase reaction, while the second stage is mostly conducted in gas-phase reaction.[4, 5] In accordance with the

restrictions of gas-phase reactor, the operating conditions have to be strictly controlled. The particle size iPP have to be moderate with narrow size distribution and the amount of iPP has to be sufficient as well. According to Kittilsen et al., who conducted propylene polymerization in both of slurry- and gas-phase.[6] They controlled the amount of produced polypropylene by observing gas consumption and found that the final polymer was agglomerated and sticky when the first stage was gas-phase, because surfaces of polymer particle were excessively exposed.

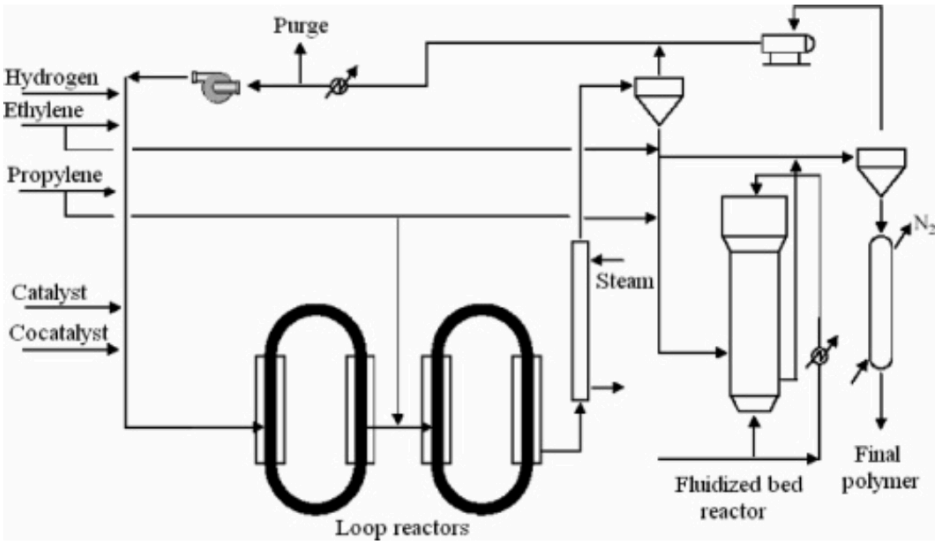

Figure 3.1 Spheripol process for hiPP production.

The produced polypropylene particle is a porous material, which active sites are located on the surfaces. Thus, in the second stage, polypropylene particle can behave like a reactor for copolymerization. The utilization of polypropylene particle as a reactor is called "Reactor granule technology (RGT)".[7, 8] As same as typical reactor, the reactor characteristics can also affect the properties of product. Many researchers purposed that pore volume of polypropylene limited copolymer capacity. Thus, to increase copolymer content, Vestberg et al.[9] attempted to enlarge polymer pore

volume through modifying catalyst. They employed nano-sized silica in catalyst preparation and reported that copolymer content increased almost double. However, as mentioned above, the characteristics of reactor directly affects the reaction and also polymer properties. Thus, it is necessary to optimize operating conditions and procedure, which are most suitable to the reactor.

In this chapter, we established the procedure for hiPP polymerization and copolymer content evaluation, as well. The kinetics of propylene polymerization was also observed and utilized to control reproductivity. According to the limitation of reactor system, correlation was developed from reaction profile to predict the amount of produced polymer. The accuracy of the correlation was acceptable and well consistent with the results from extraction.

3.2 Experiment

3.2.1 Materials

Ethanol (purity > 99.5%) was purchased from Wako Pure Chemical Industries Ltd. and then dried over 3A molecular sieves with N_2 bubbling for 2 h. Mg powder (particle size 0.06 - 0.3 mm) was purchased from Merck Co., Ltd. Iodine (I_2, purity > 99%) was used as an initiator in $Mg(OEt)_2$ synthesis. Titaniumtetrachloride ($TiCl_4$, purity > 99%), di-*n*-butylphthalate (DNBP) (purity > 98%) were used without further purification. *n*-Heptane (purity > 99.5%), toluene (purity > 99.5%) were dried over 4A molecular sieves with N_2 bubbling for 2 h. Cyclohexylmethyldimethoxysilane (CMDMS or C-donor) was distillated under reduced pressure. Triethylaluminum (TEA) was donated by Tosho finechem Co., Ltd. Propylene and ethylene of polymerization grade were donated by Sumitomo Chemical Co., Ltd. Decane (purity > 95%) was purchased from Sigma-Aldrich Co. LLC.

3.2.2 $Mg(OEt)_2$ synthesis

A 500 mL jacket-type glass reactor equipped with a mechanical stirrer was used for $Mg(OEt)_2$ synthesis. After N_2 replacement, the reactor was heated to 75°C. 0.68 g of flake I_2 and 31.7 mL of ethanol were added into the reactor. The mixture was stirred at 180 rpm for 10 min to assure the complete dissolution of I_2. Then, 2.5 g of magnesium powder and 31.7 mL of ethanol were continuously introduced for nine times with an interval time of 10 min. After the last addition, the mixture was aged under stirring for 2 h. Afterwards, the resultant solid was washed with 190 mL of ethanol before drying by rotary evaporator.

3.2.3 Catalyst synthesis

$Mg(OEt)_2$-based Ziegler-Natta catalyst was prepared by using a 500 mL three-neck round bottom flask equipped with a mechanical stirrer rotating at 180 rpm under N_2 atmosphere. 15.0 g of $Mg(OEt)_2$ and 150 mL of toluene were added into the flask under N_2 blanking. 30.0 mL of $TiCl_4$ was tardily dropped while the temperature was strictly kept at 5°C. Followed by the gradual increase of temperature to 90°C, 4.5 ml of DBP was added. Thereafter, the reaction mixture was heated to 110°C and stirred for 2 h. The product was washed with 150 mL of toluene twice at 90°C and further treated with 30.0 mL of $TiCl_4$ in 150 mL of toluene at 110°C for 2 h. Finally, the product was washed with 220 mL of heptane at 70°C for three times and at room temperature for four times to obtain the final catalyst.

3.2.4 Propylene polymerization

Propylene polymerization was conducted in a 700 mL cylindrical shape reactor equipped with a spiral shape propeller rotating at 150 rpm for 80 min. After

replacement of N_2, 200 mL of heptane was introduced to the reactor followed by 0.9 μmol of TEA, 0.09 μmol of C-donor. Then, the reactor atmosphere was replaced by propylene. The desired catalyst amount was charged to the reactor under propylene atmosphere. Finally, 100 mL of heptane was added to the reactor. The reaction was conducted at 50 °C and 0.5 MPa. The polymer was collected after gas was vented off and dried under vacuum at 60 °C for 6 h.

3.2.5 In situ high impact propylene copolymerization

An in situ propylene/(ethylene-co-propylene) copolymer (or high impact polypropylene, hiPP) was produced by two-stage reaction in series. Firstly, polypropylene was produced according to the former described procedure. After the desired polymerization time, stirring speed was reduced to 100 rpm, and then solvent was vacuumed for 1 h to ensure completely dry. The second-stage reaction, ethylene-propylene copolymerization was conducted in gas-phase reaction. The stirring speed was increased to 600 rpm. Copolymerization was conducted under equimolar feed of ethylene and propylene at the total pressure of 0.4 MPa. Finally, gas was vented off and the produced copolymer was collected and dried at 60 °C under vacuum.

3.2.6 Characterization

The morphology of $Mg(OEt)_2$ and catalyst was evaluated by scanning electron microscopy (SEM, Hitachi S-4100) at an accelerate voltage of 20 kV. The particles were coated by Pt-Pd for 60 s before the measurement. The particle morphology in SEM micrographs was quantified using an image processing software. The relative span factor (RSF) and the circularity were respectively calculated based on equations (3.1) and (3.2),

$$\text{Relative span factor} = \frac{D_{90}\text{-}D_{10}}{D_{50}} \tag{3.1}$$

$$\text{Circularity} = \frac{4 \times \pi \times \text{area}}{(\text{boundary length})^2} \tag{3.2}$$

where, D_{10}, D_{50}, and D_{90} correspond to the cumulative number-based particle sizes at 10%, 50%, and 90%, respectively. The area and boundary length for a two-dimensionally projected particle were determined over 500 particles. The Ti and donor contents were determined by UV/vis spectroscopy (JASCO V-670) and IR spectroscopy (FTIR-4100, JASCO), respectively.

The content of atactic polypropylene and random copolymer was extracted by *n*-decane. 0.4 g of polymer was dissolved in 40 mL of *n*-decane. The solution was kept stirring at 140 °C for 30 min then sequentially cooled down to 90 °C without stirring. Then, the solution was kept at 25 °C for 30 min. The solution became opaque mixture. After that, an insoluble content was separated from the mixture by centrifugation at 4000 rpm for 1 h. It can be seen that the upper part was clear solution. Then, an exact volume of clear solution was co-precipitated in acetone. The obtained solid regarded as a decane soluble content ($C_{10,sol}$). Lastly, it was filtrated and dried under vacuum at 60 °C for 6 h.

3.3 Results and discussion

In this work, high impact polypropylene (hiPP) was produced from two-stage reaction in series, which the first step was propylene polymerization. Consequently, the produced polypropylene particles behaved like small reactors in a second-stage reaction. Copolymerization occurred all over the surfaces of polypropylene particles. According to the solubility of ethylene-propylene copolymer, copolymerization is

generally conducted in a gaseous phase to avoid copolymer dissolution. Thus, the morphology and amount of produced polypropylene have to be suitable to gas-phase reactor. Generally, the basic requisitions of polymer morphology for gas-phase reactor are moderate particle size, narrow size distribution, and sufficient strength.

From the previous chapter, the enlargement of $Mg(OEt)_2$ particle size was accomplished. The synthesized catalyst also well represented the morphology of $Mg(OEt)_2$. As is known, the morphology of polymer imitates the morphology of catalyst.[10] Thus, the morphology of catalyst should be qualified as same as the properties of polypropylene, which was polymerized in gas-phase reaction.

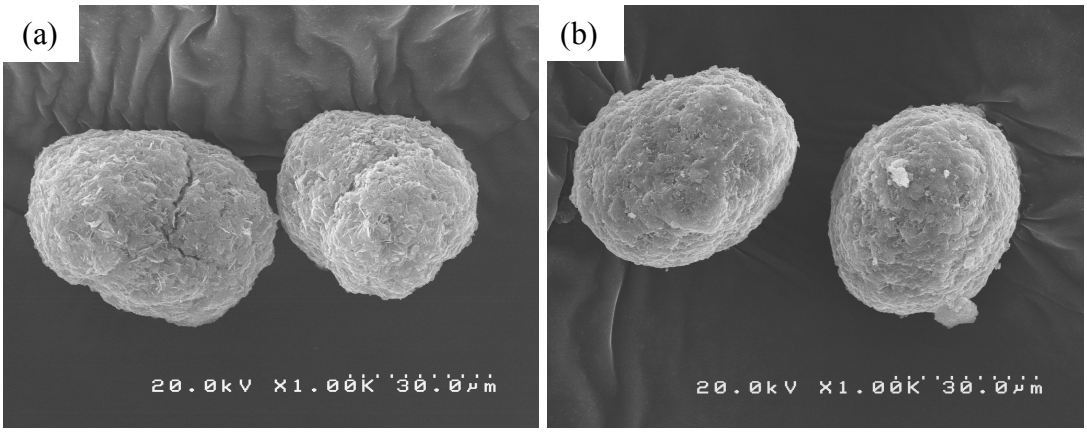

Figure 3.2 Morphology of (a) $Mg(OEt)_2$ and (b) catalyst.

The morphology and characteristic of $Mg(OEt)_2$ and catalyst are shown in **Figure 3.2** and **Table 3.1**. The morphology and characteristics of catalyst well imitated those of $Mg(OEt)_2$. The average particle size of catalyst (D_{50}), the RSF value, and the circularity of catalyst were higher than $Mg(OEt)_2$, which was consistent with the results of Taniike et al.[11] The catalyst had moderate average particle size with narrow size distribution and good circularity. These properties of catalyst well met the prerequisite requirements for gas-phase polymerization.

Table 3.1 Characteristics of $Mg(OEt)_2$ and catalyst.

	D_{10} [(a)] (μm)	D_{50} [(a)] (μm)	D_{90} [(a)] (μm)	RSF [(b)]	Circularity [(c)]
$Mg(OEt)_2$	27.5	39.3	48.5	0.53	0.82
Catalyst	27.0	41.8	52.9	0.61	0.85

[(a)] D_{10}, D_{50}, and D_{90} are the particle diameters at 10%, 50% and 90% in the cumulative number-based particle size distribution obtained by the analysis of SEM micrographs over 500 particles.

[(b)] Determined based on equation (3.1).

[(c)] Determined based on equation (3.2).

Besides the properties of catalyst, the first-stage polymerization conditions were also an important factor that needs to be considered. According to the restrictions of reactor, some portion of particle could not move and packed in the bottom part. So, it might cause product heterogeneity and poor reproducibility. A transparent plastic cylinder with the same diameter of reactor was set for testing particle lift-up ability.

The different amount of commercial polymer was stirred at different speed. The height of H in **Figure 3.2** represents the height of unmovable polymer beds. From the experiment, H value was 0.8 cm and it scarcely changed even the stirring speed or the amount of polymer was changed. The height of 0.8 cm could be implied to approximately 6 g of polymer. However, it is worth to note that this approximation was calculated according to the facts that; (1) bulk density of polymer is 0.4 g/cm^3, and (2) the volume of stirrer was discarded.

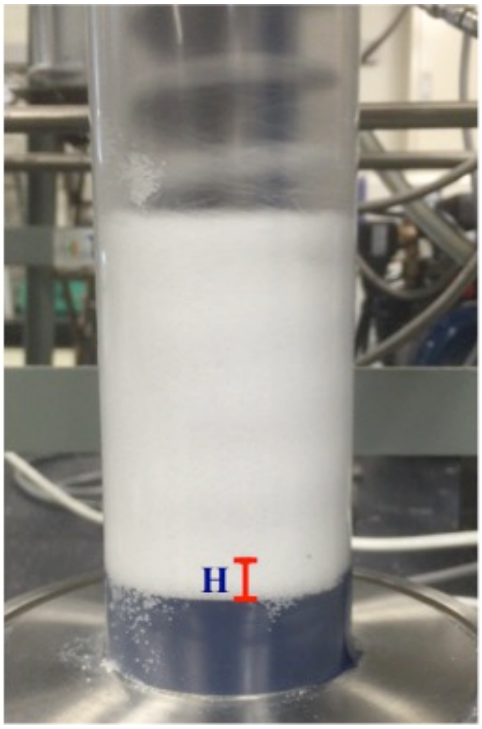

Figure 3.2 lift-up ability test setup.

One of the solutions for reducing an error, which occurred from these unmovable beds, was the increase of total polymer amount. **Table 3.2** shows polymerization results and the error from unmovable beds. The double catalyst amount could increase two times content of polymer, while the unmovable beds were sufficiently low (14.0 wt%) enough to discard.

Table 3.2 Polymer yield at different amount of catalyst and its error from unmovable beds.

Catalyst amount (mg)	**Yield [(a)] (g)**	**Unmovable bed (wt%)**
30	16.5 ± 1.8	31.5
60	37.2 ± 1.8	14.0

[(a)] Propylene polymerization was conducted at 50 °C in 300 mL of heptane with 0.9 mmol of TEA, and 0.5 MPa of continuously supplied propylene for 80 min.

The portion between polypropylene and copolymer is important to determine the properties of hiPP. However, it is difficult to control the exact amount of polypropylene, because the process was continuously conducted in series. Some researchers fed propylene from a ballast, which the exact amount of propylene was known.[6] Thus, the consumption of propylene could be converted to the amount of produced polymer. For slurry-phase, gas consumption could not represent the amount of produced polypropylene because it was disturbed by gas dissolution. In this study, propylene polymerization was conducted in a slurry-phase. The amount of produced polypropylene was investigated through reaction profile monitored by mass flow meter. The experiment setup is shown in **Figure 3.4**.

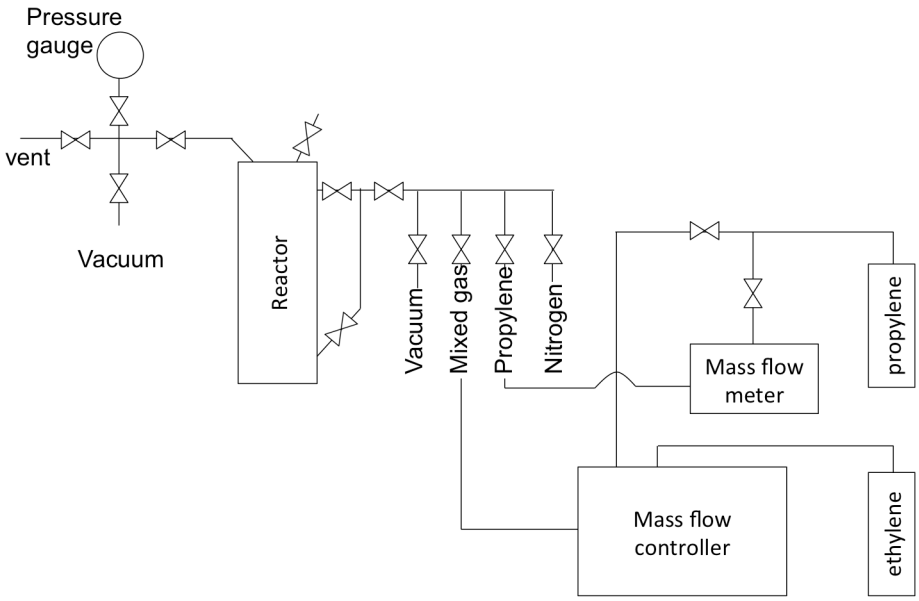

Figure 3.4 reactor system for hiPP polymerization.

Propylene was fed from the bottom of the reactor, while the slurry of catalyst was injected from the top of reactor. A mass flow meter was equipped in order to track gas consumption. Firstly, mass flow was calibrated with rotameter to correlate

between signal from mass flow meter (voltage, V) and flow rate (L/min). The obtained equation in **Figure 3.5** was used for converting the signal of mass flow meter to volume flow rate of propylene.

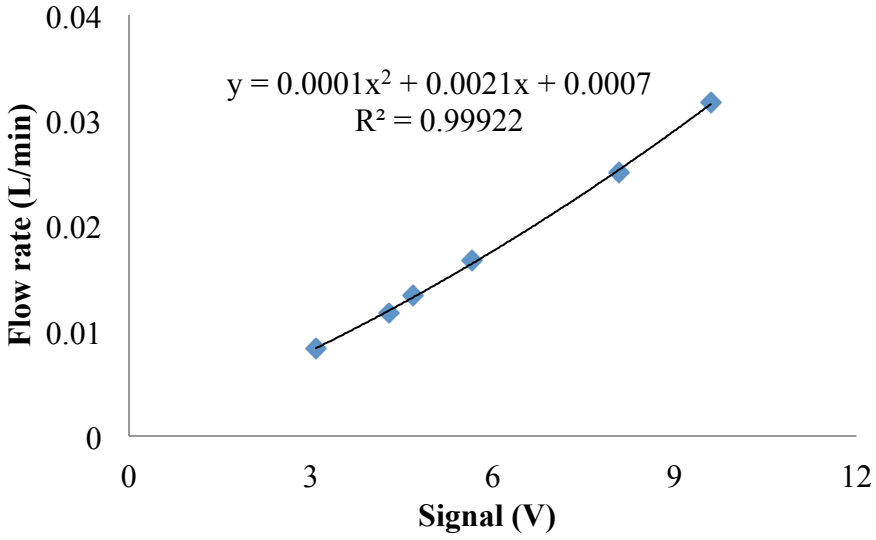

Figure 3.5 calibration curve of mass flow meter.

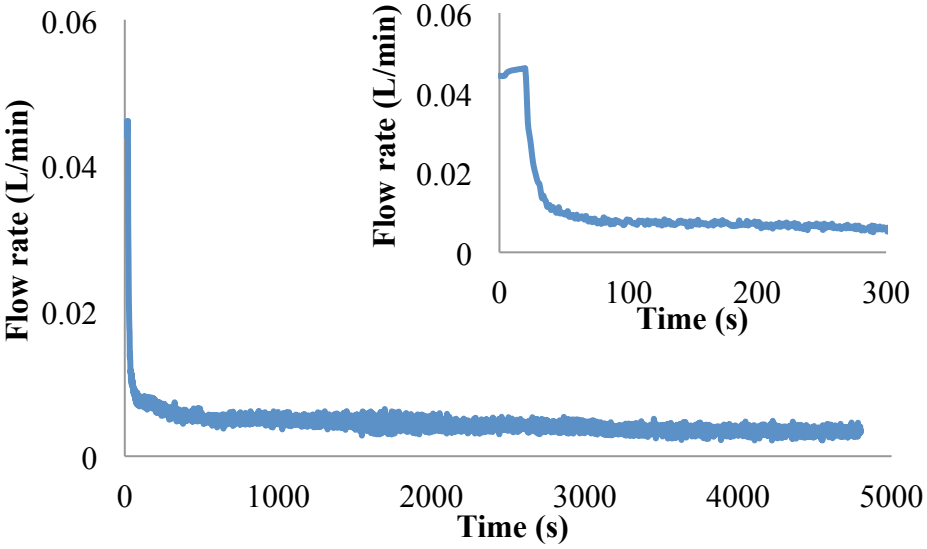

Figure 3.6 reaction profile obtained from bottom-feed gas system.

The obtained reaction profile is shown in **Figure 3.5**. Flow rate was high in the first 20 s of reaction, and then it suddenly dropped and continuously decreased along the reaction. This characteristic was different from usual reaction profile, which showed build-up type for $Mg(OEt)_2$-based catalyst.[12, 13] At the beginning, the reactor was at atmospheric pressure of propylene. Propylene was supplied from the ballast, which the pressure was set. Thus, the relatively high flow rate at the initial stage of reaction (20 s) was ascribed as a pressure difference between reactor and set pressure. After the reactor was pressurized to the set pressure, propylene was consumed by both of dissolution and reaction. However, it was difficult to distinguish between those two consumptions. Thus, the reaction profile or its area could not represent propylene consumption by the reaction. To reduce these effects, the reactor system and operating procedure was modified as shown in **Figure 3.7**.

The injection ports for catalyst and solvent were equipped on the top of the reactor. After charging alkylaluminum (TEA) and external donor, solvent was saturated. The catalyst slurry and solvent were injected from the ports. The operation was carried out under propylene atmosphere. The reaction profile was obtained as shown in **Figure 3.8**.

The reaction profiles showed almost similar to typical build-up type profile. However, even the system was saturated, there was a short period (around 5 s) which propylene was fed with high flow rate. This high flow rate was ascribed to the different pressure between the catalyst injection port and the reactor. Then, flow rate increased until the reaction time of 1200 s which indicated to induction period. After that, the flow decreased because of catalyst deactivation. In addition, the results also showed the drawback of this system. The catalyst slurry could be injected to the reactor only by pressure difference between the reactor and the injection port. Thus,

according to cylindrical shape of the reactor and spiral stirrer, the catalyst could not be completely injected to the system, and resulted in poor reproducibility.

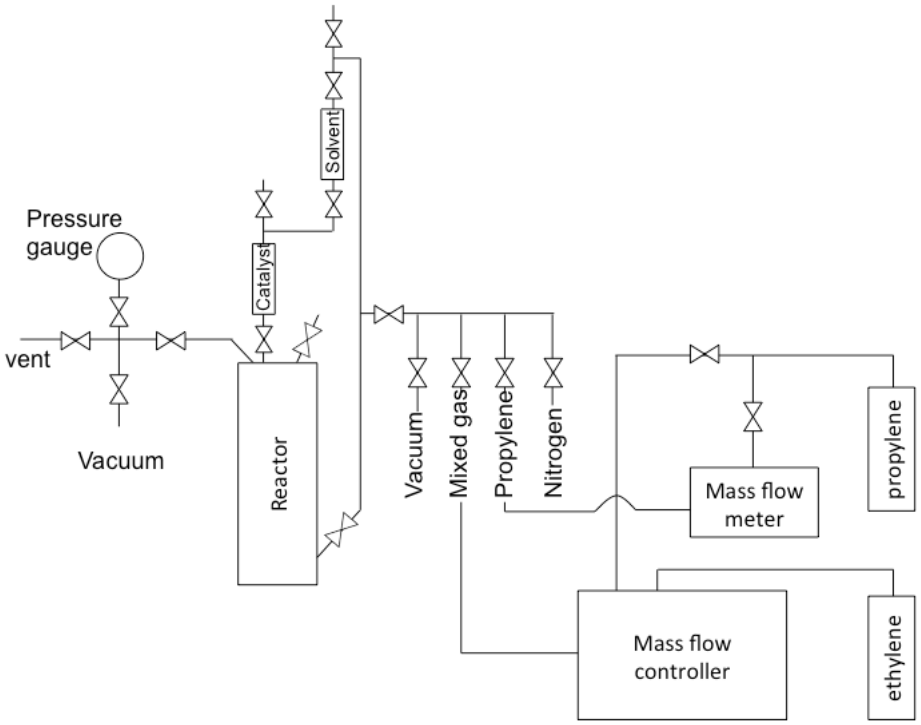

Figure 3.7 Modified reactor system.

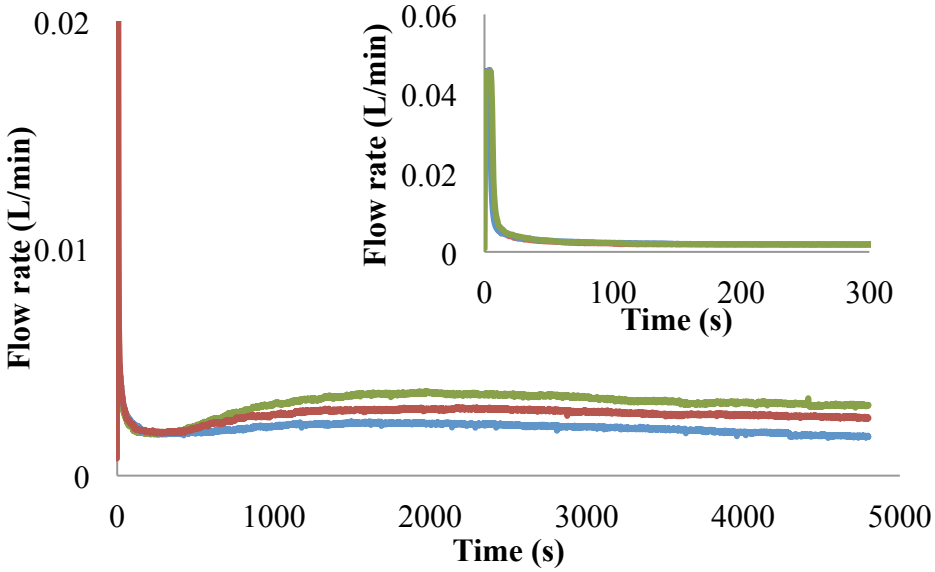

Figure 3.8 Reaction profiles from modified reactor system.

From the results, it was difficult to utilize whole reaction profile to calculate produced polypropylene amount because the initial fed gas was not totally consumed by the reaction (**Figure 3.6** and **3.8**). Moreover, even the consumption by gas dissolution could be neglected (**Figure 3.8**), reproducibility level was not acceptable. Thus, to obtain the exact amount of polypropylene, it is necessary to establish the correlation between reaction profile and polymer yield.

It is worth to note that the following developed correlation was under these bases; (1) catalyst activation and deactivation were identical among different batches of polymerization (as shown in **Figure 3.6** and **3.8**, the reaction was in deactivation period after 30 min., and it was independent of reactor system or operating procedure), (2) the saturation and activation (induction period) were finished after 30 min of reaction, which the flow rate was maximum. After catalyst was fully activated, the reaction was in the deactivation period. Thus, after 30 min, gas consumption rate could be implied to polymer yield. To establish the correlation, propylene polymerization was conducted in the system presented in **Figure 3.4** with different amount of catalyst. The gas flow rates were averaged from 1000 s of later-stage polymerization to make sure that it was not influenced by saturation and noise of signal. The average flow rates and yields were plotted as shown in **Figure 3.9**, and then the obtained equation was used to calculate polymer yield (**Table 3.3**). The obtained correlations were linear and well represent the data. The accuracy of the equation was within the error of below 10%, which was acceptable. To extend the usage of the equation, hiPP polymerization was conducted to verify the availability of the equation.

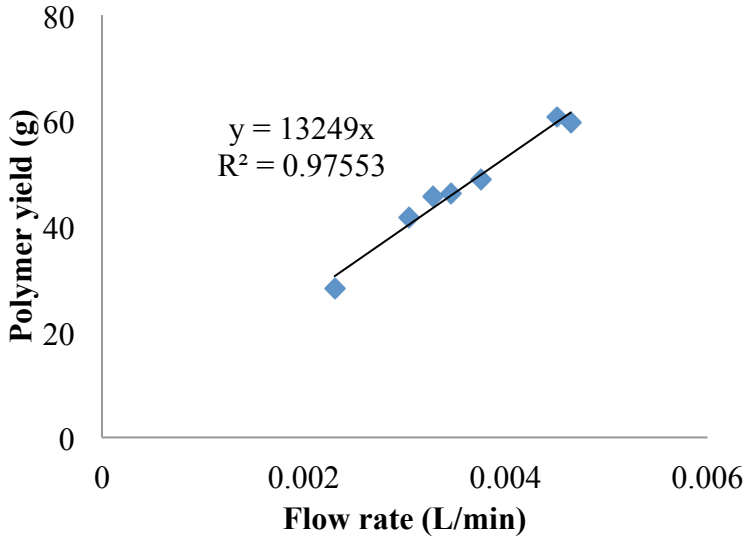

Figure 3.9 Correlations between polymer yield and average flow rate.

Table 3.3 Comparison between real and calculated polymer yield.

$Yield_{real}$ (g)	$Yield_{cal}$ (g)	Error (%)
41.7	40.3	-3.4
46.2	45.9	-0.7
60.7	59.7	-1.7
28.1	30.5	8.6
48.8	49.7	1.8
59.7	61.5	3.1
45.6	43.4	-4.9

HiPP polymerization was conducted in the system as shown in **Figure 3.4**. After propylene polymerization and solvent removal, the reaction was conducted in gas-phase. Ethylene and propylene were fed from the bottom of the reactor. Either ethylene-propylene random copolymer (EPR) or ethylene-propylene segmented copolymer (EPB) can be formed inside polypropylene particles. However, the content (and ratio) of them depends on the conditions, which can be examined by extraction.

Table 3.4 Real and calculated polypropylene yield and extraction results.

Polypropylene yield (g)		hiPP yield (g)	Copolymer (g)	$C_{10,sol}$ (wt%)	Note
Real	Calculated				
41.7	40.3	-	-	0.89	PP polymerization
-	41.3	47.2	5.9	7.17	Copolymerization time 15 min
	48.8	63.9	15.1	10.36	Copolymerization time 45 min

Table 3.4 shows real and calculated polypropylene yield and extraction results. For propylene polymerization, there was slightly different (3.6% error) between real and calculated yield, which meant the equation in **Figure 3.9** was acceptable. The extraction was also conducted for polypropylene. Generally, $C_{10,sol}$ content represents the content of polymer, which cannot crystallize at room temperature.[14] Thus, in case of polypropylene, $C_{10,sol}$ content represent an atactic polypropylene (aPP) content. From the results, aPP was 0.89 wt%, which was consistent with other literatures using $MgCl_2/TiCl_4$/DNBP catalysts. At 15 min of copolymerization, hiPP yield was 47.2 g. Based on the calculation, copolymer content was 5.9 g (or 12.5 wt% of whole hiPP). However, for hiPP, $C_{10,sol}$ content can represent only EPR content because EPB contains segmented copolymer, which can crystallize at room temperature.[14] Thus, hiPP containing 7.17 wt% of $C_{10,sol}$ content meant in 47.2 g of hiPP consisted of EPR and aPP 3.38 g. After subtracting aPP, EPR content was 2.96 g. From literatures, EPR and EPB content are supposed to be equal.[5] Thus, polypropylene was 41.3 g which almost similar to the calculated yield. Again, the results from extraction were used to confirm the accuracy of polypropylene content prediction in higher content of copolymer. From the experiment, the content of polypropylene was 51.8 g which higher than the predicted content 6.1 %.

3.4 Conclusion

The procedure for high impact propylene copolymerization including the method for first-stage yield prediction and its proof was established. In our reactor system, the exact amount of produced polypropylene could not be calculated from whole reaction profile because of unidentified fed propylene in the early stage of reaction. Moreover, the gas was also consumed by dissolution. We indirectly utilized the profile by establishing correlation between average flow rate and polymer yield. The accuracy of the correlation was checked by n-decane extraction. The error between calculated and real yield was below 10%, which was considered as high precision.

References

[1] D. B. Malpass, E. Band, *Introduction to Industrial Polypropylene: Properties, Catalysts Processes*, Wiley-Scrivener, Massachusetts, United States of America.

[2] J. B. P. Soares, T. F. L. McKenna, *Polyolefin Reaction Engineering,* WILEY-VCH, Boschstr, Germany 2012.

[3] T. Simonazzi, G. Cecchin, S. Mazzulo, *Prog. Polym. Sci.*, 16 (1991) 303-329.

[4] J. A. Debling. W. H. Ray, *J. Appl. Polym. Sci.*, 81 (2001) 3085-3106.

[5] Z.-Q. Fan, Y.-Q. Zhang, J.-T. Xu, H.-T. Wang, L.-X. Feng, *Polymer*, 42 (2001) 5559-5566.

[6] P. Kittilsen, T. F. McKenna, *J. Appl. Polym. Sci*, 82 (2001) 1047-1060.

[7] P. Galli, *Macromol. Symp.*, 78 (1994) 269-284.

[8] P. Galli, *J. Macromol. Sci., Pure Appl. Chem*., 36 (1999) 1561–1586.

[9] T. Vestberg, P. Denifl, C.-E. Wilen, *J. Appl. Polym. Sci.*, 110 (2008) 2021-2029.

[10] P. Galli, P. C. Barbe, L. Noristi, *Angrew. Makromol. Chem.*, 120 (1984) 73-90.

[11] T. Taniike, T. Funako, M. Terano, *J. Catal.*, 311 (2014) 33-40.

[12] P. J. T. Tait, G. H. Zohuri, A. M. Kells, I. D. McKenzie, Ziegler Catalysts, Springer Berlin Heidelberg, Heidelberg, Germany 1995.

[13] A. Dashti, A. Ramazani SA, Y. Hiraoka, S. Y. Kim, T. Taniike, M. Terano, *Polym. Int.*, 58 (2009) 40-45.

[14] W. Rungswang, P. Saendee, B. Thitisuk, T. Pathaweeisariyakul, W. Cheevasrirungruang, *J. Appl. Polym. Sci.*, 128 (2013) 3131–3140.

Chapter IV

Reactor granule technology for evaluating rubber distribution of high impact polypropylene in $Mg(OEt)_2$-based Ziegler-Natta catalyst

4.1 Introduction

Among various commercialized polypropylenes, polypropylene/(ethylene-co-propylene) copolymer or high impact polypropylene (hiPP) has gained overwhelmed attraction from both of academic and industrial aspects because of its special properties. HiPP is an alloy of isotactic polypropylene and ethylene-propylene copolymer.[1] In general, according to an economic point of view, hiPP is commonly produced in the sequential two-stage reactions in series, at which the first-stage is propylene polymerization. Afterwards, the produced polypropylene is transferred to the second-stage ethylene-propylene copolymerization, which is normally conducted in gas-phase reactor.[2] Since, the polypropylene granule contains active sites, so it can be utilized as a reactor for next stage copolymerization. This invention was named "Reactor Granule Technology (RGT)".[3] In the second-stage reaction, ethylene-propylene sequential copolymer (EPB) and ethylene-propylene random copolymer (EPR) are simultaneously formed inside polypropylene pores.[4, 5] The addition of copolymer leads to the enhancement of properties. Polypropylene has excellent stiffness. The cooperation of these copolymer components could greatly enhance the toughness.[6, 7] This well-balanced stiffness-toughness property makes hiPP becomes engineering grade polypropylene, which has been widely used in an automobile industry. These fabulous properties are achieved through the optimal control of reaction conditions and elegant catalyst design during several years of development.

There are many studies working on the effects of copolymer components on the properties of hiPP. According to Speri et al. studies, they reported that EPR (or rubber) has two major important roles.[8] It acts as stress concentrators that initiate craze formation. Also, it is craze arrestors that prevent craze extension by branching.

The authors additionally purposed that EPR domain should have small size (0.5 μm) and narrow distribution (0.1 – 1.0 μm with the center at 0.5 μm) in order to improve impact strength of hiPP. Besides the characteristics of rubber, the amount and the quality are also important for the properties of hiPP. Fan et al. investigated the impact strength at low temperature (−30 °C) and room temperature (23 °C) of hiPP absented random copolymer.[9] They reported that, at room temperature, impact strength was slightly lower after removing the random copolymer, while the impact strength at low temperature was strongly affected. A number of studies showed the importance of copolymerization conditions on the changes of copolymer properties and whole hiPP properties as well. It cannot be denied that the catalyst also plays an important role in determining hiPP properties. For instance, polypropylene structure was strongly affected by catalyst architecture.[10] However, the significance of catalyst design has not been enough attended.

The morphology of polymer is known that it is developed through fragmentation and replication mechanisms. The catalyst platform and its architecture have significant effect on the fragmentation, which also affects the final morphology of polymer.[10] There are two widely acceptable mechanisms for explaining fragmentation behaviors, layer-by-layer (LbL) and homogeneous fragmentations. For $MgCl_2$-based catalyst, the fragmentation tends to occur in a "layer-by-layer" (LbL) manner rather than homogeneous fragmentation.[11, 12] According to continuous transformation of polymer morphology along the reaction, the characteristics of polymer are difficult to predict and investigate.

In this research, copolymerization of ethylene-propylene was utilized to evaluate the performance of polypropylene (or reactor granule) in rubber distribution of hiPP. The polymer morphology development from $Mg(OEt)_2$-based catalyst was

investigated along the reaction time by observing internal structure of polypropylene particles. Then, ethylene-propylene copolymerization in gas-phase was conducted after propylene polymerization. The results indicated that internal structure of polymer had great influences on copolymerization activity limited by mass diffusion. Also, the importance of catalyst platform was stressed by comparing rubber distribution.

4.2 Experiment

4.2.1 Materials

Ethanol (purity > 99.5%) was purchased from Wako Pure Chemical Industries Ltd. and then dried over 3A molecular sieves with N_2 bubbling for 2 h. Mg powder (particle size 0.06 - 0.3 mm) was purchased from Merck Co., Ltd. Iodine (I_2, purity > 99%) was used as an initiator in $Mg(OEt)_2$ synthesis. Titaniumtetrachloride ($TiCl_4$, purity > 99%), di-*n*-butylphthalate (DNBP) (purity > 98%) were used without further purification. *n*-Heptane (purity > 99.5%) and toluene (purity > 99.5%) were dried over 4A molecular sieves with N_2 bubbling for 2 h. Cyclohexylmethyldimethoxysilane (CMDMS or C-donor) was distillated under reduced pressure. Triethylaluminum (TEA) was donated by Tosho finechem Co., Ltd. Commercial $MgCl_2$/diether/$TiCl_4$ Ziegler-Natta catalyst was donated from Mitsui chemicals, Inc. Propylene and ethylene of polymerization grade were donated by Sumitomo Chemical Co., Ltd. Octadecyl 3-(3,5-di-tert-butyl-4-hydroxyphenyl)propionate (AO-50, donated by ADEKA Corporation) was used as a stabilizer.

4.2.2 $Mg(OEt)_2$ synthesis

A 500 mL jacket-type glass reactor equipped with a mechanical stirrer was used for $Mg(OEt)_2$ synthesis. After N_2 replacement, the reactor was heated to 75°C. 0.68 g of flake I_2 and 31.7 mL of ethanol were added into the reactor. The mixture was stirred at 180 rpm for 10 min to assure the complete dissolution of I_2. Then, 2.5 g of magnesium powder and 31.7 mL of ethanol were continuously introduced for nine times with an interval time of 10 min. After the last addition, the mixture was aged under stirring for 2 h. Afterwards, the resultant solid was washed with 190 mL of ethanol before drying by rotary evaporator.

4.2.3 Catalyst synthesis

$Mg(OEt)_2$-based Ziegler-Natta catalyst was prepared by using a 500 mL three-neck round bottom flask equipped with a mechanical stirrer rotating at 180 rpm under N_2 atmosphere. 15.0 g of $Mg(OEt)_2$ and 150 mL of toluene were added into the flask under N_2 blanking. 30.0 mL of $TiCl_4$ was tardily dropped while the temperature was strictly kept at 5°C. Followed by the gradual increase of temperature to 90°C, 4.5 ml of DBP was added. Thereafter, the reaction mixture was heated to 110°C and stirred for 2 h. The product was washed with 150 mL of toluene twice at 90°C and further treated with 30.0 mL of $TiCl_4$ in 150 mL of toluene at 110°C for 2 h. Finally, the product was washed with 220 mL of heptane at 70°C for three times and at room temperature for four times to obtain the final catalyst.

4.2.4 Propylene polymerization

Propylene polymerization was conducted in a 700 mL cylindrical shape reactor equipped with a spiral shape propeller rotating at 150 rpm for 80 min. After replacement of N_2, 200 mL of heptane was introduced to the reactor followed by 0.9

μmol of TEA, 0.09 μmol of C-donor. Then, the reactor atmosphere was replaced by propylene. 60 mg of catalyst was introduced to the reactor under propylene atmosphere. Finally, 100 mL of heptane was added to the reactor. The reaction was conducted at 50 °C and 0.5 MPa for 45 and 60 min. The polymer was collected after gas was vented off and dried under vacuum at 60 °C for 6 h.

4.2.5 In situ high impact propylene copolymerization

An in situ propylene/(ethylene-co-propylene) copolymer (or high impact polypropylene, hiPP) was produced by two-stage reaction in series. Firstly, polypropylene was produced according to the former described procedure. After the desired polymerization time, stirring speed was reduced to 100 rpm, and then solvent was vacuumed for 1 h to ensure completely dry. The second-stage reaction, ethylene-propylene copolymerization, was conducted in gas-phase reaction. The stirring speed was increased to 150 rpm. Copolymerization was conducted under equimolar feed of ethylene and propylene at the total pressure of 0.3 and 0.4 MPa. Finally, gas was vented off and then the produced copolymer was collected and dried at 60 °C under vacuum.

4.2.6 Characterization

The morphology of $Mg(OEt)_2$ and catalyst was evaluated by scanning electron microscopy (SEM, Hitachi S-4100) at an accelerate voltage of 20 kV. The particles were coated by Pt-Pd for 60 s (and 100 s for polymer particle and film) before the measurement. The particle morphology in SEM micrographs was quantified using an image processing software. The relative span factor (RSF) and the circularity were respectively calculated based on equations (4.1) and (4.2),

$$\text{Relative span factor} = \frac{D_{90}\text{-}D_{10}}{D_{50}} \quad (4.1)$$

$$\text{Circularity} = \frac{4 \times \pi \times \text{area}}{(\text{boundary length})^2} \quad (4.2)$$

where, D_{10}, D_{50}, and D_{90} correspond to the cumulative number-based particle sizes at 10%, 50%, and 90%, respectively. The area and boundary length for a two-dimensionally projected particle were determined over 500 particles. The internal polymer structure was also observed by SEM. The razor was dipped into liquid nitrogen before cutting particles. The distribution of rubber inside hiPP particle was evaluated through a film casted by hot-pressing technique. 0.6 g of hiPP was hot pressed at 230 °C under 20 MPa for 5 min, and then quenched at 100 °C for 5 min and at 0 °C for 3 min to get a film with the thickness of 0.2 mm. The obtained film was cut into 0.5 × 2 cm^2 and soaked in 10 mL of xylene. The mixture was sonicated at 50 °C for 5 min. Lastly, the film was washed with hexane for three times and dried under vacuum at 60 °C for 6 h.

4.3 Results and discussion

4.3.1 Time-dependence PP template for hiPP copolymerization

In propylene/(ethylene-*co*-propylene) copolymerization, polypropylene produced in the first-stage behaves like a reactor for ethylene-propylene copolymerization. As the reaction was proceeding, polymer characteristics such as particle size, pore size, and pore volume were also changed ascribing to replication and fragmentation phenomena. In this research, the impacts of polypropylene template (or reactor granule) were evaluated in copolymerization performances. Propylene polymerization was conducted at 45, 60 and 70 min by using $Mg(OEt)_2$-based

Ziegler-Natta catalyst. The characteristics and morphology of $Mg(OEt)_2$ and catalyst are shown in **Table 4.1** and **Figure 4.1** respectively.

Table 4.1 Characteristics of $Mg(OEt)_2$ and catalyst.

	D_{10} [(a)] (μm)	D_{50} [(a)] (μm)	D_{90} [(a)] (μm)	RSF [(b)]	Circularity [(c)]
$Mg(OEt)_2$	27.5	39.3	48.5	0.53	0.82
Catalyst	27.0	41.8	52.9	0.61	0.85

[(a)] D_{10}, D_{50}, and D_{90} are the particle diameters at 10%, 50% and 90% in the cumulative number-based particle size distribution obtained by the analysis of SEM micrographs over 500 particles.

[(b)] Determined based on equation (4.1).

[(c)] Determined based on equation (4.2).

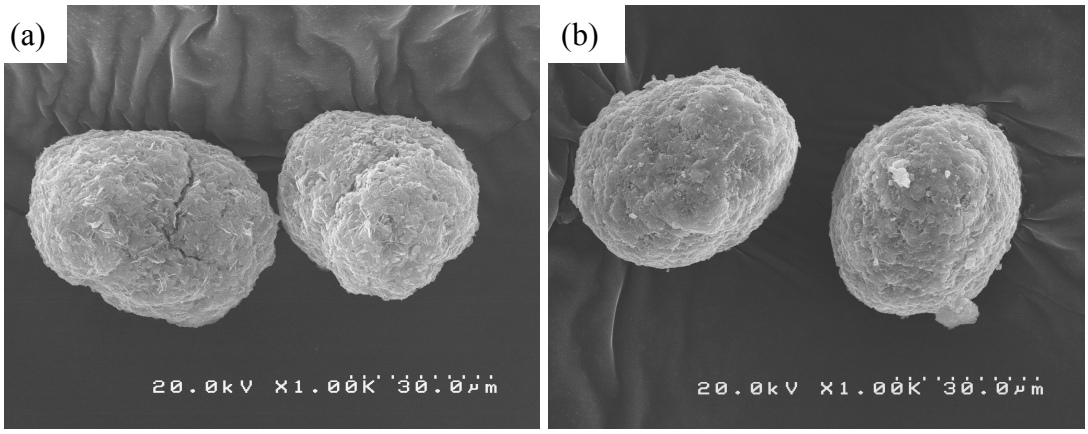

Figure 4.1 Morphology of (a) $Mg(OEt)_2$ and (b) catalyst.

The catalyst had potato-shape with smooth surface and nice circularity as same as $Mg(OEt)_2$. The average particle size (D_{50}), RSF, and circularity of catalyst were higher than $Mg(OEt)_2$, which was consistent with the results of Taniike et al. [13] The catalyst also had relatively narrow size distribution and nice circularity.

As known from literatures, catalyst morphology imitated $Mg(OEt)_2$ not only external but also internal structure.[8, 14] $Mg(OEt)_2$ is a porous material, which internal

structure composes of three different layers; an outermost layer, a porous layer, and a dense core. Under appropriate reaction conditions, $Mg(OEt)_2$-based catalyst could well maintain its original morphology. The formation of polypropylene in $Mg(OEt)_2$-based catalyst was investigated by using stopped-flow technique.[10] At the beginning, polymerization occurred in the porous layer and on the outermost surface, which resulted in reinforced polymer particles. The further reaction caused fragmentation in the porous layer, which also led to the fragmentation in the compact core. To investigate the internal structure of polypropylene, the polymer particles from different reaction time were cut. The results are shown in **Figure 4.2**. The observed inner structure of polymer well imitated that of $Mg(OEt)_2$ even the reaction was over the initial stage.

At reaction time of 45 min, cross-sectional image revealed that there were cracks mainly in the middle of particle. Although the cracks might be occurred because of the cutting technique, they could imply that the strength of particle was not enough to resist shear force during cutting. This could be implied that the particle was not dense. Also, there was an unclear borderline between the porous layer and outermost layer. As the reaction was carried out, particle size was larger. The inner structure showed that the width of the porous layer was expanded and the lamellae structure was distinctly observed. At the core, cracks still appeared but the damage was less than those of 45 min particles. According to lamellae structure of the porous layer, the expansion to the edge of particle could lead to the generation of fine particle especially in gas-phase reaction, because the lamellae were more brittle than a compact structure (**Figure 4.2c**). Thus, the second-stage gas phase copolymerization was conducted after propylene polymerization of 45 and 60 min.

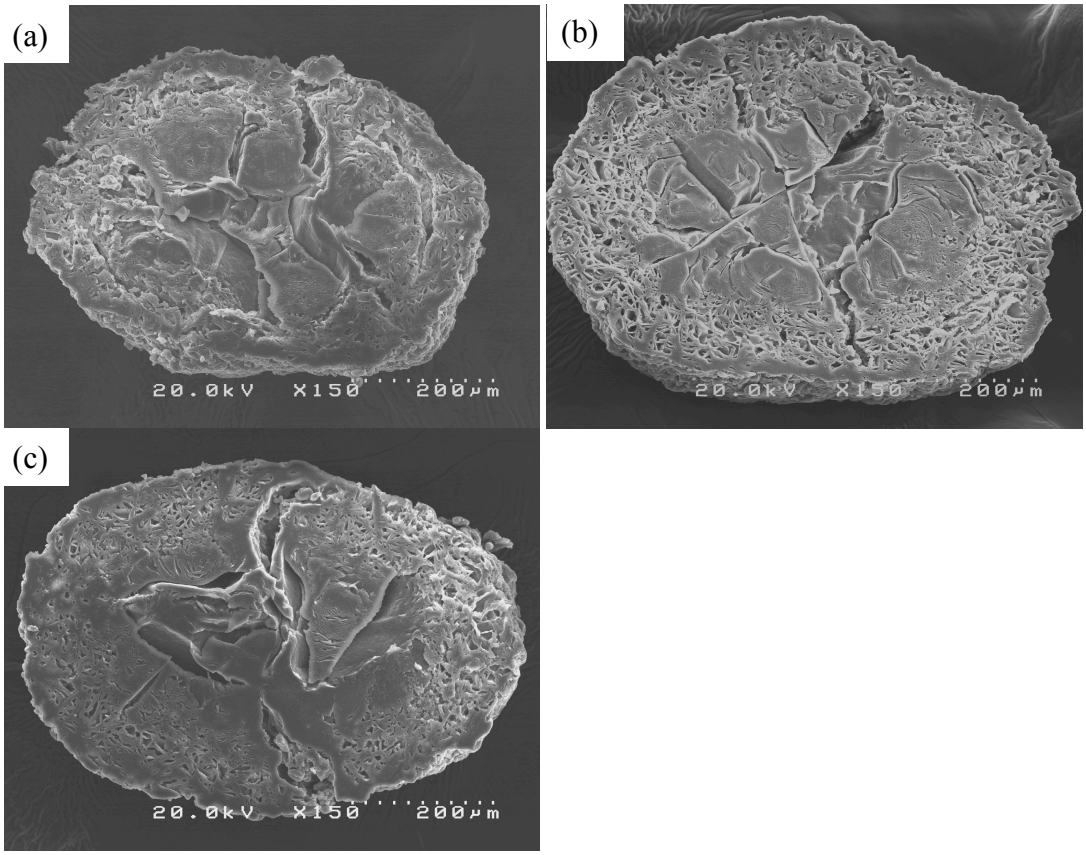

Figure 4.2 Internal structure of $Mg(OEt)_2$ and polypropylene particle produced from different polymerization time; (a) 45 min, (b) 60 min, and (c) 70 min.

The copolymerization activities and copolymer content are presented in **Table 4.2**. The samples were denoted as C-PP or C-hiPP, which mean polypropylene and high impact polypropylene produced from $Mg(OEt)_2$-based catalyst respectively. The first two digits after PP or hiPP represented propylene polymerization, and the last two digits referred to copolymerization time. For propylene polymerization time of 45 min at the pressure of 4 atm, the results showed that copolymerization activity decreased with the increase of reaction time, while copolymer content continuously increased. In order to observe the polymer structure, the obtained polypropylene and high impact polypropylene particles were cut. The SEM images are showed in **Figure 4.3**. Before further discussion, it is worth to note that the particle size of

cross-sectional particle was distorted by the direction of cutting. The morphology of polymer particles was similar to $Mg(OEt)_2$, whose shape was potato-like. Thus, the cutting direction, vertical or horizontal, could affect the size of the cross-sectional particle. As seen in **Figure 4.3**, at low content of copolymer (23-25 wt%) the internal structure of hiPP was almost similar to those of PP **(Figure 4.2)**. Even there were cracks, which were possibly generated from cutting, the core of particles were more compact comparing to those of PP particles. As the copolymer content increased, the depth of cracks was shallower which could imply that the particle was strengthened by the increase of copolymer content. Also, at the porous layer, the pores were partly filled.

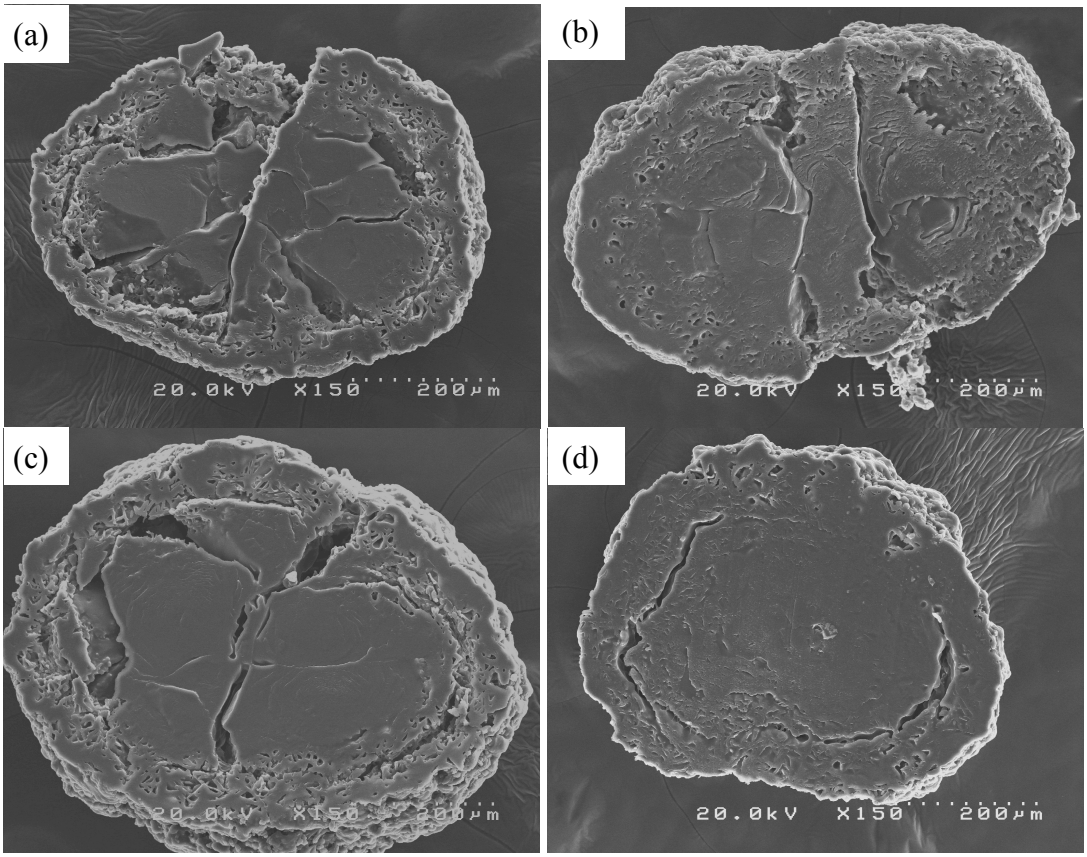

Figure 4.3 Internal structure of (a) C-hiPP4508, (b) C-hiPP4530, (c) C-hiPP6008, and (d) C-hiPP6030.

Table 4.2 propylene polymerization and hiPP copolymerization results from $Mg(OEt)_2$-based Ziegler-Natta catalyst.

Sample	Propylene polymerization		Ethylene-Propylene copolymerization[a]				
	Time (min)	$Yield_{PP}$ (g)	Time (min)	Pressure (atm)	$Yield_{hiPP}$ (g)	Activity[b] ($g_{copolymer}/g_{cat}$.h.atm)	Copolymer content[c] (wt%)
C-PP4500	45	23.9	-	-	-	-	-
C-hiPP4508	45	-	8	3	31.9	333.3	25.1
C-hiPP4507	45	-	7	4	33.7	350.0	29.1
C-hiPP4510	45	-	10	4	36.1	305.0	33.8
C-hiPP4530	45	-	30	4	41.5	146.7	42.4
C-PP6000	60	27.9	-	-	-	-	-
C-hiPP6008	60	-	8	3	36.2	345.8	22.9
C-hiPP6010	60	-	10	4	38.5	265.0	27.5
C-hiPP6030	60	-	30	4	51.0	192.5	45.3

[a] Ethylene/propylene copolymerization was conducted at 4 atm of monomer pressure after propylene polymerization without any addition of cocatalyst or external donor.

[b] Activity was calculated from $\frac{\mathrm{Yield_{hiPP}} - \mathrm{Yield_{PP}}}{\mathrm{g_{cat}} \times \mathrm{h} \times \mathrm{atm}}$

[c] Copolymer content was calculated from $\frac{(\mathrm{Yield_{hiPP}} - \mathrm{Yield_{PP}}) \times 100}{\mathrm{Yield_{hiPP}}}$

Finally, at high copolymer content (42-45 wt%), the internal structure of hiPP was totally different from those of low copolymer content or PP particles. For hiPP4530, a few cracks and moderate amount of voids still appeared while there were radial cracks and relatively small amount of void for hiPP6030. This indicated that polypropylene produced from less first-stage reaction time had more rubber capacity. The initial step of copolymerization in gas phase is the diffusion of monomers into the pores of polypropylene. The decrease of copolymerization activity was not ascribed to catalyst deactivation but mass transfer limitation.[1, 15] At the beginning of the copolymerization, monomers could easily access to the pores of polypropylene and form the copolymer. The further copolymerization led to more content of copolymer. At a certain point, copolymer occluded the pores of polypropylene.[16] Thus, the monomers had to diffuse through the copolymer layer in order to produce more copolymer. At this stage, mass diffusion limitation became dominant and led to the decrease of copolymerization activity. The results from cross-sectional images were also consistent with the decrease of copolymerization activity.

4.3.2 EPR distribution

Ethylene-propylene random copolymer (EPR) and ethylene-co-propylene sequential copolymer (EPB) are important components for improving impact properties of hiPP. They are simultaneously generated during the second-stage copolymerization. EPR is an elastomeric material, so it has strongly influences on flexural modulus of hiPP. There are many researchers paying attention on the impact of this component. In this work, I focus on the importance of polymer-template architecture on the distribution of EPR. In this section, precipitation-based Ziegler-Natta catalyst was also used for hiPP copolymerization in order to point out the

importance of catalyst design. The first-stage propylene polymerization time was fixed at 45 min and the second-stage copolymerization time was 8 min at 0.4 MPa and 30 min at 0.5 MPa, which denoted as S-hiPP4508 and S-hiPP4510, respectively.

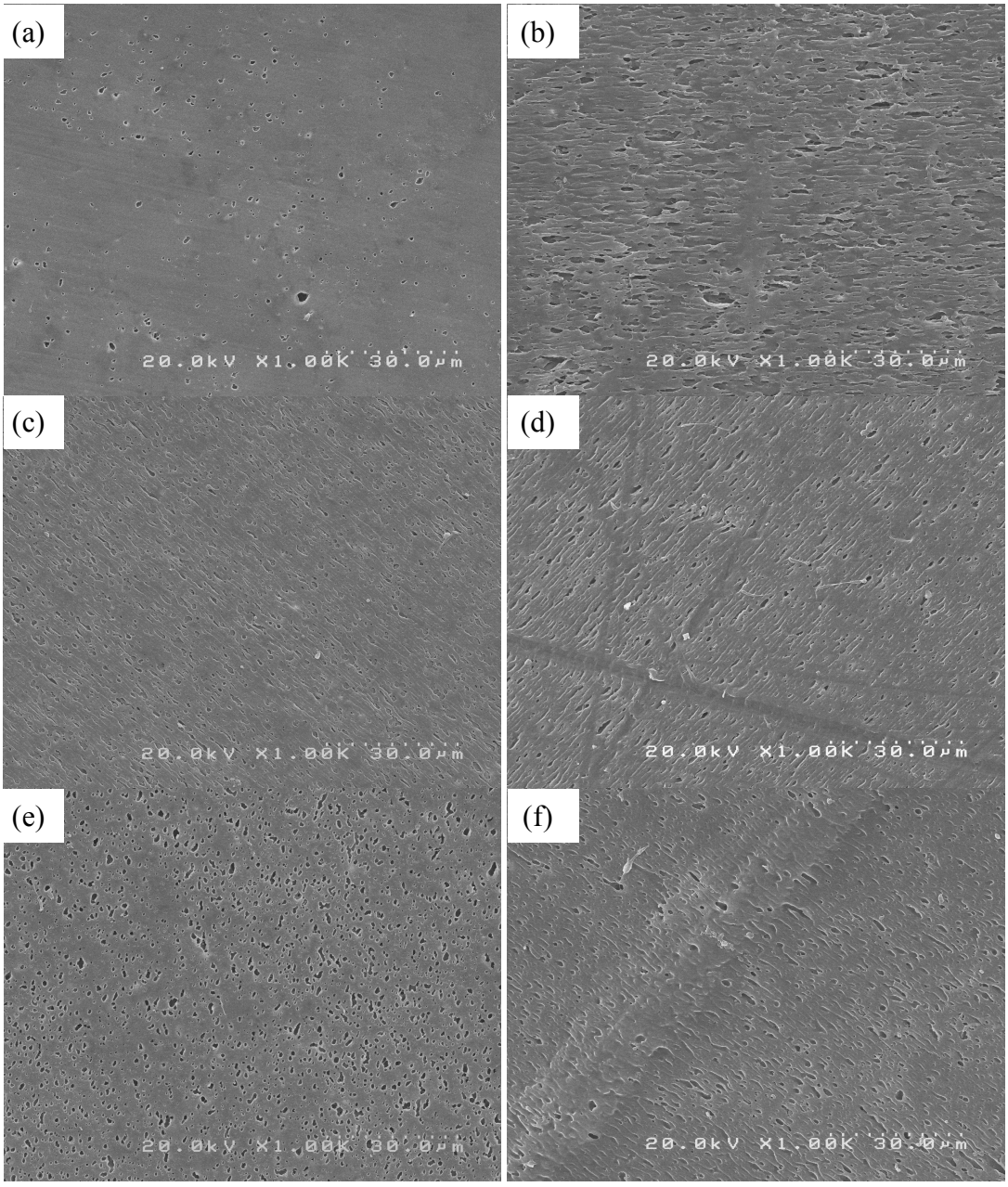

Figure 4.4 Rubber distribution of hiPP film; (a) S-hiPP4508 (copolymer content 7 wt%), (b) S-hiPP4510 (copolymer content 27.4 wt%), (c) C-hiPP4508 (copolymer content 25.1 wt%), (d) C-hiPP4530 (copolymer content 42.4 wt%), (e) C-hiPP6008

(copolymer 22.9 wt%), and (f) C-hiPP6030 (copolymer content 45.3 wt%).

The extraction by xylene could diminish only EPR on the surface of the film. After extraction, the film became turbid because of the removal of elastomeric component. Then, the extracted films were evaluated by SEM as shown in **Figure 4.4**. At the same hiPP copolymerization conditions, S-hiPP4508 and 4530 had sufficiently low amount of copolymer content compared to C-hiPP. Focusing on the effect of rubber content on the dispersion of rubber, the increase of rubber from 7 to 27.4 wt% leads to poor rubber dispersion. On the other hand, at the same copolymer content, C-hiPP4508 presented fine and well dispersion of rubber on the film. This indicated that S-hiPP4530 exceeded the copolymer capacity which led to the overflowing of rubber to the surface of polymer particles. In addition, it could imply that $Mg(OEt)_2$-based catalyst had more pore volume than precipitation-based catalyst. Considering C-hiPP, at fairly same copolymer content between C-hiPP4508 and C-hiPP6008, the rubber distribution of C-hiPP4508 was more uniform as can be seen in finely dispersed holes. Considering the internal structure of PP and hiPP as shown in **Figure 4.2** and **4.3**, C-PP4500 and C-hiPP4508 had more cavities than C-PP6000 and C-hiPP6008. For higher content, the surfaces of the films were similar to that of S-hiPP4530. As purposed by McKenna et al., copolymer was formed underneath the layer of PP and exposed to the pores. Thus, the excess capacity of copolymer content could result in overflow of rubber. Then, the copolymer (mainly EPR) partially formed on the surfaces of hiPP particles and resulted in connected cavities on the film as shown in **Figure 4.4b, d, f**.

4.4 Conclusion

The influences of polymer structure on rubber distribution in hiPP were investigated. Polypropylene polymerization was conducted at different reaction time. The results showed the internal structure of polymer could maintain that of $Mg(OEt)_2$. The internal structure became denser as the polymerization time increased. Copolymerization in gas-phase was conducted sequentially after propylene polymerization. As the copolymerization time increased the influence of mass diffusion became dominant resulting in decrease of copolymerization activity. The precipitation-based catalyst was employed in order to investigate the influence of catalyst structure on the distribution of rubber. The result showed that pore volume was important for rubber distribution. The more available pore volume, the more rubber dispersion it was.

References

[1] Y.-Q. Zhang, Z.-Q. Fan, L.-X. Feng, *J. Appl. Polym. Sci.*, 84 (2002) 445-453.

[2] P. Kittilsen, T. F. McKenna, *J. Appl. Polym. Sci.*, 82 (2001) 1047-1060.

[3] P. Galli, *Macromol. Symp.*, 78 (1994) 269-284.

[4] Y. Chen, Y. Chen, W. Chen, D. Yang, *J. Appl. Polym. Sci.*, 108 (2008) 2379-2385.

[5] Z. Fu, Z. Fan, Y. Zhang, J. Xu, *Polym. Int.*, 53 (2004) 1169-1175.

[6] Z. Fu, J. Xu, Y. Zhang, Z. Fan, *J. Appl. Polym. Sci.*, 97 (2005) 640-647.

[7] D. Bouzid, F. Gaboriaud, T. F. L. McKenna, *Macromol. Symp.*, 243 (2006) 215-224.

[8] W. M. Sperci, G. R. Patrick, *Polym. Eng. Sci.*,15 (1975) 668-672.

[9] Z.-Q. Fan, Y.Q. Zhang, J.-T. Xu, H.-T. Wang, L.-X. Feng, *Polymer*, 42 (2001) 5559-5566.

[10] T. Taniike, V. Q. Thang, N. T. Binh, Y. Hiraoka, T. Uozumi, M. Terano, *Macromol. Chem. Phys.*, 212 (2011) 723-729.

[11] X. Zheng, M. S. Pimplapure, G. Weickert, J. Loos, *Macromol. Rapid Commun.*, 27 (2006) 15-20.

[12] M. H. Nejad, P. Ferrari, G. Pennini, G. Cecchin, *J. Appl. Polym. Sci.*, 108 (2008) 3388-3402.

[11] T. Taniike, T. Funako, M. Terano, *J. Catal.*, 311 (2014) 33-40.

[12] S. Dwivedi, T. Taniike, M. Terano, *Macromol. Chem. Phys.*, 215 (2014) 1698-1706.

[13] Z. Fu, Q. Dong, N. Li, Z. Fan, J. Xu, *J. Appl. Polym. Sci.*, 101 (2006) 2136-2143.

[14] T. F. McKenna, D. Bouzid, S. Matsunami, T. Sugano, *Polym. React. Eng.*, 11 (2003) 177-197.

Chapter V

General conclusions

5.1 General summary

This dissertation mainly focused on the investigation and evaluation of the structure on the catalytic performances of Ziegler-Natta catalyst. So far, it is known that the performances of Ziegler-Natta catalyst are influences from various factors from molecular level such as active site nature to macroscopic level such as particle size and pore volume. Thus, the researches were often done in an empirical way. This research intensively investigated the origin of catalyst structure, the importance of reaction conditions, and the influences of polymer structure.

In chapter 1, basic knowledge of Ziegler-Natta catalyst including catalyst development and catalyst preparation method was described. $Mg(OEt)_2$-based Ziegler-Natta catalyst and its related researches was also reviewed. Among several grade of polypropylene-based materials, high impact polypropylene (hiPP) is one of the most attractive grades in both of academic and industrial. HiPP and its formation mechanisms are introduced. Finally, the objectives of this dissertation were stated.

In chapter 2, the particle development of $Mg(OEt)_2$ was precisely investigated. The different size of magnesium powder was employed in order to study the morphology development. The results clearly showed that magnesium powder affected reaction rate, which had influences on the formation of $Mg(OEt)_2$, especially detachment or separation step, which resulted in different final particle size. The $Mg(OEt)_2$ samples were used for catalyst preparation and tested with ethylene/1-hexene copolymerization. The copolymerization activity was also identical between two catalysts. However, the difference in 1-hexene content was observed. It was ascribed to the effect of particle size, which also affected the diffusion ability of comonomer.

In chapter 3, the procedure and the conditions for hiPP were established. The limitation was examined. Also, the conditions for both of propylene polymerization and ethylene-propylene copolymerization were optimized. The exact content of polypropylene containing in hiPP was certified by the equation obtained from the reaction profile. The results were well consistent with the rubber extraction experiment.

In chapter 4, the morphology development of polypropylene was investigated. The structure of polypropylene still maintained the structure of $Mg(OEt)_2$. Ethylene-propylene copolymerization was conducted after propylene polymerization. It showed that the copolymerization activity was obviously influenced by the structure of polypropylene due to mass transfer limitation. The rubber distribution was compared between different catalyst platforms. The results showed $Mg(OEt)_2$-based had more rubber capacity comparing to precipitation-based catalyst.

5.2 Conclusion

Polymer morphology has been researched and developed over decades since the discovery of Ziegler-Natta catalyst. It is widely accepted that the polymer morphology imitates the catalyst, so the stage of catalyst design is necessary to achieve required polymer morphology. Among several techniques for catalyst preparation, $Mg(OEt)_2$ is an effective precursor because it can give excellent catalyst morphology and high catalytic activity. However, the systematic morphology control of $Mg(OEt)_2$ has not been established yet. The polymer morphology was important not only for production efficiency but also polymer properties. For instance, hiPP copolymerization utilizes porous structure of PP to form copolymer components.

Besides the conditions and procedure of the reaction, the structure of PP is a key factor, which determines the properties and characteristics of the final product.

In this research, I investigated morphology development of polypropylene and its effects in hiPP copolymerization. At the beginning of this research, the morphology development of $Mg(OEt)_2$ was studied. It was observed that the reaction rate had great effect on the morphology of $Mg(OEt)_2$, especially on the particle size. Then, the catalyst prepared from the obtained $Mg(OEt)_2$, was used for hiPP copolymerization. In chapter 3, because of the limitation of the reactor, I proposed an alternative way to examine the properties of hiPP. Finally, the importance of polymer morphology on the properties of hiPP was clearly shown.

The results from this research can be applied to control the morphology of $Mg(OEt)_2$-based Ziegler-Natta catalyst. Also, the importance of conditions and procedure was emphasized. Finally, I also proposed an alternative way to obtain well distribution of copolymer in hiPP. The results of this study may contribute to the profound understanding and application of the heterophasic polyolefin production with $Mg(OEt)_2$-based Ziegler-Natta catalysts.

Investigation of heat generation during initial stage of gas-phase propylene polymerization on Ziegler-Natta catalyst

by

Goond Hongmanee

Submitted to

Japan Advanced Institute of Science and Technology

Supervisor : Professor Timothy F. McKenna
LCPP–CNRS/ESCPE-Lyon

1 Introduction

Industrial polyolefin production processes are classified into two main types, slurry-phase process and gas-phase process. Considering production cost, gas-phase process well serves the requirement because it consumes less amount of solvent as in the slurry process. In addition, there is some valuable polymer such as high impact polypropylene (hiPP), which is limited for gas-phase process. However, there are some limitations of gas-phase process; insufficient heat transfer ability, and fine particle of polymer. These drawbacks are primarily solved by tuning operating conditions. However, the rational explanation and the evidences on the solution are still ambiguous especially in terms of reaction kinetics.

To the best of our knowledge, there are no experimental studies on reaction kinetics of propylene polymerizations comparing between slurry and gas phase, whereas some can be found for ethylene.[1] For instance, Naderpour et al.[2] studied ethylene polymerization kinetics with a heterogeneous Ziegler-Natta (ZN) catalyst, and concluded that process variables as temperature, pressure and hydrogen concentration have different effects on the kinetic parameters and rate of polymerization of ethylene in slurry and gas phases. From a reaction engineering standpoint, Daftaribesheli[3] studied mass transfer resistances in gas and slurry processes, and determined that transport of gaseous monomer over a gas-liquid boundary can become the rate limiting step, when highly active catalysts are used. Thus, in gas phase reaction, gas can diffuse much faster than in a liquid phase, and in consequence, reaction starts more quickly and particles in the gas-phase more suffer from overheating than in slurry phase especially at the initial stage of reaction.

In fact, several authors have pointed thermal degradation as one of the possible reasons to explain low productivity in propylene gas-phase process.[4-7] During the

initial stage of reaction, large amount of heat is generated when the polymerization sites are highly active. However, the generated heat is continuously accumulated in the formed polymer particle and cannot be sufficiently removed because of low heat transfer ability. Thus, some active sites are harmed and the particles are uncontrollably cracked. Regarding to this fact, an additional step is added to control the generated heat and fragmentation. In some commercial processes, polymerization is conducted in a mild environment before changing to the desired conditions.[8] Although the problems can be technically solved, those are still a lack of evidence to identify the occurrence of thermal degradation because there is no effective tool, which is able to effectively monitor the generation of heat during the first few seconds of the reaction.

Stopped flow reactor was invented in order to investigate short-time generated polymer, which is a footprint of active sites. Slurry-phase stopped flow reactor was extensively exploited to understand the nature of active sites and polymer morphology development.[8-9] For instance, the relationship between structure and performance of electron donor was studied by applying stopped flow technique and DFT calculation.[10] The results showed that the adsorption of an alkoxysilane affected on the productivity and the coadsorption model could well explain the experimental results obtained from stopped flow. For gas-phase, the investigation and understanding of reaction kinetics and particle development were clearer since McKenna et al. developed gas-phase stopped flow reactor.[11] Thus, comprising gas-phase stopped flow and calculation of energy balance, it has high potential to reveal the origin of thermal degradation in gas-phase propylene polymerization.

In this study, semi-batch propylene polymerizations were conducted in both of slurry- and gas-phases at different reaction temperatures to clarify its impact over

kinetics and performances. The activity profile was obtained from the consumption of propylene and then fitted by mathematic models to provide kinetics parameters. Two different temperatures were conducted in gas-phase stopped flow reactor. Calculation of energy balance provided a more realistic temperature profile of the catalyst, which was higher than those showed by the system. [12-14]

2 Experiment

2.1 Materials

Commercial fourth generation $MgCl_2$ supported $TiCl_4$ Ziegler-Natta with titanium content of 2.8 % and triethylaluminium (Witco, Germany) were used for polymerization. Dicyclopentyldimethoxysilane (DCPDMS) was used as external electron donor. All heptane used was pre-treated on 3Å molecular sieves. Sodium chloride (purity > 99.5 %) was obtained from Acros Organics, France, and then dried under vacuum at 200 ºC for 5 hours and kept under argon atmosphere. Propylene and ethylene with minimum purity of 99.5 % and hydrogen with minimum purity of 99.99 % were purchased from Air Liquide (France). Propylene was purified with a three stage system of columns before use: a first one filled with BASF R3-16 catalyst (CuO on alumina), a second one filled with molecular sieves (13X, 3A, Sigma-Aldrich), and a last one filled with Selexsorb COS (Alcoa). Argon provided by Air Liquide, France, with minimum purity of 99.5 %, was used in order to keep the reaction free of oxygen.

2.2 Semi-batch polymerization method

Slurry phase and gas phase polymerizations were conducted in semi-batch mode in a 2.5 L spherical stirred-bed reactor (turbosphere), equipped with injection valves for the catalyst and monomer feeds. During reaction the system was kept under isothermal conditions. A pressure reducer was used to maintain constant pressure. Continuous measurements of the monomer pressure in ballast were interpreted using the Soave-Redlich-Kwong equation of state (SRK-EOS) to obtain the productivity as a function of time, and the derivative of the pressure drop gives us the reaction rate. The experimental setup used to carry out the polymerization reactions was similar to the one described by Cancelas et al.[7] and Kittilsen and McKenna[15], and the reader is referred to these publications for a more detailed description of the system.

The reactor was heated to the desired temperature and vacuumed for 1 h. Argon replacement was done before reaction start. For slurry phase polymerizations, the liquid mixture was prepared under argon. 30 mg of catalyst were mixed with TEA (Al/Ti of 190) and external donor (Si/Ti of 10) in 1L volumetric flask under argon atmosphere with 500 ml of heptane. The slurry was transferred to reactor with pressure of propylene slightly above atmospheric pressure and at low stirring rate. The reaction was conducted at 7.5 bar of propylene and 2 % of hydrogen for 1 h increasing stirring rate (~ 500 rpm).

For gas phase polymerizations 30 mg of catalyst were diluted in NaCl salt and transferred to a 100 cm^3 cartridge injector in the glovebox. Once the reactor had reached the desired initial temperature, required amount of 1M TEA/heptane solution was injected and agitation (300 rpm) was started. About 5 minutes after the first injection the donor/heptane solution (0.42 M) and the catalyst suspension were injected under argon. The reactions were held at 7.5 bar of propylene and 2 % of hydrogen for 1 h.

Prepolymerization was not performed in any case. Nevertheless, note that first catalyst is injected and then reaction is started by reactor pressurization, which is a softer initiation compared to industrial conditions where monomer is already present. Once the reaction is finished the monomer inlet is closed and the reactor is rapidly cooled down and depressurized. Polymer is recovered either after filtration in the slurry case, either after washing it with demineralized water, to dissolve NaCl. In any case the final powder is then dried for at least one hour at 90 °C to remove the remaining traces of liquid (heptane or water).

Gas-phase Stopped Flow Polymerization

A schematic view of the stopped flow reactor system is shown in **Figure 1**. It consists of a fixed packed bed which is crossed by a pulse of reactants during a predetermined time, typically less than one minute, where reaction temperature is controlled by plunging it into a heated water bath. Inlet and outlet gases stream temperatures are measured during reaction. For a more detailed description of the system and reactor technology reader is referred to previous publications from our group.[13-14]

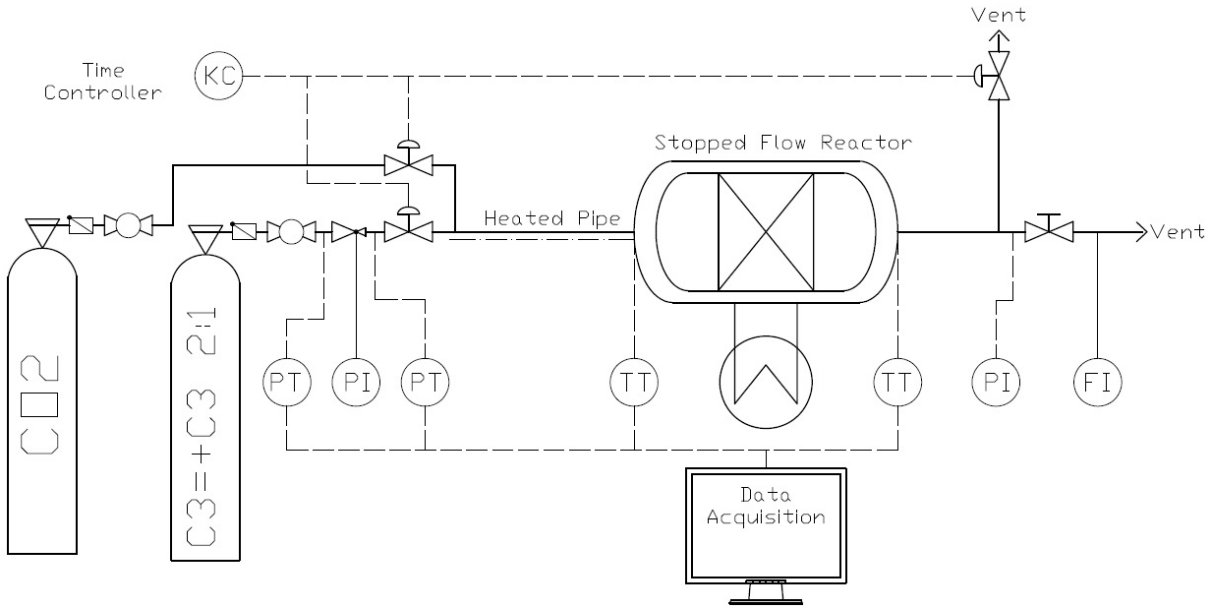

Figure 1. Stopped flow reactor experimental setup and control system.

Gas phase reactions were accomplished in a 3.14 mL packed bed reactor with 4.5 bars of a mixture propylene-propane (where 33 mol-percent was propane) at 60 and 70ºC. Propene was diluted to ameliorate heat transfer conditions inside the packed bed, and propane was chosen among other commonly gases used in industry, as for instance nitrogen, due to its higher heat capacity and similar acentric factor to propene molecule. Ziegler Natta precatalyst was packed with small NaCl salt, consisting of single cubes of 5–10 μm slightly agglomerated to give a final single object of around 30 μm. The salt was dried at 200 ºC and at least 10^{-5} bar during 4 hours. For each run an amount of 15 mg of ZN precatalyst were packed along 2 g of NaCl in a glovebox. TEA (1 M, heptane solution) was used in a molar ratio Al/Ti of 26. As compared to semi-batch reactions, Al/Ti ratio was diminished to avoid over-reduction, since a smaller volume will augment TEA concentration, while Si/Ti molar ratio was kept the same as in semi-batch reactions. Before reaction, heptane from donor and cocatalyst solutions was removed applying vacuum to the solid mixture containing the activated catalyst.

In this work, applied reaction times were 5, 10, 20 and 40 seconds, always followed by degassing during 5 seconds and then 30 seconds of a CO_2 stream, to halt the reaction.

Reaction yield is measured by weighing the reactor before and after polymerization. Afterwards salt was washed away with water and polymer recovered for further analysis.

Polymers characterization

The bulk density was determined using a method of weighing a known loosely packed polypropylene powder. A recipient with a precisely known volume of about 40 mL is used. The bulk density is indicated in gram polymer per milliliter volume.

The molecular weight distributions (MWD) of polymer samples were characterized by HT-SEC (Viscotek-Malvern Instruments). The system was equipped with three detectors (a refractometer, a viscometer and light scattering) and with three columns (PSS POLEFIN analytical 1 000 - 100 000 - 1 000 000 Å). Analyses were performed in 1,2,4-trichlorobenzene stabilized with butylhydroxytoluol at 0.2 $g \cdot L^{-1}$ at 150 ºC at a flow rate of 1 $mL \cdot min^{-1}$. The molecular weight distributions were calculated by a triple detection. Refractometer, viscometer and light scattering signals were used in order to erase possible artifacts.

Kinetic Model

For semi-batch experiments, we have chosen to describe the reaction rate by semi-empirical relations to describe the physical effects. The instantaneous rate of propylene polymerization is calculated from the rate of pressure drop in the propylene feed ballast. For each experiment, the measured reaction rates have been fitted to the

mathematic model shown in Equation 1 with 1st order deactivation for single site catalyst. Fitting is done by minimizing the deviations between the experimental and model curves. Development of the equation can be found elsewhere.[16]

$$Rp = k_p C_O \cdot C_m \cdot e^{-k_d \cdot t} \cdot \frac{1 - e^{-K_a \cdot \left(1 - \frac{k_d}{K_a}\right) \cdot t}}{1 - \frac{k_d}{K_a}} \qquad (1)$$

Values k_p, K_a and k_d stand for the propagation rate, activation and deactivation constants, respectively. C_0 is the initial amount of nonactivated catalyst and C_m is monomer concentration in the active sites. Units were adapted to obtain reaction rate (Rp) in $g \cdot gcat^{-1} \cdot h^{-1}$. Equation 1 is derived from the fundamental model for polymerization kinetics where reactions taken in account are site activation, propagation, and catalyst deactivation.

As Table 1 clearly shows, propene concentration (C_m) in the active sites differs depending on temperature and phase of polymerization. For gas phase reactions we considered it equal to the solubility of propylene in polypropylene, and we used the experimental data from Sato et al.[17] However, for slurry polymerizations it is given by the propylene solubility in the diluent, in our case heptane. In this case, data was taken from Dashti et al. [18] publication.

3. Results and Discussion

3.1 Semi-batch Polymerizations

The influence of reaction phase (gas or slurry), temperature and seedbed amount on the polymerization kinetics has been studied using the described kinetic model from Equation 1. The values obtained for the activation constant K_a, the deactivation constant k_d, and the kinetic parameter $k_p \cdot C_0$ have been used to analyze the various

process parameters in a qualitative manner. A general summary of all semibatch runs, presenting the process conditions and determined kinetic parameters, is displayed in **Table 1**.

Table 1. Summary of semi-batch polymerization reactions designed and performed in the current study in the turbosphere reactor.

Reaction Phase	Seedbed (g NaCl)	Temperature (°C)	Activity ($kgPP \cdot gcat^{-1} \cdot h^{-1}$)	$k_p \cdot C_0$ ($L \cdot g_{cat}^{-1} \cdot h^{-1}$)	$K_a \cdot 10^3$ (s^{-1})	$k_d \cdot 10^4$ (s^{-1})	Cm ($g \cdot L^{-1}$)
Slurry	-	50	0.83	9.3	5	0.1	95
Slurry	-	60	1.38	19.3	2.3	0.1	81
Slurry	-	70	2.11	36.3	1.6	0.1	70
Slurry	-	90	2.47	52.8	1.4	0.1	58
Gas	10	50	0.67	20.4	50	2.8	53
Gas	10	60	0.75	41.9	50	5	39
Gas	10	70	0.62	26.3	50	2.2	35
Gas	20	70	0.93	37.5	50	1.9	35

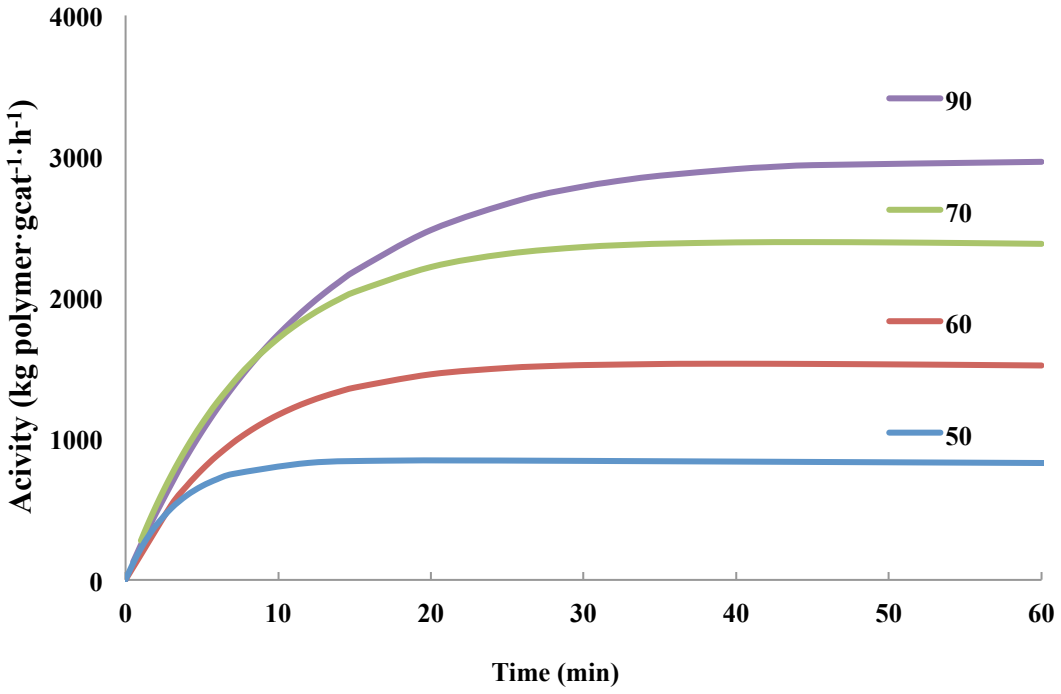

Figure 2. Instantaneous rate of propylene polymerization at 70 °C with 7.5 bars of propylene in slurry phase at 50, 60, 70 and 90 °C.

Figure 2 shows the influence of temperature on the instantaneous rate of propylene polymerization in slurry phase with a supported ZN catalyst with 7.5 bar of partial pressure of propylene in the reaction environment. It can be seen that activity profiles are build-up type for slurry phase polymerizations. During reaction, activity increased until it reached the maximum and remained constant throughout the reaction. Induction period is the reaction time taken to reach the maximum rate, and it was extended by the increase of reaction temperature. At 50 °C, the induction period was within first 10 min of the reaction while there was around 40 min for 90 °C. Activation constant, K_a, can be used to quantify this effect, since this parameter represents how fast reaction takes to reach maximum catalytic activity. As we see in **Table 1**, it decreased with increasing temperature. Monomer has to pass several barriers for slurry polymerization to go on. In our three phases system (gas, liquid and solid) first monomer diffuses into heptane, then to the pores of the particle and gets sorbed in the polymer layer covering the active sites, where it reacts. With higher temperature propene solubility decreases, but monomer consumption rises. Therefore, while monomer flow decreases over the gas-liquid boundary, its driving force augments, making a greater resistance that controls monomer transport.[3] Thus, induction period augments (along with a K_a diminution) and equilibrium is reached later.

As exposed in **Table 1**, the catalytic activity at 70 °C was higher than that of 50 °C and it slightly increased at 90 °C. This trend was not exactly the same for the kinetic parameter $k_p \cdot C_0$, which showed an increase almost linear with the increasing reaction temperature. Variations of propene concentration cause these dissimilarities. Additionally, in this set of experiments, the deactivation was not influenced by changing temperature as seen in constant k_d value in every temperature.

Figure 3 exhibits the influence of temperature (50, 60 and 70 °C) on the instantaneous rate of propylene polymerization in gas phase with a ZN catalyst with 7.5 bar of partial pressure of propylene in the reaction environment. They show declining kinetics for all temperatures and high activities in the early stage. The run performed at 60 °C presented highest average activity, as well as greatest $k_p \cdot C_0$, whereas at same amount of salt the run performed at 70 ºC produced the lowest amount of PP.

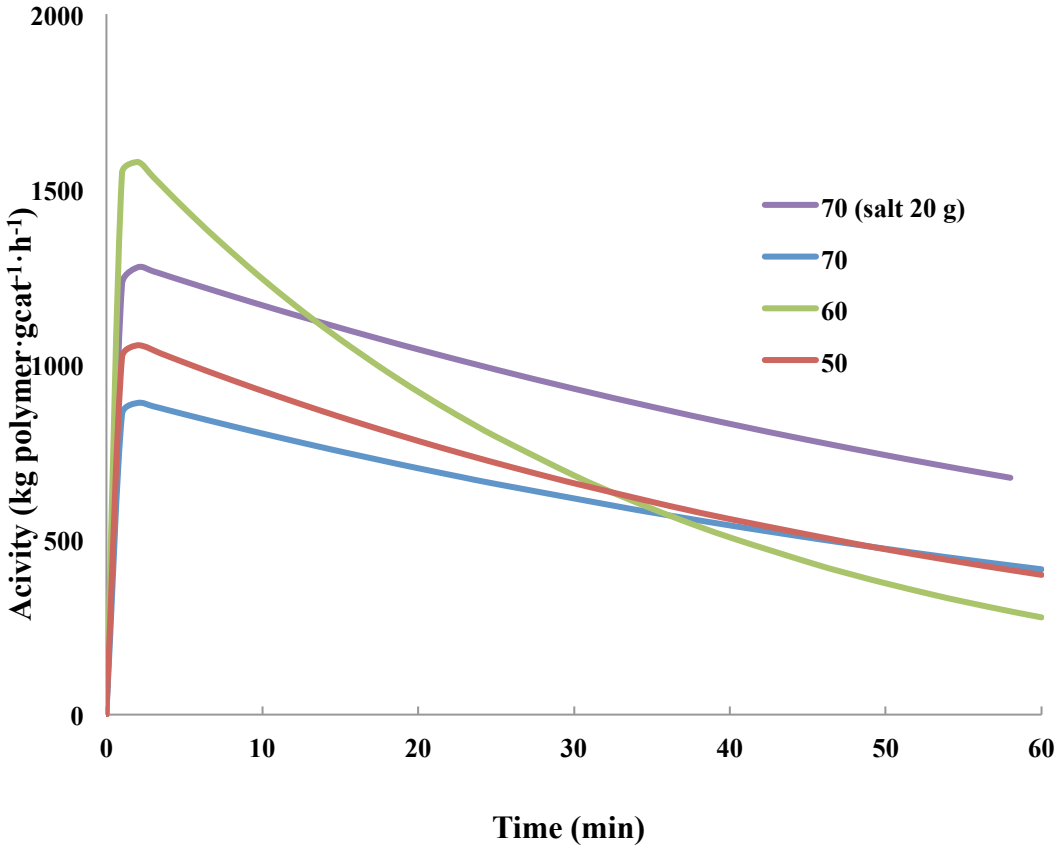

Figure 3. Instantaneous rate of propylene polymerization at 70 °C with 7.5 bars of propylene in gas phase at 50, 60 and 70 °C. For the last temperature two different amount of seedbed were used, 10 and 20 g.

The reaction profiles from slurry and gas phase polymerizations obviously showed different kinetics pattern even though the same catalyst was used in the reaction. In slurry phase reaction, the build-up type profile did not show deactivation

within 1 h of reaction. These could be explained as the advantage of solvent. It has an important role in adsorbing generated heat during the reaction and delaying monomer arrival to active centers. Likewise, temperature was well controlled, and thus catalyst was not harmed by overheating. On the other hand, gas-phase reaction showed decay-type reaction profile. Interestingly, the highest rate of deactivation was coming from the highest rate of reaction, at 60 °C. Possibly, large amount of heat was generated as the result of an initial high rate of reaction, almost certainly due to higher macroparticle diffusivity as compared to slurry reactions.[19] The generated heat was not sufficiently removed according to poor heat transfer in gas-phase reaction. Thus, the heat was accumulated and deactivated the catalyst. To improve heat transfer in gas phase processes, some components can be added along catalyst when injected. For instance, the previous work in our group adapted a catalyst injection method.[7],[20] The addition of catalyst together with solvent or mineral oil could effectively improve catalyst activity and polymer morphology. In this work, another alternative was investigated: adding more amount of seedbed (NaCl salt) at the reaction temperature of 70 °C to improve heat transfer. The results showed an activity enhancement as compared to the same reaction temperature but less amount of salt. $k_p \cdot C_0$ value augmented while k_d decreased. Thus, early stage of reaction was obviously affected by temperature.

If our postulates are true, heat transfer differences between both methods (slurry and gas phase) should affect other aspects of polymerization, as morphology of the obtained powders. **Figure 7** shows the effect of reaction phase on bulk density of PP powders for a supported ZN catalyst.

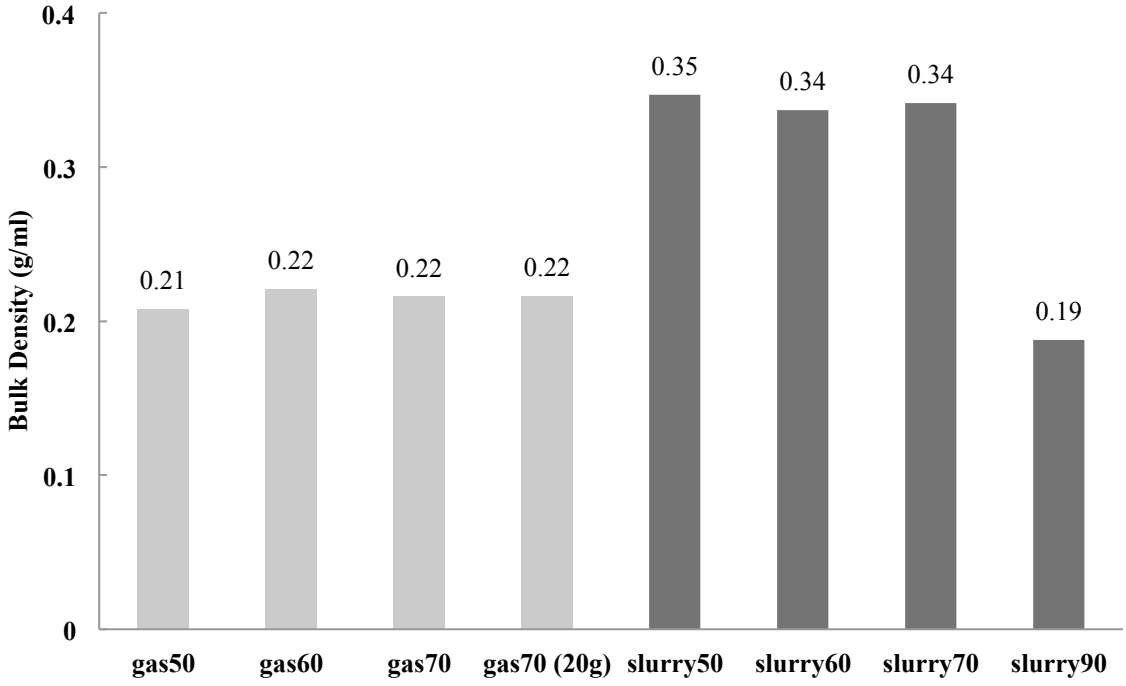

Figure 3. Bulk densities of polypropylene powders from runs shown in Table 1.

It is revealed here how bulk densities are lower for gas phase without dependence on seedbed amount, when compared to similar reaction temperature in slurry phase. While PP particles with regular and more or less spherical shape were being obtained from the slurry polymerizations, (except reaction at 90 °C, which yielded big agglomerates of polymer) gas phase ones produced mainly fines with some flaky particles. The fragmentation process that occurs is obviously different in the gas and slurry phases, and this might be in part the result not only of the presence of the solvent in the slurry reactions but also of better initial temperature control, as already indicated by Kittilsen et al.[15] It is also well known that rapid initial reactions are correlated with poor control of the particle morphology. Pater et al.[21] concluded that bulk densities are low when initial reaction rates are high. This certainly supports our previous assumption of heat accumulation in the catalyst and its consequent deactivation, due to high initial reaction rates.

Although obtained reaction profiles, kinetic parameters and bulk densities evidenced the effects of temperature on the runs, gas phase reactions at 60 and 70 ºC were conducted within very short time to further explore heat generation during initial stage, in the stopped flow reactor.

3.2 Gas Phase Stopped Flow Polymerizations

Reactions were conducted at 60 and 70 °C during 5, 10, 20 and 40 s in a gas phase stopped flow reactor. **Figure 4** shows obtained temperature profiles from outlet thermocouple of 40 s reaction plotted versus time.

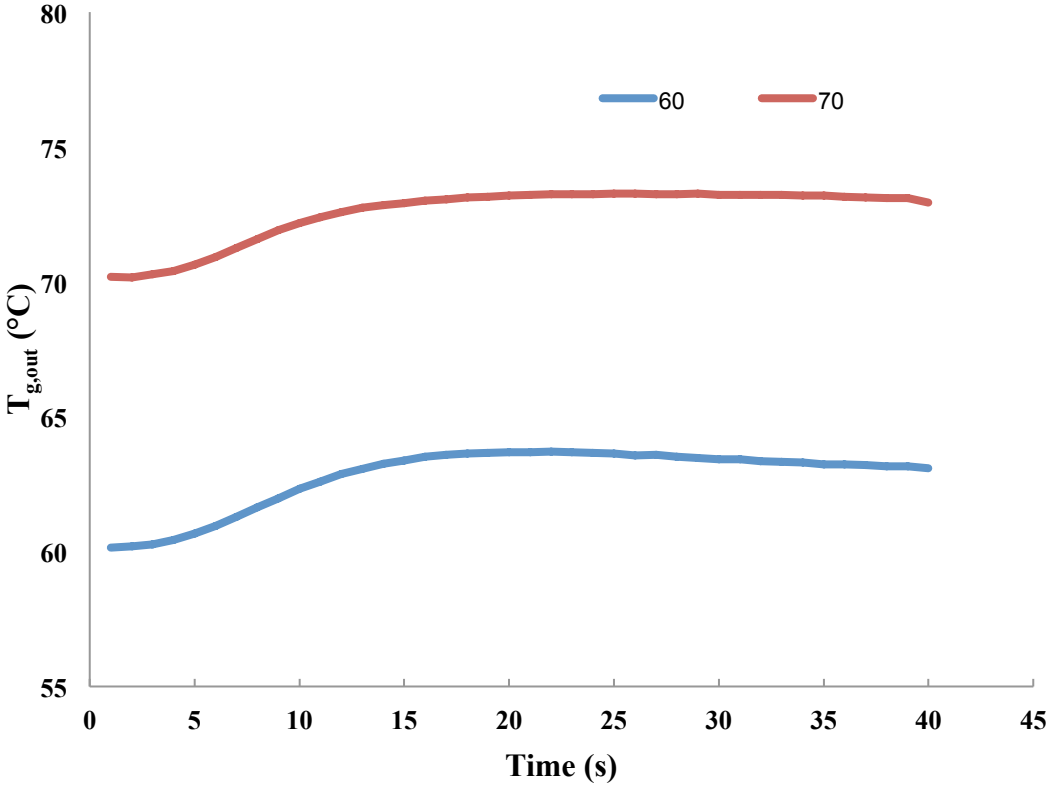

Figure 4. Outlet gas temperature profile for 40 s propylene homopolymerization using supported ZN catalyst at 60 and 70 °C and 4.5 bar of propylene/propane 2:1 molar mixture.

As shown in **Figure 4**, temperatures raised approximately 4 °C within 15 s and remained constant for both temperatures studied. It seems that we are working with very good heat transfer conditions with our equipment, but, as explained before, it is reasonable to suspect that particle temperatures are higher. A solid average temperature of the bed (catalyst and salt, T_{solid}) can be calculated, following the next steps. Initially, outlet gas temperatures ($T_{g,out}$) combined with inlet temperatures ($T_{g,in}$) can be used to estimate the total amount of heat evacuated by the gas stream, (Q_{evac}) as presented in Equation 2:

$$Q_{evac} = \dot{q}\rho_f C_{pf} \int_0^t \left(T_{g,out} - T_{g,in}\right) dt \tag{2}$$

Where $\dot{q}$ is the volumetric flow rate of the gas phase and ρ_f its density. Polymer yield ($m_{polymer}$) with the enthalpy of polymerization (ΔH_r) was used to calculate heat generated (Q_{gen}) in the packed bed, following Equation 3:

$$Q_{gen} = m_{polymer} \cdot (-\Delta H_r) \tag{3}$$

The accumulated heat (Q_{acc}) in the reactor can be calculated with an energy balance as shown in Equation 4. Rearranging the expression to Equation 5 a solid average temperature of the bed at the end of each reaction (T_{solid}) is obtained. Here, T_0 is the initial solid temperature and m_{solid} is the mass of the bed.

$$Q_{acc} = Q_{gen} - Q_{evac} = m_{solid} C_{p,solid} (T_{solid} - T_0) \tag{4}$$

$$T_{solid} = T_0 + \frac{Q_{acc}}{m_{solid} C_{p,solid}} \tag{5}$$

Therefore, we will get a lower bound on the average temperature of catalyst particles at 5, 10, 20 and 40 s. Once more, interested readers are referred to preceding papers from our group for a more detailed description in its calculation. [13, 14] **Figure 5** displays the calculated accumulated heat in the reactor (Q_{acc}) and the solid average temperature (T_{solid}) at 5, 10, 20 and 40 s at 60 and 70 °C.

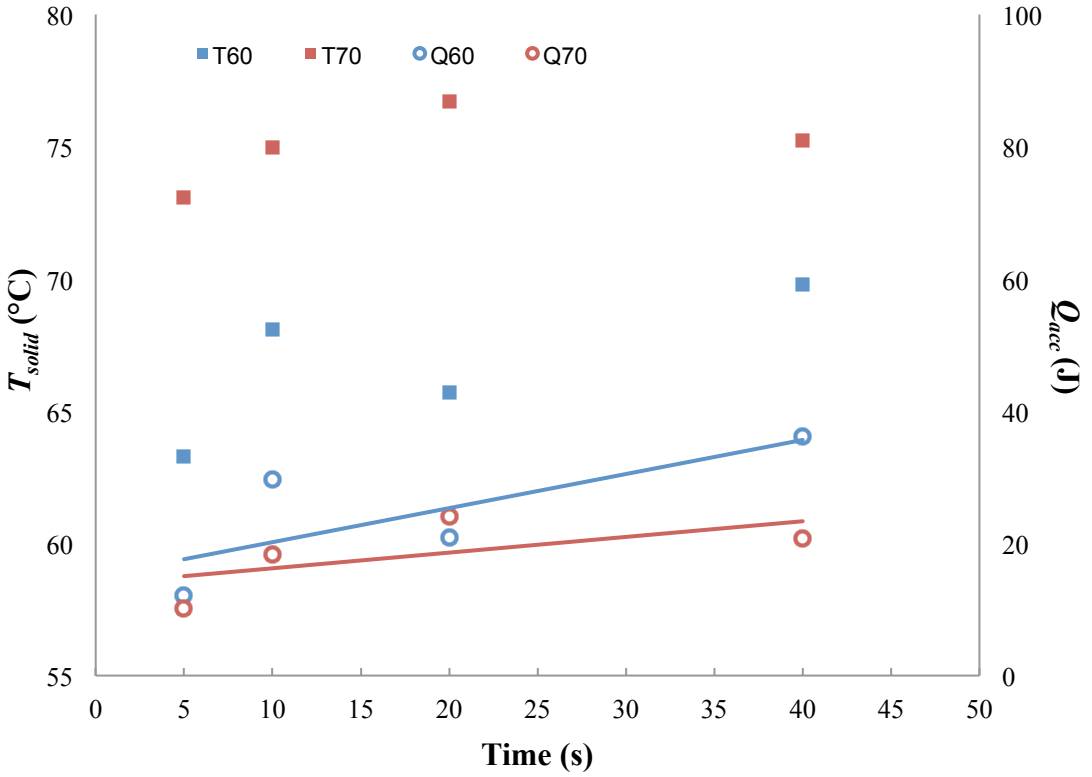

Figure 5. Accumulated heat (Q_{acc}) and solid average temperature of the bed (T_{solid}) at different times of propylene polymerization at 60 and 70 °C.

Figure 5 exhibits how, for each temperature, T_{solid} is higher than the observed outlet temperature from **Figure 4**. Therefore heat transfer limitations exist and we can verify that packed bed (and in consequence catalyst particles) from 60 ºC reactions series are overheating more. Accumulated heat results (Q_{acc}) are in agreement. A possible explanation for this behavior is active sites were somehow partially destroyed by temperature before reaction in gas phase polymerizations.

This is also in accordance with gas phase semi-batch experiments (**Figure 3**), where for the same reaction conditions there is more activity at 60 than 70ºC. At lower temperature, active sites were less harmed. Additionally, when reaction started, heat generated accumulated in the catalyst. According to poor heat transfer ability of gas, heat continued accumulating and resulted in a bigger damage to active sites, resulting in a higher value of k_d for 60 °C semibatch gas phase polymerization.

Our assumptions can also explain observed results when a greater seedbed mass was used at 70 ºC gas phase semibatch polymerizations. At this point is important to remember that precatalyst-salt mixture is always injected at room temperature to an already heated reactor. This would result in a lower catalyst starting temperature of polymerization, since heat transfer is delayed. In consequence, $k_p \cdot C_0$ value augmented, while k_d decreased since heat was accumulating less in the catalyst particles.

3.3 Molecular Weight

The results from the GPC measurements (Mw and Mw/Mn) are presented for all gas phase samples produced at different process conditions (**Table 2**). As shown in the literature,[22] the dominant chain transfer reaction is with hydrogen if it is present. In consequence, Mw from semibatch experiments from **Table 2** are very similar, and it does not depend on temperature. On the other hand, when hydrogen was not present in the reaction environment, as in stopped flow reactions, Mw increased when reaction temperature decreased. This is further supported by $k_p \cdot C_0$ values from **Table 1**. Definitely, temperature in the gas phase polymerization of propylene has a great effect on the active sites.

Table 2. Weight average molecular weight (Mw) and polydispersity (Mw/Mn) of every sample synthetized in gas phase. Note that hydrogen was not present in stopped flow reactions.

Reactor	Seedbed (g NaCl)	Temperature (°C)	Hydrogen (mol %)	Mw (kDa)	Mn/Mw
Semi-batch					
Gas Phase	10	50	2	295	3.9
Gas Phase	10	60	2	304	3.6
Gas Phase	10	70	2	303	3.6
Gas Phase	20	70	2	299	3.6
Stopped Flow					
40 s	2	60	0	528	3.3
40 s	2	70	0	318	3.3

4. Conclusions

Instantaneous rate profiles from gas phase and heptane-slurry propylene polymerizations were obtained from a supported Ziegler-Natta catalyst at different temperatures, and were fitted with a kinetic model. It is shown the big effect that temperature has on catalyst performance, and, in particular, over catalyst deactivation in gas phase reaction. Thermal degradation was expected as the main cause of degradation because of insufficient heat removal. The addition of salt together with the catalyst could improve heat removal as can be seen in lower deactivation constant and higher activity. The results from gas phase stopped flow reactor showed that generated heat was lower in higher reaction temperature. This suggested that some active sites were deactivated because they were temperature sensitive.

References

[1] M. F. Bergstra, G. Weickert, *Macromol. Mater. Eng.*, 290 (2005) 610-620.

[2] N. Naderpour, E. Vasheghani-Farahani, M. H. N. Famili, M. Vatankhah, *Iran. Polym. J.*, 19 (2010) 895-906.

[3] M. Daftaribesheli, *Comparison of Catalytic Ethylene Polymerization in Slurry and Gas Phase*, University Of Twente [Host], Enschede, **2009**.

[4] R. Spitz, C. Bobichon, A. Guyot, *Makromol. Chem.*, 190 (1989) 707-716.

[5] G. Guastalla, U. Giannini, *Makromol. Chem. Rapid Commun.*, 4 (1983) 519-527.

[6] J. J. C. Samson, B. van Middelkoop, G. Weickert, K. R. Westerterp, *AIChE J.*, 45 (1999) 1548-1558.

[7] A. J. Cancelas, V. Monteil, T. F. L. McKenna, *Macromol. Symp.*, 360 (2016) 133-141.

[8] B. Liu, H. Matsuoka, M. Terano, *Macromol. Rapid Commun.*, 22 (2001) 1-24.

[9] A. Di Martino, J.-P. Broyer, D. Schweich, C. de Bellefon, G. Weickert, T. F. L. McKenna, *Macromol. React. Eng.*, 1 (2007) 284-294.

[10] S. Poonpong, S. Dwivedi, T. Taniike, M. Terano, *Macromol. Chem. Phys.*, 215 (2014) 1721-1727.

[11] B. Olalla, J.-P. Broyer, T. F. L. McKenna, *Macromol. Symp.*, 271 (2008) 1-7.

[12] T. F. L. McKenna, E. Tioni, M. M. Ranieri, A. Alizadeh, C. Boisson, V. Monteil, *Can. J. Chem. Eng.*, 91 (2013) 669-686.

[13] E. Tioni, J. P. Broyer, V. Monteil, T. McKenna, *Ind. Eng. Chem. Res.*, 51 (2012) 14673-14684.

[14] E. Tioni, R. Spitz, J. P. Broyer, V. Monteil, T. McKenna, *AIChE J.*, 58 (2012) 256-267.

[15] P. Kittilsen, T. F. McKenna, *J. Appl. Polym. Sci.*, 82 (2001) 1047-1060.

[16] J. B. P. Soares, T. F. L. McKenna, *Polyolefin Reaction Engineering*, Wiley-VCH, 2013.

[17] Y. Sato, M. Yurugi, T. Yamabiki, S. Takishima, H. Masuoka, *J. Appl. Polym. Sci.*, 79 (2001) 1134-1143.

[18] A. Dashti, S. H. Mazloumi, A. B. Ani, A. Akbari, *J. Chem. Eng. Data*, 59 (2014) 2258-2262.

[19] Q. Wu, H. Wang, S. Lin, *Macromol. Chem. Phys.*, 197 (1996) 155-163.

[20] A. R. Martins, A. J. Cancelas, T. F. L. McKenna, *Macromol. React. Eng.* 2016, Accepted.

[21] J. T. M. Pater, G. Weickert, W. P. M. V. Swaaij, *J. Appl. Polym. Sci.*, 87 (2003) 1421-1435.

[22] Y. V. Kissin, R. Ohnishi, T. Konakazawa, *Macromol. Chem. Phys.*, 205 (2004) 284-301.

[1] Y.-Q. Zhang, Z.-Q. Fan, L.-X. Feng, *J. Appl. Polym. Sci.*, 84 (2002) 445-453.

[2] P. Kittilsen, T. F. McKenna, *J. Appl. Polym. Sci.*, 82 (2001) 1047-1060.

[3] P. Galli, *Macromol. Symp.*, 78 (1994) 269-284.

[4] Y. Chen, Y. Chen, W. Chen, D. Yang, *J. Appl. Polym. Sci.*, 108 (2008) 2379-2385.

[5] Z. Fu, J. Xu, Y. Zhang, Z. Fan, *J. Appl. Polym. Sci.*, 97 (2005) 640-647.

[6] W. M. Sperci, G. R. Patrick, *Polym. Eng. Sci.*,15 (1975) 668-672.

[7] Z.-Q. Fan, Y.Q. Zhang, J.-T. Xu, H.-T. Wang, L.-X. Feng, *Polymer*, 42 (2001) 5559-5566.

[8] T. Taniike, V. Q. Thang, N. T. Binh, Y. Hiraoka, T. Uozumi, M. Terano, *Macromol. Chem. Phys.*, 212 (2011) 723-729.

[9] X. Zheng, M. S. Pimplapure, G. Weickert, J. Loos, *Macromol. Rapid Commun.*, 27 (2006) 15-20.

[10] M. H. Nejad, P. Ferrari, G. Pennini, G. Cecchin, *J. Appl. Polym. Sci.*, 108 (2008) 3388-3402.

[11] T. Taniike, T. Funako, M. Terano, *J. Catal.*, 311 (2014) 33-40.

[12] S. Dwivedi, T. Taniike, M. Terano, *Macromol. Chem. Phys.*, 215 (2014) 1698-1706.

[13] Z. Fu, Q. Dong, N. Li, Z. Fan, J. Xu, *J. Appl. Polym. Sci.*, 101 (2006) 2136-2143.

[14] T. F. McKenna, D. Bouzid, S. Matsunami, T. Sugano, *Polym. React. Eng.*, 11 (2003) 177-197.